Miniaturized Fluorescence Biosensor for Studying Neuronal Events

Thuvan Nguyen
University of New Orleans

MINIATURIZED FLUORESCENCE BIOSENSORS FOR STUDYING NEURONAL EVENTS

A Dissertation

Submitted to the Graduate Faculty of the
University of New Orleans
in partial fulfillment of the
requirements for the degree of

Doctor of Philosophy
in
The Department of Chemistry

by

Thuvan Hoang Nguyen

B.A., University of New Orleans, New Orleans, 1998
M.S., University of New Orleans, New Orleans, 2001

May 2003

ACKNOWLEDGMENTS

TABLE OF CONTENTS

ABSTRACT

When developing new techniques to analyze neuro-chemical microenvironments, it is important to realize the incredible variability in the cellular content and the response to stimulation between cells and within a single cell. Conventional analysis techniques yield an average result to describe the content and function of cells. This approach often misses important information since the onset of pathological conditions is always initiated in a small number of cells. New minimally invasive single cell analysis techniques are required for single cell studies in order to gain new insights and understanding of cells' functions. The objective of my Ph.D. study was to fabricate, characterize, and apply submicrometric fluorescence sensors for the analysis of neuron cells. This dissertation will report the fabrication of miniaturized fluorescence sensors for Ca^{2+}, pH and Zn^{2+} analysis. In the first approach, liposomes (phospholipid vesicles) were used as miniaturized containers for fluorescent sensing reagents. Liposome-based fluorescence sensing technology offers several advantages over commonly used fluorescence sensing techniques including high spatial resolution, protection of the sensing dye from quenchers and high biocompatibility. However, liposome based sensors were found to be unstable in the cellular environment. The second approach was to synthesize submicrometric particle-based fluorescence sensors named lipobeads to replace the fluorescent liposomes in cellular studies. Lipobeads are polystyrene particles that are coated with

a phospholipid membrane. One unique advantage of fluorescent sensing lipobeads is the ability to immobilize hydrophobic indicator molecules in the phospholipid membrane. This enables the use of these indicators in aqueous media since the lipobeads are fully water miscible. The lipobeads also proved to be highly biocompatible in cellular studies. This is attributed to their phospholipid bilayer membrane, which is similar in structure to cell membranes. The dissertation will describe the analytical properties of fluorescence sensing lipobeads and their application in studying zinc ion release and pH changes near neuron cells under physiological conditions, conditions of neuronal injury and stress and acidic cortical spreading depression during stroke like conditions.

CHAPTER 1: BACKGROUND OF SINGLE CELL ANALYSIS

When developing new techniques to perform intracellular analysis at the single cell level, it is important to realize the incredible variability not only in chemistry from cell to cell but also in physiological response time and compartments within single cells. Analyses of extracellular fluid as well as single whole cells must be considered primary goals for eventual understanding of single cell function. Recent advances in biotechnology enabled the development of biochemical sensors with single cell measurement capabilities. Biosensors are applied in many areas of biological monitoring including studying the functions of the brain and clinical monitoring of brain health. Biosensors are attractive because they use the specificity and high turnover rates of enzymes to give excellent selectivity for important bioactive species in a simple continuously recording device. Biosensor systems used in such demanding environments must be sensitive, stable, reproducible, and give a quick response [1]. Chemical sensors, which are defined as a combination of a sensing element and a transducer, share the same requirements as biosensors. Moreover, biosensors or chemical sensors must be real- time, noninvasive tools for the analysis of chemical processes in living cells and their sub-compartments [2].

Biological studies at the single cell level have attracted the attention of researchers from various disciplines for decades. However, the analysis of individual cells provides an extreme analytical challenge due to the complexity of the cellular

environment and its dynamic nature. Recent advances in biotechnology enabled the development of biochemical sensors with single neuron cell measurement capabilities. Several useful techniques exist for single cell analysis. The patch-clamp technique has an impressive sensitivity for characterizing individual ion channels in single cells [3]. Microelectrodes using amperometry and voltammetry modes were successfully applied to provide significant new insights into mechanisms of exocytosis and stimulus–secretion coupling in neurons [4-7]. The pioneering work of Adams [8-9] and Wightman [10] has demonstrated that important issues in neurophysiology and neuropharmacology could be addressed using microelectrodes based sensors. Neurotransmitter release and uptake were investigated in single cells, brain slices, and the intact brain. Wightman et al [11] showed that catecholamine is secreted from neurons in the form of sharp spikes, which is evidence of quantal release occurring from non-neurite-bearing endocrine cells. Their work provided the first temporally-resolved measurements of chemical secretion expected for quantal release and also proved the advantages of microelectrodes in possessing the sensitivity and temporal resolution to detect single cellular activities. Capillary electrophoresis separation in conjunction with electrochemical detection has also been applied to single cell analysis [12-16]. Swanek et al. developed a new method for the direct identification of dopamine from two separate vesicle compartments of a fully developed neuron in Planorbis corneus by capillary electrophoresis with scanning electrochemical detection. This method allows for both qualitative and quantitative identification in cellular analysis and demonstrates the utility of scanning electrochemical detection for both [17]. However, many neuromodulators, neurotransmitters, and neuropeptides are not intrinsically electroactive and the response depends on the

geometry of the cell/electrode pair. As in the case of patch clamp recording techniques, the stimulation of the secretion is not controllable. Most of the cells could not be stimulated by electrical depolarization [18-19]. More importantly, the information obtained with microelectrodes from a cell sample is limited. It is not feasible to place a large number of microelectrodes with sensitivity and selectivity toward multiple analytes and measure cellular events simultaneously in a large number of cells. Furthermore, the analytical properties of microeletrodes are limited by poor stability and interferences, their fabrication is cumbersome, and if and how they affect signaling events in neuron cells remain unknown. Therefore, alternative techniques have to be applied for single neuron analysis. Microdialysis combined with discrete sampling, separation by capillary electrophoresis, and subsequent determination can provide a comprehensive picture of metabolic processes occurring in the sampling region. Unfortunately, microdialysis has a relatively poor temporal and spatial resolution [20]. Besides capillary electrophoresis, mass spectrometry, and electrochemical techniques, fluorescence techniques for single cell studies are considered as an alternative.

1.1. Fluorescence and Fluorescence Sensing

Fluorescence is a luminescence phenomenon that occurs in poly-aromatic hydrocarbons or heterocycles molecules called fluorescent molecules. It is the process in which absorption of light of a given wavelength by a fluorescent molecule is followed by the emission of light at longer wavelengths. Fluorescence, chemiluminescence and phosphorescence are examples of luminescence, which are defined based on the nature of the excited state. Fluorescence occurs when the molecule returns to the electronic ground

state, from the excited singlet state, by the emission of a photon. Phosphorescence is the emission of light from the spin forbidden transition of the electron from the triple excited state to the ground state. Chemiluminescence occurs when a chemical reaction produces an electronically excited species which emits a photon in order to reach the ground state.

Below are several principles, which are important to understand the phenomenon of fluorescence and fluorescence sensing techniques.

1.1.1. Jablonski diagram

Once a molecule has been absorbed in the form of electromagnetic, there are a number of routes by which it can return to the ground state (the statistically most common energy state for room temperature chemical species). Jablonski diagram (Figure 1.1) illustrates the processes involved in the creation of an excited electronic state by optical absorption and subsequent emission.

http://www.deltadot.com/technologies/background/flourescence/
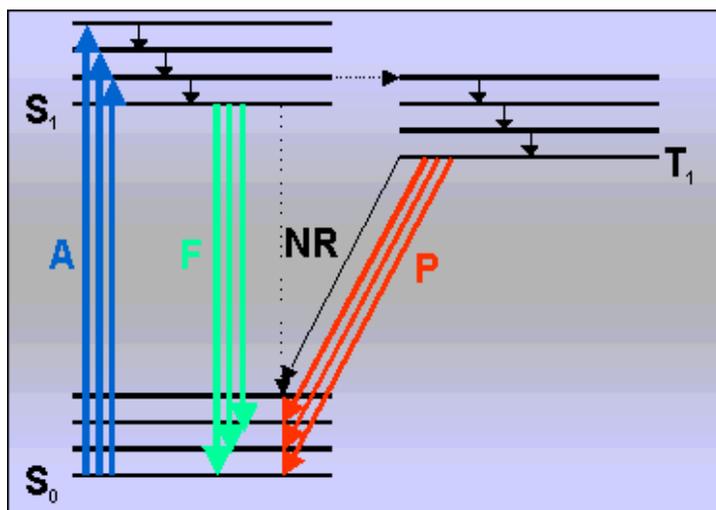
Figure 1.1. A Jablonski diagram describing radiative and non-radiative transitions following excitation. A: Absorbance; F: Fluorescence; P: Phosphorescence

$S_0, S_1, S_2,$ and S_n represent the singlet grounds of 1st, 2nd, and n^{th} electronic states. A number of vibrational energy levels exist in each of these electronic states. There are few processes occurring following the absorption of light. A fluorophore is excited to higher vibrational levels of S_1 or S_2. The molecule is then relaxed to the lowest vibrational level of S_1 through a process called internal conversion, which occurs very quickly ($<1 \times 10^{-12}$ seconds). Returning to the ground state occurs to a higher excited vibrational ground state level, which then quickly reaches thermal equilibrium. Due to energy dissipation during the excited-state lifetime, the energy of the emission photon $h\nu_{EM}$ is lower, and therefore of longer wavelength, than the excitation photon $h\nu_{EX}$. The difference in energy or wavelength represented by ($h\nu_{EX}$ – $h\nu_{EM}$) is called the Stokes shift. The Stokes shift is fundamental to the sensitivity of fluorescence techniques because it allows emission photons to be detected against a low background, isolated from excitation photons. If the photon emission occurs between states of the same spin state (e.g. $S_1 \longrightarrow S_0$), this is termed fluorescence. If the spin state of the initial and final energy levels is different (e.g. $T_1 \longrightarrow S_0$), the emission is called phosphorescence. The fluorescence lifetimes are very short; about 1×10^{-5} to 10^{-8} seconds. The phosphorescence lifetimes are longer; about 1×10^{-4} seconds to minutes or even hours.

There are three significant nonradiative deactivation processes: internal conversion (IC), intersystem crossing (ISC) and vibrational relaxation. Internal conversion is the radiationless transition between energy states of the same spin state (compare with fluorescence-a radiative process). Intersystem crossing is a radiationless transition between different spin states (compare to phosphorescence).

Vibrational relaxation, the most common of the three-for most molecules, occurs very quickly ($<1 \times 10^{-12}$ seconds). Vibrational relaxation is enhanced by physical contact of an excited molecule with other particles with which energy, in the form of vibrations and rotations, can be transferred through collisions.

1.1.2. Fluorescence quantum yield and lifetime

The fluorescence quantum yield (Q) is the ratio of the number of emitted photons to the number of absorbed photons. Substances with a large quantum yield display bright emission. Fluorescence lifetime (t_F) is the average length of time a molecule remains in its excited state. The fluorescence lifetime determines the time available for the fluorophore to interact with or diffuse in its environment.

1.1.3. Fluorescence spectra

The fluorescence process is cyclical. The same fluorophore can be repeatedly excited and detected. A single fluorophore can generate thousands of detectable photons and this is fundamental to the high sensitivity of fluorescence detection techniques. The distribution of wavelength-dependent intensity that causes fluorescence is known as the fluorescence excitation spectrum. The fluorescence emission spectrum is the distribution of wavelength-dependent intensity of emitted energy. Excitation and emission spectra depend on the chemical structure of the fluorophore and the solvent in which it is dissolved.

1. Excitation maximum
2. Stokes shift
3. Emission maximum
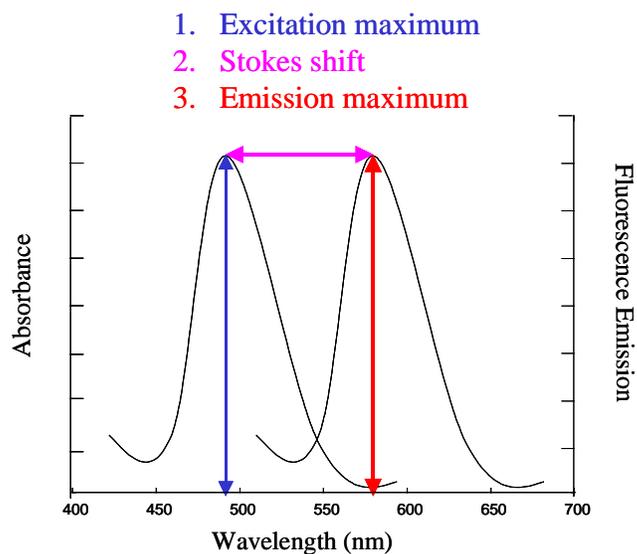
Figure 1.2. Excitation and emission spectra of a typical fluorophores

1.1.4. Fluorescence quenching

Fluorescence quenching can be defined as a bimolecular process that reduces the fluorescence quantum yield or decreases the intensity of the fluorescence emission without changing the fluorescence emission spectrum. It can result from collisional or dynamic quenching, self-quenching, static quenching, quenching by energy transfer, excited state reactions, and molecular arrangement. Collisional quenching occurs when the excited state fluorophore is deactivated upon contact with some other molecule in solution, which is called the quencher. When quenching occurs by a collisional mechanism, the quenching is an additional process that deactivates the excited state besides radiative emission. Because dynamic quenching depopulates the excited state without allowing fluorescence emission, the decrease in fluorescence intensity equates to the decrease in fluorescence lifetime. The dependence of the

emission intensity, F on quencher concentration [Q] is given by the Stern-Volmer equation:

$$F_0/F = \tau_0 / \tau = 1 + k_q\tau_0[Q] \qquad [1.1]$$

Here, F_0 and F are the intensities observed in the absence and presence of quencher. τ and τ_0 are the lifetimes in the presence and absence of quencher, respectively. k_q is the bimolecular rate constant for the dynamic reaction of the quencher with the fluorophore. The product of $k_q\tau_0$ is referred to as the Stern-Volmer constant or K_{SV}.

Fluorescence can be quenched by other mechanisms. Self-quenching or 'concentration quenching' happens when a molecule quenches its own fluorescence at high concentration. The mechanism can be through radiationless transfer of energy between identical molecules (particularly where the Stokes Shift is small), through formation of aggregates (common for large molecules such a porphyrins), or via a Stern-Volmer mechanism in solution. Common fluorescent dyes such as fluorescein and its derivatives show marked concentration quenching, both in solution and when used to label macromolecules. Static quenching occurs when an interaction between the fluorophore and quencher is involved. Static quenching can result from the formation of a ground state complex that is non-fluorescent or weakly fluorescent in the presence of quenchers. This process occurs in the ground state and does not rely on diffusion or molecular collisions. Additionally, the fluorophore may react with reactive species such as singlet oxygen and destroy its chromophoric struture. Or the fluorophore is irreversibly destroyed in the excited state under high intensity

illumination conditions. This type of quenching is called photobleaching. Photobleaching originates from the triplet-excited state, which is created from the singlet state S_1 via intersystem crossing. Another quenching process is based on resonance energy transfer (RET). This is a radiationless process where excited species transfer excitation energy to a neighbor having an absorption that overlaps the fluorophore's emission spectrum. RET is only efficient for molecules in very close proximity (typically within <10nm). It is only seen in concentrated solutions in absence of specific interactions. In addition, quenching can occur by non-molecular mechanisms, such as attenuation of the incident light by the fluorophore itself or other absorbing species. These processes do not contain molecular information, and are not of great interest.

1.1.5. Molecular information from fluorescence

The spectra of extrinsic probes are used to determine a probe's location on a macromolecule because the emission spectra are sensitive to the fluorophore's environment. A variety of small molecules or ions, such as iodide (I^-), oxygen, and acrylamide, can act as quenchers of fluorescence. They decrease the intensity of the emission. The accessibility of fluorophores to these quenchers can be used to determine the location of probes on macromolecules or the porosity of proteins and membranes to quenchers. In addition, fluorophores absorb light along a particular direction with respect to the molecular axes. The extent to which a fluorophore rotates during the excited-state lifetime determines its polarization or anisotropy. Fluorescence polarization can be used to measure the apparent volume or molecular

weight of proteins. On the other hand, RET can be used also to measure the distance between sites on macromolecules when the donor and acceptor are within the Forster distance typically in the range of 15-60 A°. The extent of donor quenching can be used to calculate the donor- to-acceptor distance in association [21].

1.2. Fluorescence Probes

Fluorescence probes can be divided into two main classes: intrinsic and extrinsic. Intrinsic fluorophores are those which occur naturally, including the aromatic amino acids, flavins, and derivatives of pyridoxal and chlorophyll. When no fluorescence or no changes in the spectral properties of the samples exists, extrinsic fluorophores are added to the sample to provide fluorescence. Examples of extrinsic fluorophores are Alexa Fluor® 488 carboxylic acid, and fluorescein-5-isothiocyanate (FITC).

a) Intrinsic or natural fluorophores

The quantum yield of a fluorophore is a function of the molecular structure. The common groups found in biological macromolecules (and their assemblies) have significant fluorescence (high enough quantum yield) including tryptophan, tyrosine, nicotinamide adenine dinucleotide reduced form (NADH), and flavin adenine dinucleotide (FAD). Intrinsic protein fluorescence originates with the aromatic amino acids such as trytophan, tyrosine, and phenylalanine. The indole groups of trytophan residues are the dominant source of UV absorbance and emission in proteins. Enzyme cofactors like NADH frequently are fluorescent. NADH (reduced form) is highly fluorescent with absorption and emission maxima at 340 and 460 nm. The oxidized form of NADH, NAD^+, is non-fluorescent. The lifetime of NADH in aqueous

solution is near 0.4 ns. Depending on the protein, NADH fluorescence can increase or decrease upon protein binding. FAD absorbs light in the visible range (at ~ 450 nm) and emits around 525 nm. Typical lifetimes for flavin mononucleotide and FDA are 4.7 and 2.3 ns. In contrast to NADH, which is highly fluorescent when bound to protein, flavo-proteins are generally non-fluorescent.

b) Extrinsic fluorophores:

It is necessary to add an external molecule, which is fluorescent (an extrinsic fluorescent probe) to the system of interest; or to obtain fluorescence from samples that have little or no intrinsic fluorescence (i.e. lipids). There are two common types of extrinsic fluorescent probes: intensity- based sensing probes, and wavelength-ratiometric probes.

- <u>Intensity- based sensing probes</u>: Fluorescent probes display changes in intensity and do not display spectral shifts. Changes in the fluorescence intensity are typically due to different quantum yields of the free and complexed forms, rather than differences in the absorption spectrum. The analyte concentration [A] can be obtained from Equation 1.2.

$$[A] = K_D \{(F\text{-}F_{min}) \, / \, (Fmax \text{-} F)\} \qquad\qquad [1.2]$$

F_{min} is the fluorescence intensity when the indicator is in the free form. F_{max} is the fluorescence intensity when the indicator is totally complexed. F is the intensity when the indicator is partially complexed by the analyte. K_D is the dissociation constant. This is the critical factor in using probes, which bind specific analytes. The useful range of analyte concentrations is typically

restricted to 0.1 K_D < [A]< 10K_D. Concentrations lower than 0.1 K_D or higher than 10K_D will produce little change in the observed signal.

- Wavelength- ratiometric probes: Probes display spectral shifts in their absorption or emission spectra upon binding analytes. In these cases, the analyte concentrations can be determined from the ratio of intensities, independent of the overall probe concentration. The use of wavelength-ratiometric probes makes the measurements independent of the probe concentration, unlike intensity-based measurements.

This dissertation focuses on pH, calcium ions, and zinc ions, which are very important in neurotransmission. The significance of measuring these species at the single cell level will be discussed in later chapters. These species are naturally non fluorescent, so extrinsic intensity-based fluorophores must be used for their analysis.

1.3. Fluorescence detection techniques for single cell studies

The advantages of using fluorescence detection, rather than absorbance methods, as an analytical tool in medical testing, biotechnology, and drug discovery include higher sensitivity, and selectivity [22]. Most commonly used fluorescence techniques include flow cytometry [23] and fluorescence microscope [24]. Flow cytometry is a powerful technique for single cell analysis and high throughput screening applications. Flow cytometry allows rapid screening of individual cells and is used to individually analyze a large number of cells at the single cell level. The rate of analysis in flow cytometry can reach 10,000 cells/second. Each cell is observed once as it flows through the detection

region. This technique is not able to follow the kinetics of the cellular response because the analysis is performed in an irreversible manner. On the other hand, fluorescence microscopy is used for real time continuous observation of cells over time. A general problem in both flow cytometry and fluorescence microscopy is the lack of quantitative accuracy due to incomplete reaction between the tagging molecules and their target analytes, heterogeneous distribution of fluorophores in cells, and interferences from other cellular species.

Combined with a variety of optochemical probes and sensors, fluorescence microscopy has become a primary choice for single cell analysis despite its accuracy limitations. The development of highly sensitive and relatively inexpensive charge coupled device (CCD) cameras has led to a dramatic improvement of the accuracy and reliability of fluorescence microscopy measurements [25-29]. Furthermore, fluorescence sensors were also proposed as an alternative to microelectrodes in cellular analysis. Potential advantages of fluorescence sensors compared to microelectrodes include non-invasiveness, insensitivity to electroactive interferences, increased simplicity and sensitivity.

1.4. Fluorescence Sensors

A fluorescence bio/chemical sensor designed for single cell measurements must be highly compatible with the cellular environment, show low cytotoxicity, and high chemical stability as well as photostability. To prevent cytotoxicity upon insertion of the sensor into the cell, the sensing reagent must be isolated from the cellular environment by a biocompatible matrix barrier that is selective to the intracellular analyte. In principle, it

is possible to fabricate a sensor that contains several fluorophors and bioactive macromolecules such as enzymes, protein receptors and antibodies for multiple analyte sensing. It is also possible to incorporate ligands on the sensor that are not soluble in aqueous solution and can be used for site -specific extracellular measurements.

Cellular labeling, which is a classical fluorescence sensing technique, uses fluorescent dyes sensitive to a given analyte of interest. It provides a strong, average, fluorescent signal that can be calibrated to a specific concentration level of analyte [30-31]. The monitoring changes of the fluorescence properties provide information on the cellular responses to external stimuli. The problems with this technique are the toxicity to the cells by excessive dye loading, protein binding, and lack of site- specific information. A new experimental approach to address problems associated with whole cell fluorescence labeling has been the development and utilization of submicrometer fiber optic chemical sensors, where a fluorescent dye is immobilized at the distal end of the fiber in a polymerization matrix, to measure the level of intracellular analytes and cellular dynamics [32-34]. The miniaturization of the sensors results in at least a million-fold reduction of the sample volume and in milliseconds or less response times. Such sensors offer a great potential as they are applicable for chemical analysis in limited volume samples like single biological cells and for scanning of chemical reactions on surfaces or in small domains [35]. However, cellular analysis with a fiber optic sensor is limited to one cell at a time. In addition, the insertion of the tapered fiber optic sensor into the observed cell may still cause a physical damage to the cell membrane. Miniaturized particle-base fluorescence sensors were proposed as an alternative to microelectrodes and fiber optic sensors in cellular analysis. Potential advantages of particle based fluorescence

sensors compared to microelectrodes include non-invasiveness, insensitivity to electroactive interferences, increased simplicity and sensitivity. In these polymer particle based sensors, the sensing dyes are immobilized to the particle surface through chemical bonding or physical absorption [36-37]. The sensing dyes can be also embedded within a hydrogel particle during the polymerization [38]. The sensors can be directed into a specific region of interest in a cell to provide site-specific information. They can obtain information from a large number of cells simultaneously. The nanometric size of the sensors increases the resolution of site-specific analysis. In 1999, Kopelman et al [39] developed a new type of fluorescence nanosensor called PEBBLEs (Probes Encapsulated by Biologically Localized Embedding). In PEBBLEs, probes are embedded within a hydrogel particle during polymerization. The size of the sensor range is from 20 nm to 200 nm. The PEBBLEs show high selectivity, reversibility, and fast response time. They have been applied for intracellular pH, calcium ion, nitric oxide, and glucose measurements [40-41]. Nevertheless, these sensors have some structural problems that limit their cellular applications. The direct contact between the polymer and cells may have negative impact on cell mortality. The particles often aggregate and their analytical capability is limited by rapid photobleaching of the sensing indicators embedded in the polymer particles. The use of unilamillar phospholipid vesicles, liposomes, as fluorescence nanosensors provides a novel way to overcome the biocompatibility problem of particle based sensors. In this dissertation, the development of fluorescence liposome based sensors is described and discussed in later chapters. The latest developed sensors that are described in this dissertation are phospholipid coated sensing beads,

called lipobeads. They combine the strength of liposomes, and polymer particle based sensors.

1.4.1. Liposome-based sensors

Phospholipid vesicles, e.g. liposomes, have been used as drug-delivery vesicles in the last three decades [42-46]. This dissertation introduces for the first time the use of liposomes as nanosensors. The main advantages of liposomes based sensors include their biocompatibility, ability to effectively encapsulate hydrophilic or hydrophobic indicators and the sensitivity of their fluid-like membrane to temperature and pH.

a) Basics of liposomes

Liposomes are spherical phospholipid vesicles that form spontaneously when phospholipids are introduced to aqueous media. Upon dispersion in aqueous solution, entropic and hydrophobic effects cause phospholipids to align themselves closely in a bilayer membrane and nearly spherical emulsion, known as liposomes, which encapsulating a certain volume of the surrounding media. The bilayer membrane could also contain cholesterol and fatty acids to increase its fluidity and flexibility. The size, size distribution, and morphology of liposomes greatly depend on the method used for liposome preparation.

The morphology of liposomes is classified according to the compartmentalization of aqueous regions between bilayer shells. In unilamellar liposomes, the aqueous compartment is segregated from the external solution by

only one membranal bilayer. Unilamellar liposomes are further classified according to their size. Small unilamellar liposomes (SUV) average 100 nm in diameter while large unilamellar liposomes (LUV) are greater than 100 nm with a maximal size of up to 10 μm. In multilamellar liposomes, there is more than one bilayer surrounding each aqueous compartment. Multilamellar liposomes typically form large complex honeycomb structures that are difficult to reproduce.
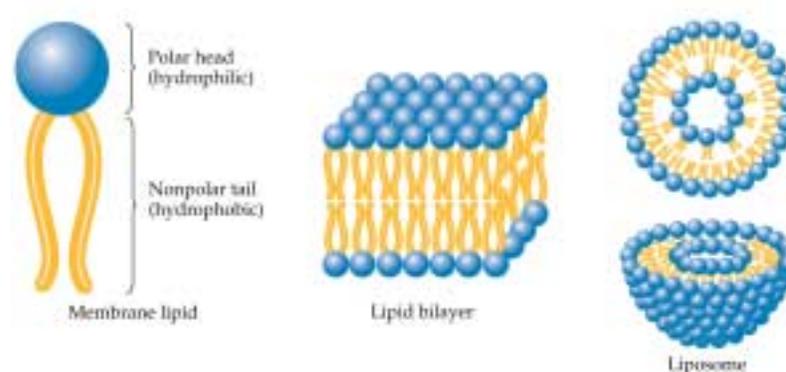
http://wps.prenhall.com/wps/media/objects/376/385232/MediaPortfolio/chapter_24/text_images/FG24_06.JPG

Figure 1.3. Lipid vesicles (Liposomes)

When introducing sensing indicators into the liposome formation process, depending on the hydrophobicity of the dyes and methods of preparation, they can be either entrapped within liposomes aqueous compartment or within the membrane. The injection method [47] is used to encapsulate hydrophilic dyes in the internal compartment of liposomes (figure 1.4a). Hydrophobic compounds and dye labeled phospholipid derivatives are incorporated into the bilayer membrane of liposomes by drying the phospholipids from an organic solvent that

already contains the hydrophobic compounds (figure 1.4b). Another preparation technique is based on dehydration and then rehydration of phospholipids in the presence of the encapsulated material. This method is primarily used to encapsulate water-soluble macromolecules or bio-conjugates, i.e. fluorescent conjugates of dextrans and proteins (figure 1.4c) [48-49]. Liposomes containing phospholipids labeled with fluorophores are prepared using the injection technique (figure 1.4d). The fluorophores in these lipsomes are attached covalently to the phospholipid headgroup or to the hydrophobic alkyl tail of the phospholipids.

(a) (b) (c) (d)
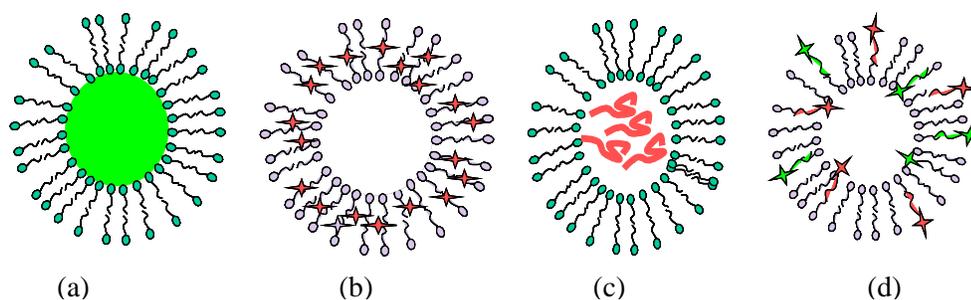
Figure 1.4 - Tailoring liposomes (a) Dyes encapsulated in the internal compartment of the liposomes.(b) Dyes encapsulated in phospholipid membrane of the liposomes (c) Dextran-conjugated dyes encapsulated in the internal compartment of the liposomes (d) Dye-DHPE as a part of the phospholipid membrane of the liposomes.

b) Characterization of liposomes

The main characterization techniques are based on light scattering, electronic and atomic force microscopy, and capillary electrophoresis. Static and dynamic light scattering measurements are used to characterize the size, size distribution, and shape of extruded vesicles under isotonic conditions [50].

Transmission electron microscopy (TEM) and atomic force microscopy (AFM) are used to determine the morphology of liposomes. While light scattering techniques provide average values of the physical characteristics of liposome suspensions, TEM and AFM provide information on individual liposomes that may or may not represent the entire liposome population. AFM imaging measurements could be conducted on untreated samples in air or in solution, avoiding all processing such as fixation, dehydration embedded sectioning, and staining required in TEM [51]. Since liposomes appear to be stable under conditions of high electric fields like the ones applied in capillary electrophoresis (CE), it is possible to use CE to obtain qualitative and quantitative information about the size to charge ratio of liposomes [52-53]. The size to charge ratio of liposomes is directly related to their mobility in the capillary when a high potential difference is applied. Since an equal distribution of charge on the liposomes is assumed, the electrophoretic distribution observed is primarily due to liposome size. The peak shape of the electropherogram is indicative of liposome size distribution and uniformity. Under normal CE conditions, liposomes produce electropherograms with a smooth broad Gaussian distribution with few spiking events.

c) Liposomes as fluorescence nanosensors

The use of unilamillar phospholipid vesicles, called liposomes, was brought to the attention of the scientific world by A.D. Bangham and his students in 1965. In liposome-based sensors, the sensing reagents are encapsulated in the

internal aqueous compartment of the liposomes and maintained their free solution properties [54]. The encapsulation of sensing reagents in liposomes increases the physical dimensions of the sensing elements, and lead to an increase in the chemical stability of the sensor. Unlike in dextran conjugation, it is expected that the encapsulated fluorescent molecules would maintain their free solution properties, including high emission quantum yield and sensing capability. The long-term stability of fluorescence-based sensing liposomes with respect to leakage of internalized compounds has been a concern because the permeability of the liposome bilayer membrane is strongly temperature dependent. A transition temperature, Tc, can be identified for phospholipids used to make the liposomes [55]. The transition temperature is defined as the point below which assembled liposomes display a gel like phase, and the bilayer permeability is minimized, reducing the effects of leakage. Close to the transition temperature, the liposome bilayer membrane will adopt a more permeable fluid like structure, and leakage rates of encapsulated materials may increase. It is therefore important to select phospholipids with a Tc, which is clearly below or clearly above room temperature. The use of unilamellar phospholipid vesicles, liposomes, as fluorescent nanosensors for pH and calcium ion levels in aqueous solutions has been demonstrated [56-57]. The sensing reagents were encapsulated in the internal aqueous compartment of the liposomes and maintained their free solution properties. This improves the response characteristics of the sensors since matrix effects common to covalent bonding or entrapment of sensing reagents in solid-state supports are eliminated.

Liposomes have been used to target specific cells or tissues using ligand-receptor strategies [58]. The same process that enables for site-specific sensing strategy becomes an obstacle when applying these fluorescence based liposome sensors to site-specific extracellular sensing approaches. When incubated with cells in vitro, liposomes are expectedly seen to deliver the encapsulated fluorescent dyes into the cytoplasm in a diffuse and non- specific manner [59]. The result of this approach is an averaged analytical signal (with an associated decrease in resolution) for each cell, which is similar to that seen in cellular labeling technique. Clearly, for effective, site-specific cellular analysis, a fluorescent sensor needs to have a sensing geometry, which can maintain mechanical stability and can preclude damage to the cell upon uptake or attachment.

1.4.2. Lipobead based sensors

While the sensing properties of liposome-based sensors were adequate for aqueous solution measurements, their application as cellular sensors was impaired by high leakage rate and poor chemical stability in the cellular environment. Although the liposome based sensors failed in cellular analysis, the advantages of applying the phospholipid membrane in sensor design are still remarkable and recognize. Hence, phospholipid coated particles, called lipobeads, are the latest developed sensors. Lipobeads combine the strength of liposomes, dye-labeled sensing beads and PEBBLEs.

a) Basics of lipobeads

      Particle-based fluorescence nanosensors named lipobeads have hydrophobic indicator embedded in the lipid-like layer. This will not only improve the chemical and photostability of these nanosensors, but also to enable hydrophobic indicators to be used for sensing applications in aqueous samples. These lipobeads (shown in Figure 1.5) have a polystyrene core and phospholipid shell. The phospholipid membrane formed on the surface of the polystyrene core is biocompatible and provides protection for the sensing fluorophore from the surrounding environment. The new hybrid sensing particles with cell-like lipid bilayer surface similar to natural cells combine complementary advantages of liposomes and polymeric beads. Overall, in the lipobead model, the binding force is the affinity between the hydrophobic phospholipid tail and the hydrophobic surface of polystyrene beads in a hydrophilic environment. The hydrophobic sensing indicator is also bound onto the beads surface and trapped in between the bead surface and the phospholipid tail through the physical stability. The technique is highly versatile since it is possible to incorporate biomolecules such as antibodies, enzymes, and receptors into the membrane of the particles and use them as selective and sensitive biosensors.

From Liposome model

To Lipobead model

Phospholipid membrane with
hydrophobic dye trapped
within the membrane

Polystyrene bead,
hydrophobic surface
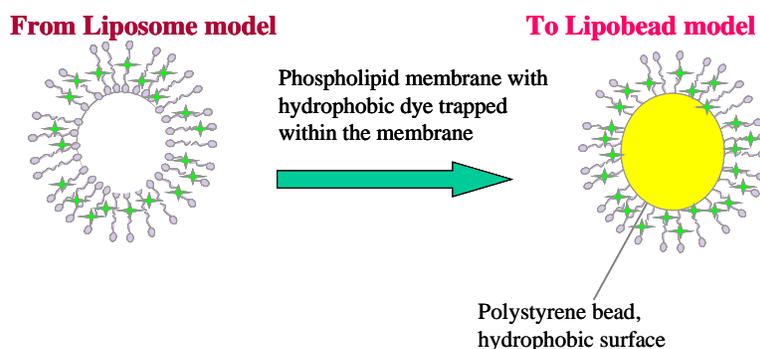
Figure 1.5. Lipobead model

b) Characterization of lipobeads

The main characterization techniques used in my studies are transmission electron microscopy (TEM), fluorescence spectroscopy, and digital fluorescence imaging microscopy. TEM is used to determine the morphology of lipobeads. Fluorescence spectroscopy and digital fluorescence imaging microscope are used for studying analytical properties of lipobead - based sensors.

c) Lipobead based sensors

These unique particles could be applied to measure the level of intracellular/extracellular ion analytes in a non-invasive manner with high reproducibility, selectivity and sensitivity. It is possible to incorporate biomolecules such as antibodies, enzymes and receptors into the membrane of the particles and use them as selective and sensitive biosensors. These lipobeads combine the mechanical stability of polymer particles with the biocompatibility of liposomes. Furthermore, hydrophobic indicators could be immobilized in the membrane of the lipobeads and used to measure the level of ion analytes in

aqueous and cellular samples. The phospholipid membrane formed on the surface of the polystyrene core is biocompatible and provides protection for the sensing fluorophore from the surrounding environment. Lipobeads offer greater flexibility in fluorescent indicator selection compared to previously prepared particle based fluorescence sensors. Particularly, water insoluble hydrophobic indicators could be employed successfully in sensing applications of lipobeads because of the amphiphylic nature of the phospholipid membrane. Lipobeads with pH, zinc ion and glucose measurement capabilities were fabricated and applied for intracellular measurements in murine macrophages and for extracellular measurements in rat cortical neurons [60-62].

1.5. Neurons

Neurons were chosen to evaluate the development of fluorescence based liposome and lipobead sensors. The brain is a collection of about 100 billion interconnected neurons. Neurons are cells specialized for the conduction and transmission of electrical signals in the nervous system. They communicate with each other thousands of times a second through an electrochemical process. Although other cells die and are replaced, many neurons are never replaced when they die.

1.5.1. Morphology of neurons
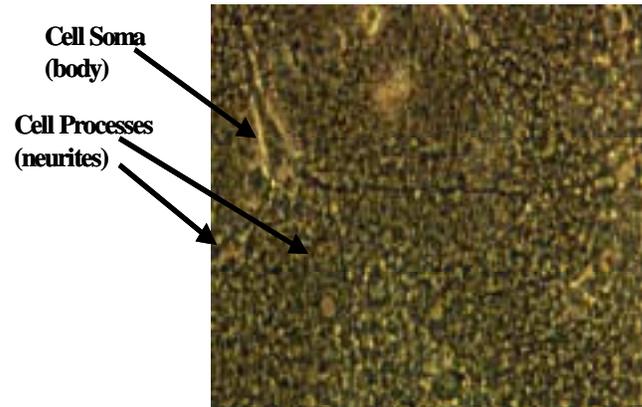
Figure 1.6. Neuron morphology

A neuron (shown in figure 1.6) has a soma, which is body of the cell. The soma houses the nucleus, in which the neuron's main genetic information can be found. Neurons have specialized projections called dendrites and axons. Dendrites bring information to the cell body and axons take information away from the cell body. The presynaptic terminal is where the nerve cell transmits a signal.

1.5.2.Synapse

Functional communication between neurons occurs at specialized junctions called synapses. The most common types of synapses in the brain use chemicals (more specifically, neurotransmitters, which are the messengers that travel between one brain cell and another) to communicate between neurons. These are called *chemical synapses*. The synapse is a small gap separating 2 neurons. The synapse consists of a presynaptic ending that contains neurotransmitters, mitochondria and other cell organelles, a postsynaptic ending that contains receptor sites for

neurotransmitters, and the synaptic cleft which is a space between the presynaptic and postsynaptic endings.

1.5.3. Nerve cell communication

Neurons communicate through a process called synaptic neurotransmission. Neurons make use of one of two basic forms of synaptic transmission: electrical and chemical. Synaptic communication in the brain relies mainly on chemical mechanism. Chemical transmission is central to understanding brain function and behavior. There is no structural continuity between the presynaptic and postsynaptic cells. They are separated by synaptic clefts, which are usually 20-40 nm wide. As a result, chemical synaptic transmission depends on the release of neurotransmitters from presynaptic neurons.

1.6. pH regulation

pH regulation in the nervous system and other tissues is considered to be an important homeostatic process. In response to neuronal activity and cell activation by neurotransmitters, other messengers or receptor agonists, intra- and extracellular pH can rapidly and transiently change just like the activity of other ions. Changes in pH affect many processes in the nervous systems including neuronal excitability, synaptic transmission, and intercellular coupling via gap junctions.

1.6.1. Intracellular pH (pH$_i$) regulation

pH$_i$ is an important modulator of metabolic processes. Regulation of intracellular pH (pH$_i$) can compromise the four processes: (1) cytosolic H^+ buffering, (2) H^+ sequestration into intracellular organelles, (3) release or metabolic production of H^+,

and (4) transmembrane movement of acid/base equivalents [63]. pH_i may play an important role in neurotransmission process. pH_i may 1) influence the uptake of some neurotransmitters in synaptic vesicles [64], 2) regulate synaptic vesicle endocytosis [65], and 3) possibly influence some of the multiple protein-protein interactions involved in the process of synaptic vesicle exocytosis [66].

1.6.2. Extracellular pH (pH_0) transients

Electrical stimulation induces extracellular pH changes accompany with alkaline-acid shifts in most nervous systems. Synaptic activation of glutamate and the recombinant type-A γ- aminobutyric acid ($GABA_A$) receptor channels leads to a fast extracellular alkaline transient. The extracellular alkalinizations are likely to emerge several minutes after a brief electrically evoked depolarization. This alkalinization changes are associated with a net efflux of bicarbonate ions across $GABA_A$ receptor channels [67-68]. The stimulus induced extracellular acidification may involve metabolic increases in the production of CO_2 and/or lactate. The proton accumulating intercellularly may be extruded via the Na^+/H^+ co-transporter, or buffered by HCO_3^- shifts across HCO_3^- transporters. These ion movements cause extracellular acidification down to pH 6.8 [69]. Lactate could leak out of the neurons across large holes induced within the cell membrane during depolarization or through non-ionic diffusion [70].

1.6.3. Model of H$^+$-dynamics during neuronal activity

The nervous system is composed of neurons and glial cells, and the extracellular spaces. The extracellular spaces are a channel like network between the cells that establishes the medium for communication between the cells. Intra- and extracellular pH changes in the nervous system may occur as follows:

Step1: Neuronal activity leads to the release of a neurotransmitter and K$^+$ during action potential.

Step2: The release of neurotransmitters leads to the opening of neurotransmitter-gated ion channels, allowing the flux of acid/base equivalents along their electrochemical gradient into and out both neurons and glial cells.

Step3: In neurons, the increase in intracellular Ca^{2+}, either due to Ca^{2+} influx via voltage-gated and transmitter gated ion channels, or due to Ca^{2+} release from intracellular stores, may lead to a secondary increase in intracellular protons by activating Ca^{2+}/H$^+$ - ATPase. Each of these processes and the uptake of neurotransmitters cause extracellular alkalinization and intracellular acidification of neurons [71].

The enzyme carbonic anhydrase is a key enzyme in these processes and necessary for the fast buffering of the extracellular alkalinization by supporting acid/base equivalents from the CO$_2$/HCO$_3^-$ buffer system. The acid accumulated in the neurons is transported out of the neurons via the Na$^+$/H$^+$ exchanger due to CO$_2$ diffusion contributing to the transient acidification of the extracellular spaces [72].

1.7. Zinc and its significant functions in the brain

Zinc is one of the most abundant transition elements in the body and essential for neuronal activities. The zinc concentration in the brain increases with growth after birth and is maintained constant in the adult brain. Approximately 90% of the total brain zinc is zinc metalloproteins. The rest is in the presynaptic vesicles and histochemically reactive [73]. Extracellular free zinc is absent in the extracellular fluid, with the estimated concentration being below the detection limits for most analytical methods (<1pM). The appropriate concentration of zinc ion in storage (releasable) pools is about 3-30 mM in presynaptic vesicles [74]. The distribution of zinc in the brain is non-uniform and its concentration is highest in the hippocampus, amyglada, and cortex [75]. It is very important for neurons to maintain cellular zinc content within a very narrow window. Low zinc levels inhibit cell growth and division and can lead to cell death. High zinc levels are toxic.

1.7.1. Zinc containing neurons

Zinc containing neurons are defined as neurons that sequester weakly bound (histochemically stainable) zinc in the vesicles of their presynaptic boutons [76]. It is critically important to note here that there is no histochemically reactive zinc anywhere but in the secretory vesicles of zinc containing boutons (or en route in their axons). Any staining for zinc in the nucleus, or dendrites of a neuron in the brain indicates either cell injury or artifact [77]. In a brain, the only neurons that have vesicular zinc are glutamatergic. Not all glutamatergic neurons are zinc-containing neurons, but all zinc- containing neurons are glutamatergic [78]. As a general rule, the

large neuron, long axon systems of the brain are non-zinc containing. Specific examples include all of the first order sensory fibers of the cranial nerves, ascending sensory pathways, and essentially all of the long fiber pathways descending from the cerebral cortex to the brain stem or spinal cord [79].

1.7.2. Zinc movement in the brain

The life cycle of zinc containing synaptic vesicles include storage, release and reuptake. There are several routes of entry and exit for zinc in neurons. These pathways include (1) presynaptic release along with glutamate when synaptic vesicles empty their contents into the synaptic cleft [80], (2) voltage-gated L-type Ca^{2+} channels and glutamate –gated channels that provide an entry route when cells are depolarized and that mediate extracellular zinc toxicity [81], and (3) a plasma membrane transporter potentially present in all neurons important for cellular zinc homeostasis [82]. The least understood of these pathways in term of mechanisms is the transporter pathway.

a) Zinc transport in the brain and uptake into neurons

Zinc transports into the brain via both the blood brain and blood cerebrospinal fluid barriers. Zn^{2+} can enter neurons by multiple routes. First, Zn^{2+} can permeate through NMDA receptor-gated Ca^{2+} channels. Secondly, Zn^{2+} can also entry through voltage gated Ca^{2+} channels. The third route of entry may be via transporter-mediated exchange with intracellular Na^{+}. A fourth route of neuronal Zn^{2+} entry is through the Ca^{2+} permeable channels gated by certain subtypes of α-

amino-3-hydroxy-5-methyl-4-isoxazolepropionic acid (AMPA) or kainite receptors [83-84].

b) Zinc release and reuptake from zinc containing neuron terminals

Zn^{2+} is released from presynaptic terminals of neurons upon depolarization and calcium dependent [85]. It is presumed that zinc release is the result of synaptic vesicle fusion with the presynaptic membrane. The release of zinc from the presynaptic vesicles of zinc containing neurons probably occurs via the mechanism of exocytosis. Zinc can be taken up back into neurons to replenish depleted synaptic vesicle stores [86]. Synaptic Zn^{2+} can be released and achieve 100 µM concentrations in the extracellular space. It is also widely assumed that the synaptic zinc that is released from boutons actually enters the extracellular fluid as Zn^{2+} [87]. The release is completely blocked at room temperature (20-26^0C) and vigorous in the range of normal rat body temperature (37-39^0C) [88]. Essentially there is nothing known about the kinetics of zinc release. Zn^{2+} is potentially neurotoxic to neurons. The movement of Zn^{2+} from pre- to postsynaptic neurons contributes to the selective nerve cell injury observed in conditions of epilepsy, and brain trauma. The modulation of zinc release and reuptake is potentially important therapeutic strategy for protection against neurotoxicity [89].

There is a hypothesis that the pH gradient across the plasma membrane, in particular its direction being opposite to the direction of Zn^{2+} flux, is a principal determinant of the extent of Zn^{2+} transport. After electrical stimulation of neurons and Zn^{2+} depletion, pH dependent plasma membrane Zn^{2+} transport can supply Zn^{2+} directly

to subcellular compartments and effect a rapid refilling of these stores in the presence of an inwardly directed Zn^{2+} gradients and physiological pH values [90]. The plasma membrane pH dependent pathway may provide the means for release Zn^{2+} to reenter neurons under physiological and non- physiological conditions. A better understanding of plasma membrane pH dependent Zn^{2+} transport will help to clarification of the role of Zn^{2+} playing in selective neuronal death after brain injury.

In this dissertation, the development of fluorescence based sensors for single neuron cell analysis is described. Research accomplishments include the development of fluorescence based liposomes and lipobeads as sensors for calcium, zinc ion and pH in primary rat cortical neurons. The development of these sensors, their advantages and limitations, and their applications in monitoring the effect of physiological and non-physiological simulation conditions and kinetic studies of biological processes at single neuron cell levels are discussed more details in the following chapters.

CHAPTER TWO: EXPERIMENTAL

This chapter describes the experimental methods and instruments used to carry out the studies that are summarized in this dissertation. Specific technical and experimental details are described in related chapters.

2.1. Materials and Reagents

1-ml syringes were purchased from Becton Dickinson. Hamilton syringes and Corning glass cover slips used for microscopy (12x12 mm) were purchased from Fisher Scientific. Dimyristoylphosphatidylcholine (DMPC) was purchased from Avanti Polar Lipids. Cholesterol and dihexadecyl phosphate were purchased from Aldrich. Sephadex G-100 was purchased from Sigma. Alexa-labeled calmodulin (Calmodulin-Alexa-Fluor 488) was purchased from Molecular Probes. Polystyrene particles (mean diameter: 1.6 μm, -/+ 0.5%) were purchased from Bangs Laboratories, Inc. (Fishers, IN) in powder form. $ZnCl_2$ (AR), N- (6-methoxy-8-quinolyl)-p-toluenesulfonamide (TSQ) was obtained from Molecular Probes, In. (Eugene, OR). *N-* (fluorescein-5-thiocarbamoyl)- 1,2-dihexadecanoyl-*sn*-glycero-3- phosphoethanolamine, triethylammonium salt (fluorescein DHPE) was purchased from Molecular Probes, Inc. (Eugene, OR). Poly-L-lysine was purchased from Sigma. Lab-Tek II chambered coverglass used for microscopy and pH buffers were purchased from Fisher Scientific. Aqueous solutions were prepared with 18

MΩ deionized water purification system (Barnstead Thermolyne Nanopure). Dihexadecyl phosphate (DP), cholesterol, and spectroscopic grade ethanol were purchased from Aldrich Chemical Company (Milwaukee, WI). Succinyl-concanavalin A (SuccCon A) and cytosine (beta)-D-arabinofuranoside (AraC) were purchased from Sigma (St. Louis, MO). Sodium hydroxide and hexane were purchased from EM Sciences and used without further purification. Spectroscopic grade ethanol was purchased from Aldrich Chemical Company (Milwaukee, WI). All aqueous preparations were made using nano-pure distilled water. 22 x 22 mm glass coverslips were obtained from Fisher Scientific, Pittsburgh, PA. Matrigel was purchased from Becton Dickinson, Bedford, MA. 35mm diameter petri plates were from Falcon-Becton Dickinson Labware, Franklin Lakes, NJ. Essential medium without phenol red containing 10 % horse serum was from Gibco, Grand Island, NY. All reagents were used as received without further purificaton.

2.2. Protocols and Procedures

2.2.1. Sol-gel for immobilization of liposomes to glass slides or vials

(a) 4-morpholino-propanesulfonic acid (MOPS) solution

- 0.0419 g MOPS + 0.0584 g NaCl + 10 ml PBS buffer pH 7.4

(b) The acidic sol

- 15.25 ml TMOS (tetramethylorthosilicate) + 3.35 ml of distilled water+ 0.22 ml of 0.04 M HCl

Mix (a) and (b) together (1:1 v/v), chill in an ice bath for 20 minutes in order to retard gelation, rapidly mix with the liposome solution, and place on a microscope

slide or into a vial sealed with a cap until the mixture becomes clear, colorless and monophasic.

2.2.2. Sephadex column solution and Sephadex column separation using a microcolumn centrifuge technique

a) Sephadex column preparation

Sephadex G50: 10 g of G50 + 120 ml of distilled water + 0.9 g NaCl

Sephadex G100: 10 g of G100 + 175 ml of distilled water + 1.575 g NaCl

- Allow the sephadex solution to swell overnight at room temperature before preparing the sephadex columns for separation.

- Place glasswool at the bottom of an empty 1-ml syringe.

- Pipette 1 ml of Sephadex suspension into the syringe to form a plug above the glasswool.

- Centrifuge the Sephadex containing syringe in a low-speed centrifuge at 2000 rpm for 5 minutes to form a dry solid Sephadex column, absent of cracks or voids.

- Further add Sephadex solution and centrifuge the syringe until a plug of dried Sephadex of ~8-9 cm long formed in the column.

- Make sure the Sephadex columns have no cracks or void and are not wet before separation process.

b) Microcolumn centrifuge technique for separation
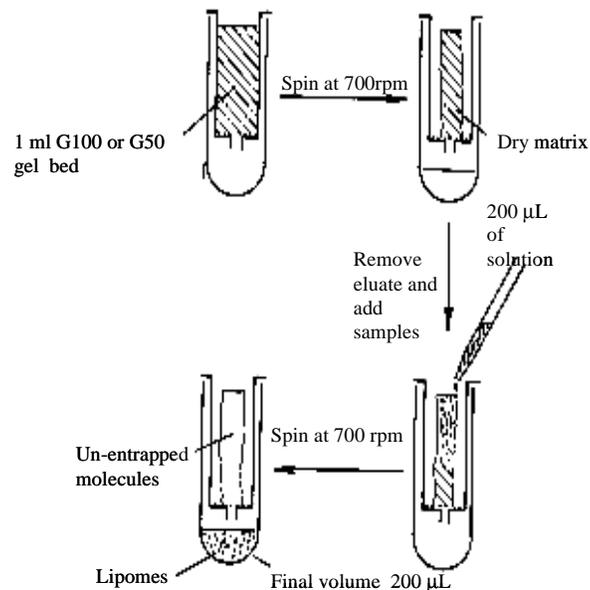
Figure 2.1. A schematic of a microcolumn centrifuge technique

- Add 200 µL of the liposome solution drop wise to the top of the column and the syringe is placed in a 10 mm diameter, 13 cm height centrifuge tube.

- Centrifuge the syringe, inserted into the tube, at 700 rmp for 15 minutes (Fisher, Model Marathon 8K).

- Collect the liposomes in the centrifuge tube while the Sephadex column retains the free bio-conjugate molecules.

- Repeat the process at least three times to ensure complete washing of free bio-conjugates from the liposome solution with a new Sephadex column every time. The washed liposome solution is stored at room temperature in a light tight environment.

2.3.3. Preparation of adhesive slides

- Immerse the slides in 70% ethanol/water for 15 minutes.

- Air dry slides or place in 60^0C oven for 2 minutes.

- Place slides in poly-L-lysine solution (1ml/ml) for 4 hours.

- Drain slides and leave at room temperature overnight or dry in 60^0C oven for 15 minutes.

2.2.4. Locke's buffer for neuron cell culture

- 154 mM NaCl, 5.6 mM KCl, 3.6 mM $NaHCO_3$, 2.3 mM $CaCl_2.2H_2O$, 5.6 mM glucose, 1.2 mM $MgCl_2.6H_2O$, and 5 mM HEPES (pH 7.4).

2.2.5. Phospholipid cocktail for liposome and lipobead coating

- 50 mM lipid stock solution prepared with a 5:4:1 molar ratio of DMPC, cholesterol, and DP in chloroform, store at -20^0C until used.

2.3. Liposome preparation (details of each method will be described in chapter 3 and chapter 4)

a) **Injection method**

- Dry 40 µl aliquot of phospholipid cocktail in a glass tube under N_2 stream gas until all the chloroform is removed.

- Add 40µl dry 2-propanol with rapid vortexing.

- Inject this solution while vortexing into 1 ml of hydrophilic fluorescence dye or probe, which will be encapsulated inside liposomes. The optimal concentration of dye encapsulating is determined by a concentration dependence of the fluorescence intensity of the dye prior to the liposome

preparation. The fluorescence intensity of each individual dye encapsulating liposome depends on the number of dye molecules encapsulated in the liposomes, which in turn depends on the concentration of the dye in the liposome preparation solution.

- In the case of hydrophobic dye, the dye will be added into the phospholipid cocktail and dry under nitrogen gas stream all together. The mixture will be reconstituted in dry 2-propanol and then added in 1 ml of a suitable buffer for liposome formation as steps shown above.

b)   Dehydration-Rehydration method for bio-conjugates encapsulating liposomes

- 50 mM lipid stock solution prepared with a 5:4:1 molar ratio of DMPC, cholesterol, and DP in 0.5 mM EGTA/ 5.0 mM Tris-HCl buffer (pH 7.0), and dispersed using probe sonicator (Fisher Model 60 Sonic Dismembrator) at 40W for 2 minutes. Filtrate undisolved components with 0.4μm (in diameter) membrane filter.

- Add 200 μL aliquot of the phospholipid stock solution to 200 μL of bio-conjugated solution in 0.5 mM EGTA/ 5.0 mM Tris-HCl buffer (pH 7.0). This may be scaled up as desired.

- Dry the solution at room temperature using a rotating flask evaporator under nitrogen to form a film of phospholipids and bio-conjugate at the bottom of the flask.

- Re-hydrate the film by adding 0.4 ml of 0.5 mM EGTA/ 5.0 mM Tris-HCl buffer (pH 7.0) to form liposomes with embedded bio-conjugate molecules in their bilayer membrane.

- Incubate the re-hydrated sample for 1 hour at room temperature to form small unilamellar vesicles.

- Separate the bio-conjugate containing liposomes from the excess, unbound molecules remaining in the solution by using a micro-column centrifuge technique described above.

2.4. Lipobead preparation (specific details will be described in chapter 5 and chapter 6)

- Disperse 4 mg of polystyrene microsphere in 100 μl of ethanol/hexane (1:1 v/v). Sonicate for 15 minutes using a 47 KHz Bransonic sonicator.

- Sonicate the mixture of 250 μl of phospholipid cocktail solution and 10-100 μl of hydrophobic encapsulated dye with an optimal concentration for 15 minutes using a 47 KHz Bransonic sonicator.

- Add both the particle suspension and the mixture of phospholipid and dye together. Sonicate for another 15 minutes using a 47 KHz Bransonic sonicator.

- Incubate the whole mixture at room temperature for 2 hours.

- Dry the whole mixture overnight under nitrogen gas stream.

- Add 1 ml of phosphate buffer pH 7.0 to the dried suspension, and sonicate for 15 minutes with a 47 KHz Bransonic sonicator.

- Incubate the suspension for 2 hours to allow the indicator and the phospholipid molecules to absorb onto the surface of the particles.

- Remove unbound dye molecules, liposomes, and unbound particles by centrifugation at least 3 times at 2000 rpm/ 15 minutes each time. The dye-coated lipobeads are collected at the bottom of the glass centrifuge while the supernatant and unbound beads/ dye molecules are discarded.

- Store in a glass test tube at room temperature until used.

2.5. Preparation of Rat Cortical Neurons and Cell Culture Plates

Primary cultures of rat cortical neurons were prepared and grown in neuronal culture medium [91-92] by dissecting cerebral cortices from embryonic day 15 rats. The cells were cultured in neuronal culture media consisting of 10% fetal calf and 10% horse serum. The cells were then treated with cytosine arabinoside to control astrocyte proliferation. For the current studies, cells were grown on glass slides (22x22x1 mm) coated with Matrigel (Collaborative Research). For these experiments, cells were plated onto 22 x 22 mm glass coverslips, which had been coated with a 1:2.5 dilution of matrigel. Matrigel was diluted with minimum essential medium. All coverslips were placed, one each, in 35mm diameter petri plates and maintained at 37° C in humidified, 5% CO_2 incubators (Gallenkamp- Sanyo Scientific, Chicago, IL). Cells were allowed to attach to coverslips for one day in vitro (DIV), and then each petri dish was flooded with2 ml of cell culture media. At 4 DIV, 10^{-5} M cytosine (beta)-D-arabinofuranoside was added to cultures to minimize astrocyte proliferation. AraC was removed at 8 DIV, at which time cells were switched to minimum essential medium without phenol red

containing 10 % horse serum. Experiments were carried out on coverslips with cells after 12 DIV.

2.6. Adhering the lectin-coated lipobeads to cell culture

- Add 200 µl of prepared lipobeads into the 2 ml of culture media already in the petri dish or coverglass slide chamber for 2 hours.

- Wash extensively but very gently (5 exchanges of 2 ml volume) with Locke's solution pH 7.4, lacking $MgCl_2$.

- Take images immediately after washing.

2.7. Data Analysis

2.7.1. Spectrofluorometer Measurements

The fluorescence spectra are obtained by holding the excitation wavelength constant and scanning through the emission wavelengths. The spectrum is the intensity vs. wavelength. The obtained highest peak intensity in the emission spectrum is used to construct the calibration curve. The instrument does the background correction automatically. The data is saved as a text file and transferred to Microsoft Excel to reproduce the spectrum for presentation purposes. The data analysis and manipulation capabilities of Excel are used to obtain ratiometric spectra and averaged spectra. Each spectrum that is presented in this dissertation was the average of three replicate spectra unless otherwise noted.

2.7.2. Digital Fluorescence Imaging Microscopy Measurements

a) Spectral analysis

A CCD camera collects the fluorescence spectrum of the particles. The spectrum is presented as intensity vs. number of pixels, which ranges from 1 to 1024 in our CCD camera. Given the properties of the 500 nm blazed grating with 600 grooves/inch the spectral range of the spectrograph under these conditions is about 300 nm. This implies that the spectral resolution of our CCD spectral measurements is about 0.3 nm, which is more than sufficient to resolve our solution-typical broad emission peaks. The instrument does the background correction automatically. The obtained highest peak intensity is used to construct calibration curves of signal against concentration. The data is saved in a unique Roper scientific software format that could be converted to ASCII format and from it to a Microsoft Excel format for further data treatment. The CCD camera used for spectral imaging is a 16 bit resolution camera with gray levels range from 0 to 65536 (2^{16}). Each spectrum that is presented in this dissertation is the average of three spectra unless otherwise noted.

b) Digital imaging analysis

Analysis of our digital fluorescence images involves measuring the average fluorescence intensity of the observed particles either by manually selecting the particles for analysis or by using the automatic features of our digital imaging analysis software image Pro plus. The software enables the automatic selection of multiple particles and analyze their size and average intensity. It is also equipped with image enhancement features such as contrast adjustment and

edge emphasis. The signal (S) to noise (N) ratio in a fluorescence image is determined as following

$$S/N = (S_{sample} - S_{background}) / 2 \, \sigma_{background})$$

Where S_{sample} is the average signal of a fluorescent particle

$S_{background}$ is the average signal of the background near the observed particle

$\sigma_{Background}$ is the signal deviation of the background

The digital images are saved as TIFF files or GIF files. TIFF and GIF are general formats that enable us to further enhance the image quality using a photo enhancement software like Adobe Photoshop 5.

c) Error analysis

Error bars indicate signal variation between 3 fluorescence intensity measurements of an observed particles or a group of particles. The results are presented as the average reading +/- the standard deviation from the average. The standard deviation (SD) is the square root of the variance, which is a measure of how spread out a distribution is. It is computed as the average squared deviation of each number from its mean.

2.7.3. Sources of Errors:

Various experimental parameters contribute to uncertainties in the analysis. First, the fluctuation of the light source used in the work, mercury lamp. It is absolutely essential that the light source energy output remains constant and stable during the measurement, as the fluorescence intensity is directly proportional to the exciting intensity. In reality, the lamp is not stable. There is up to 5% fluctuation in the energy output during our experiments. Secondly, heterogeneities in the field of illumination

and in the samples contribute greatly to the large variation observed in the kinetic data. Inconsistencies in sample handling also contribute to the experimental uncertainties. Overall, +/- 5% in digital imaging microscopy experiments is reasonable using currently available state of the art microscopy systems. This will definitely improve in the future with the expected replacement of mercury burners with highly stable diode lasers as excitation sources and further improvement in automation of sample handling.

2.8. Spectrofluorometer

A schematic diagram of the spectrofluorimeter is shown in Figure 2.2. Excitation and emission spectra, the spectral response of fluorescence probes and sensors in solution to analytes of interest were conducted using a PTI model QM-1 spectrofluorimeter (PTI, Quantamaster, Ontario, Canada) as shown in Figure 2.2.

In general, light from the source passes through the excitation monochromator, which selectively passes a narrow band of the spectrum centered about the excitation wavelength. This light hits the sample. Light given off by the sample is collected and passed through the emission monochromator, which selects a narrow band of the spectrum for the detector to look at. For an emission scan, the excitation monochromator is fixed at a wavelength absorbed by the sample, and the emission monochromator is scanned to obtain the spectrum of light emitted by the sample. For an excitation scan, the emission monochromator is fixed at a wavelength emitted by the sample and the excitation monochromator is scanned to obtain a spectrum of the light, which excites

fluorescence in the sample. Often an excitation spectrum looks just like an absorption spectrum.
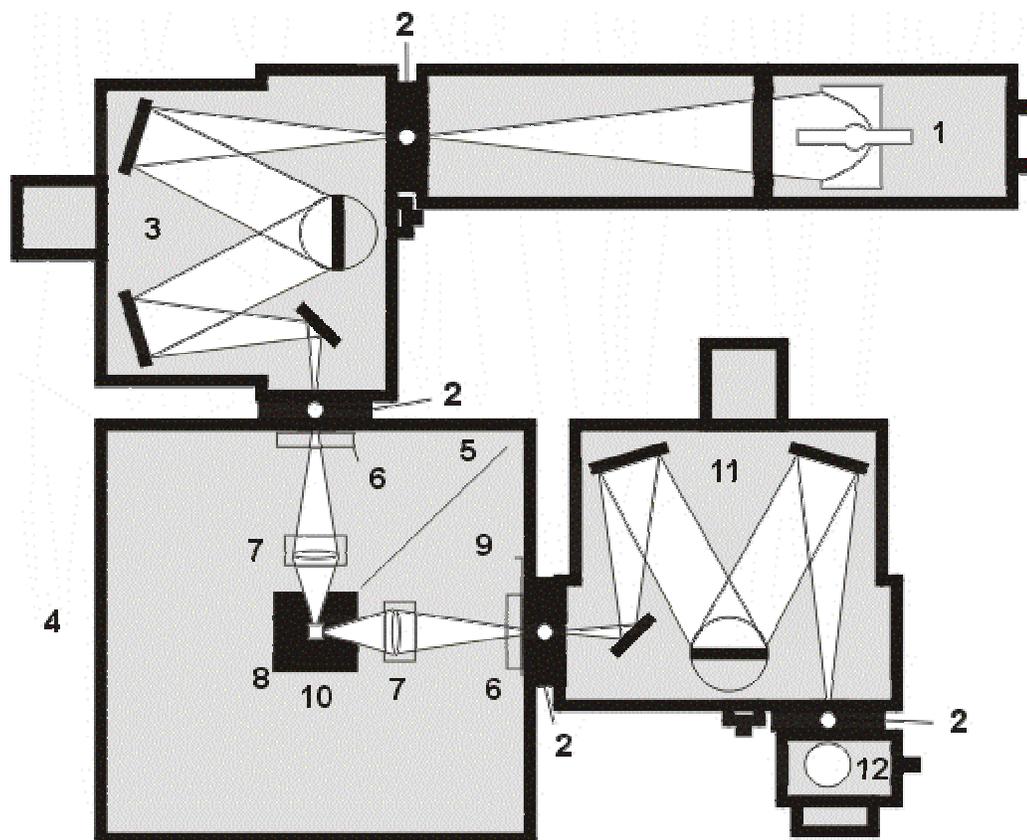
Figure 2.2. Schematic diagram of the PTI spectrofluorometer used in our studies

1.Lamp housing; 2. Adjustable slits; 3.Excitation Monochromator; 4. Sample compartment; 5. Baffle; 6. Filter holders; 7. Excitation/emission optics; 8. Cuvette holder; 9. Emission port shutter; 10. Peltier cooling & temperature probe; 11 Emission Monochromator; 12. PMT detector.

For general- purpose applications, the instrument has a xenon lamp as the source of excitation light. It is equipped with two monochromators, which are used to select the excitation and emission wavelengths, and are monitorized to allow automatic scanning of wavelengths. The fluorescence is detected with photomultiplier tubes and quantified with the appropriate electronic devices. The excitation spectrum represents the relative

emission of the fluorophore at a fixed emission wavelength at each excitation wavelength. The emission spectrum represents the photon emission rate or power emitted at each wavelength when the excitation wavelength is fixed, over a wavelength interval determined by the slit widths and dispersion of the emission monochromator. For most fluorophores, the quantum yield and emission spectra are independent of excitation wavelength.

There are four characteristics for an ideal optical components: 1) The light source must yield a constant photon output at all wavelength; 2) The monochromator must pass photons of all wavelength with equal efficiency; 3) The monochromator efficiency must be independent of polarization; 4) The detector (photomultiplier tube) must detect photons of all wavelengths with equal efficiency. Unfortunately, light sources, monochromators, and PMT with such ideal characteristics are not available. As a result, there is always a compromise to select components, and to correct for the non-ideal response of the instrument. The general characteristics of individual components of a spectrofluorometer are described as follow, along with the reasons for choosing specific components.

a) Light source

A 75 W high- pressure xenon (Xe) lamp is used as the excitation light source. The lamp provides a relatively continuously light output from 250 to 700 nm. The lamp consists of two electrodes sealed under high pressure in a quartz glass bulb containing Xe. Xe arc lamps emit a continuum of light as a result of the recombination of electrons with ionized Xe atoms. These ions are generated by

collisions of Xe atoms with electrons, which flow across the arc. Complete separation of the electrons from the atoms yields the continuous emission. Xe lamps are contained within specially designed housing as shown in Figure 2.2.
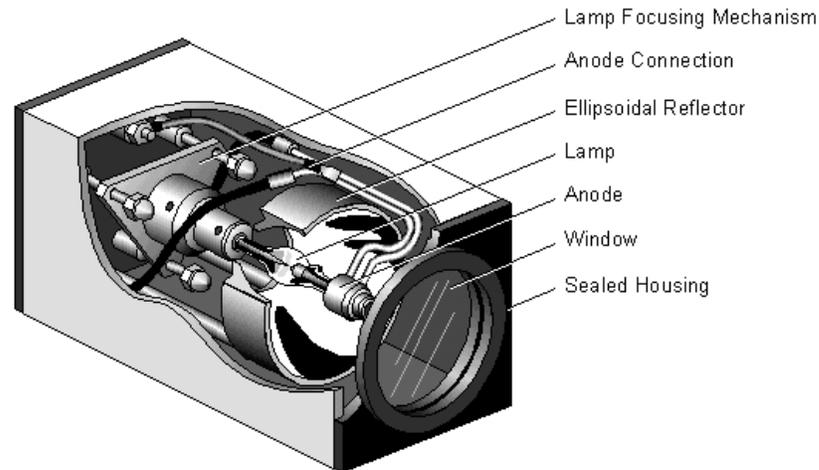
Figure 2.3. The arc lamp housing

The housing protects the user from the lamp and from its intense optical output because of the high-pressure gas in xenon lamps, and their extreme brightness. The house also serves to direct air over the lamp and remove excess heat and ozone. Another role of the housing is to collect and illuminate the lamp output, which can be focused into the entrance slit of the monochromotor.

b) Monochromator

A monochromator (as shown in Figure 2.4) is a wavelength selector. All monochromators contain the following component parts: an entrance slit, a collimating lens, a dispersing device (usually a prism or a grating), a focusing lens, and an exit slit. Polychromatic radiation (radiation of more than one wavelength)

enters the monochromator through the entrance slit. The beam is collimated, and then strikes the dispersing element at an angle. The beam is split into its component wavelengths by the grating or prism. By moving the dispersing element or the exit slit, radiation of only a particular wavelength leaves the monochromator through the exit slit. Excitation and emission wavelength selection in this system is composed of two monochromators, one for exicitation and one for emission. The monochromators are autocalibrated and are under computer control for scanning and positioning.
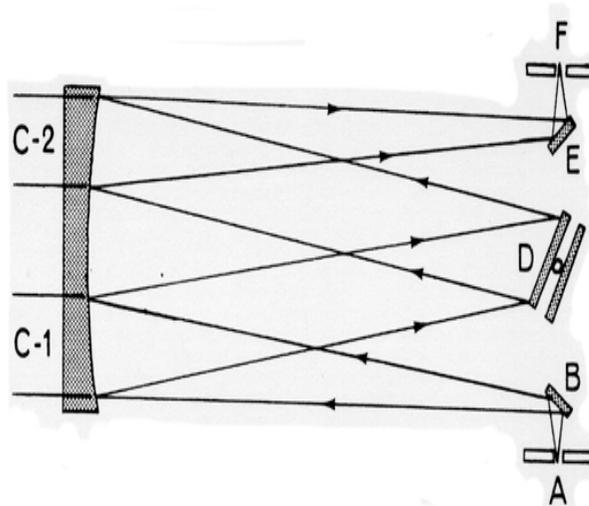
http://www.phys.virginia.edu/classes/318/atom_spec/atom_spec.html

Figure 2.4. A typical monochromator design: A = Entrance slit; B = Mirror; C1 = Collimating mirror; C2 = Focusing mirror; D = Grating; E = Mirror; F = Exit slit

c) Photomultiplier tube (PMT) detector

Photomultiplier tubes (PMTS) (shown in Figure 2.5) are designed to convert photons to an electrical signal.
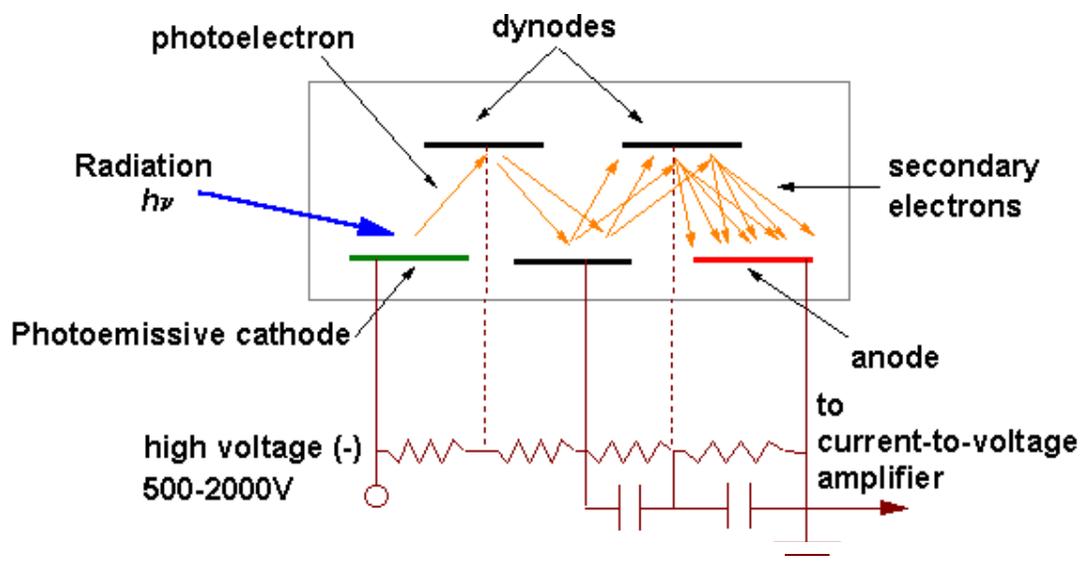
Figure 2.5. Schematic of a photomultiplier tube (PMT)

They have a high internal gain and are very sensitive light detectors for low intensity applications. They consist of a photocathode, a series of dynodes, and an anode in an evacuated glass enclosure. A photocathode is a mixture of alkali metals, which make the PMTS sensitive to photons throughout the visible region of the electromagnetic spectrum. When a photon of sufficient energy strikes the photocathode, it ejects a photoelectron due to the photoelectric effect. The photocathode is at a high negative voltage from –500 to –1500 volts. The photoelectron is accelerated towards to the first dynode. Upon the photon encounter, the first dynode emits several photoelectrons, which are attracted to the second dynote. Additional electrons are generated at each dynode due to successive photoelectric effects. As a result of each dynode the photons encounter, 10^5 to 10^7

electrons are created for each photoelectron ejected from the initial photocathode. This effectively drives the photons consecutively from the first dynode to another and finally to the anode. The amplified signal is finally collected at the last anode where it can be measured and interpreted. The overall amplification depends on the number of dynodes and the accelerating potential difference between the electrodes.

2.9. Digital Fluorescence Imaging Microscopy System

The detection system used for fluorescence measurements of the fluorescence probes and sensors in single cell is shown in Figure 2.6. The system consists of an inverted fluorescence microscope (Olympus IX 70) equipped with three detection ports. The major components are excitation light source, wavelength selection devices, objective and grating, and a charge- coupled -device (CCD).
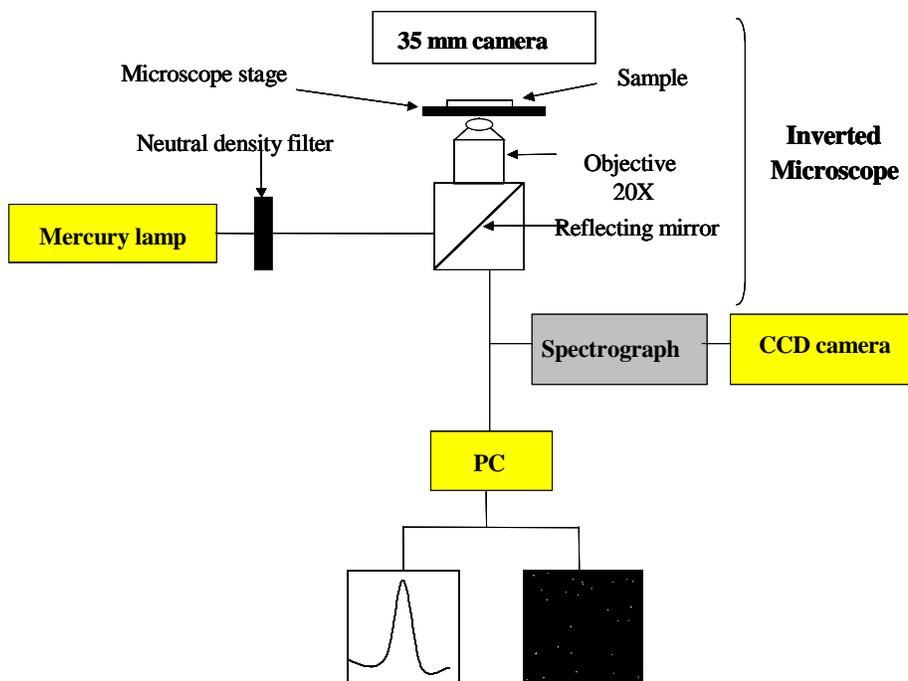
Figure 2.6. Digital fluorescence imaging microscopy system

a) Excitation light source

To generate enough excitation light intensity to furnish emission capable of detection, powerful light sources are needed, usually arc (burner) lamps. A100W mercury (shown in Figure 2.7a) consists of two electrodes sealed under high pressure in a quartz glass envelope, which also contains mercury. It is used as the light source to evaluate free fluorescence probe sensing and phospholipid coated particle based sensing techniques. Mercury burners have a life of 200 hours. When the burners reach their rated lifetime, the spectral emissions may change and the quartz envelope weakens. The mercury burners do not provide even intensity across the spectrum from ultraviolet to infrared (Figure 2.7b). The intensity of the mercury burner is expended in the near ultraviolet, with peaks of intensity at 313, 334, 365, 406, 435, 546, and 578 nanometers. At other wavelengths of visible light, the intensity is steady but not nearly so bright, but still usable for blue excitation.

(a)   (b)

http://www.olympusmicro.com/primer/techniques/fluorescence/fluorosources.html
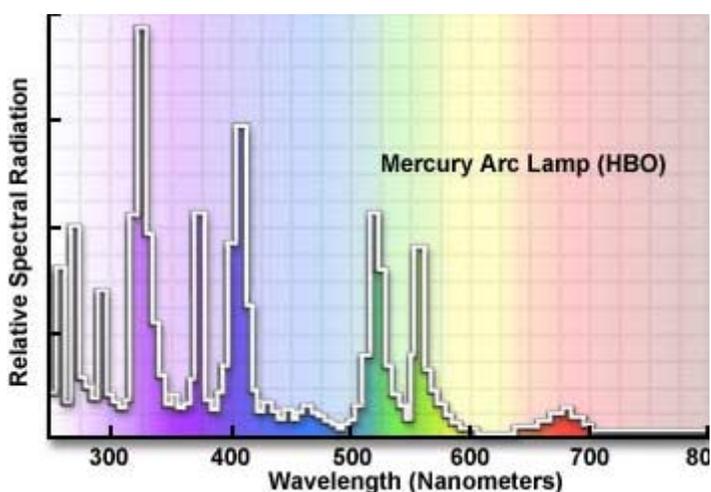
Figure 2.7. a) Mercury arc lamp; b) Mercury arc lamp UV and visible emission spectrum

The separation of excitation and emission wavelengths is achieved by the proper selection of filters to block or pass specific wavelengths of the spectrum. Optical filters are commonly used to select a certain part of the light for transmission, while preventing the rest of the light from passing through. Proper selection of filters is the key to successful fluorescence microscopy. There are three filters: exciter filters, barrier filters and dichromatic beamsplitters (dichroic mirrors) that are usually combined to produce a filter cube as illustrated in Figure 2.8.

Exciter filters permit only selected wavelengths from the illuminator to pass through on the way toward the specimen. Barrier filters (or emission filters) are used to suppress or block (absorb) the excitation wavelengths and permit only selected emission wavelengths to pass toward the eye or other detector. Dichromatic beamsplitters (dichroic mirrors) efficiently reflect excitation wavelengths and pass emission wavelengths. They are used in reflected light fluorescence illuminators and are positioned in the light path after the exciter filter but before the barrier filter.

http://www.olympusmicro.com/primer/techniques/fluorescence/filters.html
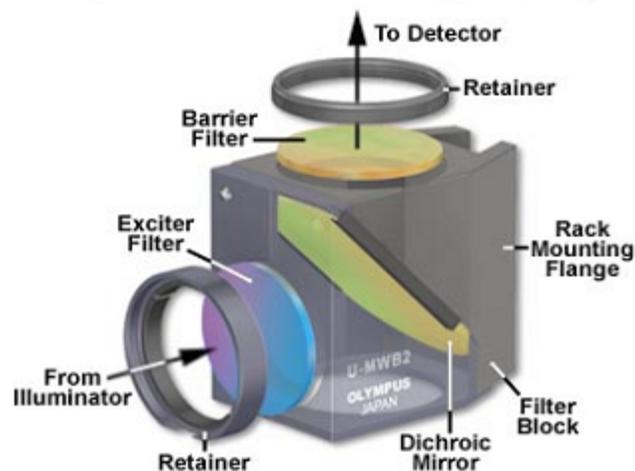
Figure 2.8. A fluorescence filter cube

b) Objectives and grating

After going through the emission filter, the fluorescence from the specimen is collected by a 20X or 40X objective with a numerical aperture 0.5 or 0.9. The signal is then reflected to the detector directly to obtain images, or dispersed by a spectrograph and detected to obtain a spectrum. The spectrograph is 150mm 3 mirror-spectrograph (Acton Research Inc.) equipped with a 600 groves/mm grating blazed at an optimum wavelength of 500nm.

c) Charge-coupled devices (CCD)

http://www.olympusmicro.com/primer/digitalimaging/concepts/ccdanatomy.html
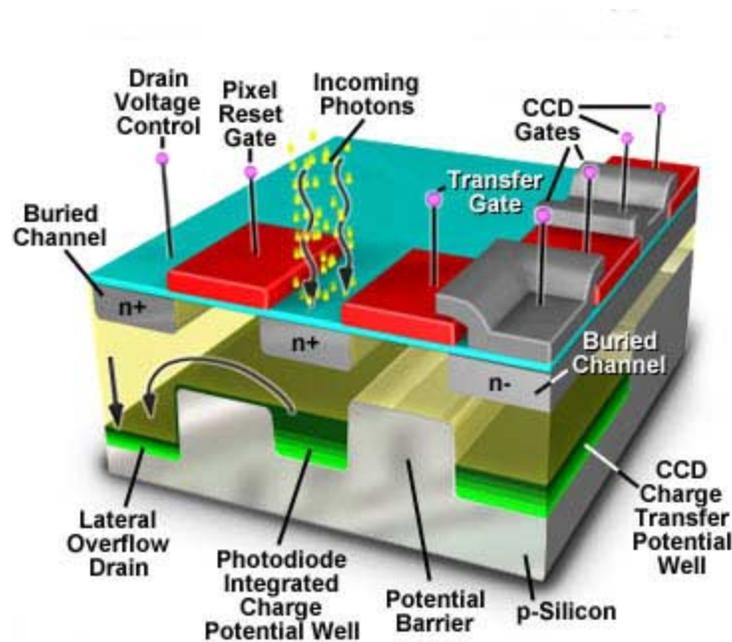
Figure 2.9. Schematic diagram of a charge-coupled device (CCD)

Charge-coupled devices (CCDs) shown in Figure 2.9 are silicon-based integrated circuits consisting of a dense matrix of photodiodes that operate by converting light energy in the form of photons into an electronic charge. Electrons

generated by the interaction of photons with silicon atoms are stored in a potential well and can subsequently be transferred across the chip through registers and output to an amplifier that reads out the quantity of accumulated charge. The charge accumulation is proportional to the total light exposure. The charge at each pixel point can be read out when desired to obtain a two dimensional image. The most common CCD designs have a series of gate elements that subdivide each pixel into thirds by three potential wells oriented in a horizontal row. Each photodiode potential well is capable of holding a number of electrons that determines the upper limit of the dynamic range of the CCD.

There are three commonly used CCD designs: the full-frame CCD, the interline transfer CCD, and the frame transfer CCD. Full-frame charge-coupled devices (CCDs) feature high-density pixel arrays, which are capable of producing high- resolution digital images. After photons composing, the image is collected by the pixel elements and converted into electrical potential. The CCD undergoes readout by shifting rows of image information in a parallel fashion, one row at a time, to the serial shift register. The serial register then sequentially shifts each row of image information to an output amplifier as a serial data stream. All integrated charge must be clocked out of the serial register before the next parallel line of image data can be transferred to the horizontal array. The entire process is repeated until all rows of image data have been directed to the output amplifier and off the chip to an analog-to-digital signal converter integrated circuit. The image in a digital format is constructed and the final photograph or photomicrograph is formed. Full-frame CCD architecture has a 100 percent fill factor. The entire pixel array is used to detect

incoming photons during exposure to the object being imaged. Full frame CCDs typically have square pixel dimensions to avoid image distortion and are fabricated with pixel sizes ranging from 7 to 24 microns in arrays containing up to 6 million pixels. A mechanical shutter or synchronized strobe illumination scheme must be used to prevent smearing for most exposure periods.

Frame-transfer CCDs have a design similar to full-frame CCDs. These devices have a parallel shift register that is divided into two separate areas, called the image and storage arrays. During the period in which the parallel storage array is being read, the image array is busy integrating charge for the next image frame. A major advantage of this architecture is the ability of the frame-transfer device to operate without a shutter or synchronized strobe, allowing for an increase in device speed and faster frame rates.

Interline- CCDs are composed of a hybrid structure incorporating a separate photodiode and an associated parallel readout CCD storage region into each pixel element. The functions of these two regions are isolated by a metallic mask structure placed over the light shielded parallel readout CCD elements. Major advantage of this architecture is the ability of the interline transfer device to operate without a shutter or synchronized strobe, allowing for an increase in device speed and faster frame rates.

In this work, a high performance frame transfer CCD (Roper Scientific, model 256 HB) with a 512x512 pixel arrays is used in order to increase the sensitivity of the imaging system. A computer is employed for data acquisition. The Princeton

Instrument software WinSpec 1.4.3 is used for spectra data analysis. The Roper Scientific software Winview 3.2 is used for image analysis.

CHAPTER THREE: OPTOCHEMICAL SENSING BY

IMMOBILIZING FLUOROPHORE-ENCAPSULATING

LIPOSOMES IN SOL-GEL THIN FILMS

3.1. Introduction

Immobilization of sensing reagents in the host matrix of optochemical sensors greatly affects their stability.   In general, covalent immobilization of the sensing reagent to the support is the preferred method since it eliminates leaking of the dye molecules from the host matrix [93-94].   However, the sensing reagent must have an appropriate functional group suitable for covalent immobilization.   Furthermore, functionalization of the sensing dye or covalent immobilization itself may alter the structural and spectral properties of the sensing reagent and lead to a loss of analyte response. While physical immobilization of the sensing reagent to the sensing support prevents these problems, it may result in dye leaking, which decreases the stability of the sensor [95].   Several research groups have recently reported the physical immobilization of dextran-fluorophore conjugates instead of free fluorescent molecules as sensing reagents in fluorescence-based sensors [96-98]. Conjugation of the fluorophores to high molecular weight dextran (70,000 Da) increases the molecular size of the sensing reagent, thus minimizes the rate of dye leaking of the sensing dye from the supportive matrix [99]. However, similar to covalent immobilization, the sensing dye must have a functional group suitable for

conjugation with dextran.   Furthermore, recent reports indicate that covalent attachment of fluorophores to dextran chains decreases their emission quantum yield [99-100].

The use of fluorescent dye encapsulating liposomes for nano-scale sensing of pH and molecular oxygen in aqueous media [101-102] has been reported in our research laboratory. These vesicles self-assemble when mono-dispersed phospholipids are introduced to an aqueous medium due to the hydrophobic nature of the aliphatic hydrocarbon chain and the hydrophilic nature of the polar head group [103-104]. The self-assembly results in an internalized volume of water, which may contain one or more water-soluble compounds (dyes, biological material, etc.). The long-term stability of fluorescence-based sensing liposomes with respect to leakage of internalized compounds has been a concern because the permeability of the liposome bilayer membrane is strongly temperature dependent. A transition temperature, Tc, can be identified for phospholipids used to make the liposomes [105]. The transition temperature is defined as the point below which assembled liposomes display a gel like phase, and the bilayer permeability is minimized, reducing the effects of leakage. Close to the transition temperature, the liposome bilayer membrane will adopt a more permeable fluid like structure, and leakage rates of encapsulated materials may increase. It is therefore important to select phospholipids with a Tc, which is clearly below or clearly above room temperature.

In this chapter, a new approach for immobilizing fluorescent reagents in a sensing support is presented.   The fluorophores are encapsulated in the internal compartment of liposomes that are entrapped in a sol-gel film. Sol-gel films have been used extensively as supporting matrices for fluorescence sensors [106-109]. Some advantages associated with sol-gel supports include high mechanical and chemical stability, lack of spectral interference, minimal quenching of fluorescence reagents and ease of fabrication.   Leaking of

macromolecules from sol gel films is minimal [110-111]. However, the leakage rate of hydrophilic fluorescence dyes from sol-gel films is significant. For example, Brennan et al. have recently used the fluorescence of tryptophan to probe the environment and reaction kinetics within protein-doped sol-gel-derived glass monoliths [112]. They have measured the leaking rate of the protein monellin and the fluorescence dye N-acetyltryptophanamide (NATA) from sol-gel monoliths. For wet-aged sol-gel monoliths, complete leakage of the fluorophore occurred over a period of 8 hours. For dry-aged monoliths, 30% of the NATA leaked over 8 hours. No leakage of protein molecules from either dry or wet-aged sol-gel monoliths has been observed.

Fluorescent liposomes have frequently been used to amplify the signals in fluorescence immunoassays [113-116]. The effect of insoluble compounds on the phospholipid transition temperature has also been used to detect anesthetics [117]. In a recent study, Yamanaka et al. immobilized dye labeled liposomes in a sol-gel support and used the sol gel films for heavy metal ion sensing [118]. In this work, liposomes were used as miniaturized containers for fluorescent sensing reagents as an alternative to covalent conjugation of the fluorescence molecules to phospholipid membranes or to dextran chains. The encapsulation of sensing reagents in liposomes increases the physical dimensions of the sensing elements, and lead to an increase in the chemical stability of the sensor. Unlike in dextran conjugation, it is expected that the encapsulated fluorescent molecules would maintain their free solution properties, including high emission quantum yield and sensing capability. The objective of this study is to evaluate the analytical properties of this new sensing geometry in aqueous solution. The fluorescein derivative carboxyfluorescein is used as a pH-sensing reagent as it is easily encapsulated in liposomes, displays high quantum efficiency, and a wide dynamic range over the physiological

pH range. These characteristics make it ideal for determinations of encapsulation efficiency, leakage rate and pH sensitivity.

3.2. Specific Experimental and Technical Details

a) The detection systems

The detection systems used to measure the fluorescence of the pH responsive solgel films in aqueous solution are the digital fluorescence imaging microscope, fluorometer, and transmission electron microscope (TEM). The fluorescence of the pH sensitive liposomes is collected by a 20X microscope objective with N.A. = 0.5. A 480 nm narrow band excitation filter, a 500-nm dichroic mirror, and a 515-nm long pass emission filter are used to ensure spectral imaging purity. Typically, an exposure time of 100 mseconds is used for image collection. TEM images of the dye encapsulating liposomes are obtained using a Zeiss-10C TEM microscope. A staining technique using 0.5% uranyl acetate is applied to observe the liposomes.

b) Preparation of carboxyfluorescein-encapsulating liposomes

A 40μl aliquot of the phospholipid cocktail is dried under nitrogen in a glass vial until all the chloroform is removed. The sample is immediately reconstituted in 50 μl of dry isopropanol with rapid vortexing. To prepare carboxyfluorescein- encapsulating liposomes, the reconstituted phospholipid mixture is added to 1 ml of a 1 mM 6-carboxyfluorescein aqueous solution at pH 7.4. The solution is then vortexed for 1 minute to form carboxyfluorescein-encapsulating liposomes. Liposomes that are larger than 100 nm are removed by passing the liposome sample back and forth several times using an

extrusion device through a 100 nm pore size polycarbonate membrane (Avanti Polar Lipids, Inc.). All reagent transfers during the preparation of the liposomes are made with a Hamilton glass syringe. The small size of the liposomes (<100 nm) is verified by transmission electron microscopy (TEM) and dynamic light scattering (DLS) measurements.

A microcolumn centrifuge technique, previously described by Fry et. al. [119] is used to separate the dye encapsulating liposomes from the excess unencapsulated free dye remaining in the liposome solution. A Sephadex G-50 column is used for this separation. To prepare the column, 10 grams of Sephadex G-50 are allowed to swell overnight in 120 ml of 0.9% NaCl solution. Glass wool is placed at the bottom of an empty 1-ml tuberculin syringe. A volume of 1-ml Sephadex solution is pipetted into the syringe to form a plug above the glass wool. The Sephadex containing syringe is then centrifuged in a low speed centrifuge (Adams Dynac) at 2,000 rpm for 3 minutes to form a dry solid Sephadex column, absent of cracks or voids. Sephadex solution is added and the syringe is again centrifuged until a plug of dry Sephadex of about 7 cm long is formed in the column. To remove the free dye from the liposomes, 200 μl of the stock liposome solution is added dropwise to the top of the column and the syringe is placed in a 10 mm diameter, 13 cm height centrifuge tube. The syringe, inserted into the tube, is centrifuged at 2,000 rpm for 4 minutes. The liposomes are collected in the centrifuge tube while the Sephadex column retains the free dye. The process is repeated at least three times to ensure complete washing of free dye from the liposomes solution. The washed liposome solution is sealed and stored in a light free environment at room temperature.

c) Preparation of a sol-gel thin film containing carboxyfluorescein encapsulating liposomes

Sol-gel thin films were prepared as described elsewhere [108]. Briefly, sols are prepared by sonicating a mixture of tetramethylorthosilicate (TMOS), water and 0.1 N HCl in a ratio of 4.5:1.4:0.1 (v/v/v) for 2 hours until the mixture becomes clear, colorless and monophasic. The solution is then stored at -20^0C for 7 days to ensure complete hydrolysis of unreacted TMOS. Then, 0.5 ml of TMOS, 0.7 ml of MOPS buffer at pH 7.2 and 50 uL of washed carboxyfluorescein encapsulating liposomes are rapidly mixed and placed on a microscope slide or in a sealed vial until gelation occurs.

3.3. Results and Discussion

3.3.1. pH sensitivity of sol-gel films containing carboxyfluorescein-encapsulating liposomes

As previously mentioned, carboxyfluorescein encapsulating liposomes are immobilized in micrometer thick sol-gel films. Photographs of sol-gel films containing carboxyfluorescein- encapsulating liposomes are shown in Fig. 3.1. Fig. 3.1a shows a sol-gel film containing a small number of fluorescent liposomes. Individual liposomes can be clearly seen, indicating that the liposomes maintain their structural integrity when immobilized in the sol-gel support. Fig. 3.1b shows a sol-gel film with a liposome density that is typically used in our pH measurements. The fluorescence spectra of this pH responsive film in aqueous solutions of pH 5, 6, 7 and 8 are shown in Fig. 3.2a. A ratiometric method is used to determine the pH of analyte samples of unknown pH. The fluorescence response is expressed as I (490) / I (440) where I (490) and I (440) are the

peak fluorescence intensities at 525 nm when the excitation wavelengths are 490 nm and 440 nm respectively. The pH of analyte samples is determined by converting the fluorescence of carboxyfluorescein to proton activity, which is approximately equal to proton concentration according to the following expression:

$$[H^+] = K_a \times [(R_{max} - R)/(R - R_{min})] \times [F_{base440} / F_{acid440}] \tag{1}$$

K_a, the acid dissociation constant, is 316 nM (pKa = 6.5) [115], R is the fluorescence response of the sensor when excited at 490 and 440 nm, and when the emission is measured at 525 nm, R_{max} is the ratio I_{490}/I_{440} when the fluorescence intensity at 525 nm reaches its maximum at pH 9, and R_{min} is the ratio I_{490}/I_{440} when the fluorescence intensity at 525 nm reaches its minimum at pH 4. Eq. (1) is derived from acid dissociation equation.

$$pH = pK_a - \log \{[(R_{max} - R) / (R - R_{min})] \times [F_{base440} / F_{acid440}]\} \tag{2}$$

$F_{base440}/F_{acid440}$ is the ratio of the fluorescence signals at 525 nm with an excitation wavelength of 440 nm under the conditions used to determine R_{max} (pH 9) and R_{min} (pH 4). Since the excitation wavelength of 440 nm is the isosbestic point of carboxyfluorescein, the fluorescence intensity of the sensor is relatively insensitive to pH changes from pH 4 to pH 9 when the sensor is excited at this wavelength. In these measurements, $F_{base440}/F_{acid440}$ is found to be 0.97 ± 0.02. As a close approximation for the ratiometric method it is possible to calculate the pH based on the following expression:

$$pH = pK_a - \log [(R_{max} - R) / (R - R_{min})] \tag{3}$$

A calibration curve describing the pH dependence of the ratio $(R_{max} - R) / (R - R_{min})$ of the liposome containing sol-gel pH sensor in standard samples is shown in Fig. 3.2b.

Data points obtained from standard solutions are shown as filled circles while pH data points calculated using Eq. (3) are shown as unfilled circles. Up to 5% variation between the calculated pH and the actual pH, as measured with a pH meter, is typically observed. In agreement with pH dependent fluorescence measurements of carboxyfluorescein solutions, the dynamic range of the sensor is between pH 6 and pH 7.5.

The employment of a ratiometric approach greatly improves the precision of the pH measurements over fluorescence intensity based measurements. The ratio I (490)/I (440) is unaffected by dye photobleaching, dye leaking, and fluctuations in the intensity of the light source and signal collection geometry. Consequently, the sensor shows higher long-term stability compared to fluorescence intensity based sensors. The sensor is highly reproducible. Each data point in the calibration curve is the average of 5 consecutive measurements with a variation of about 3%.

(a)   (b)
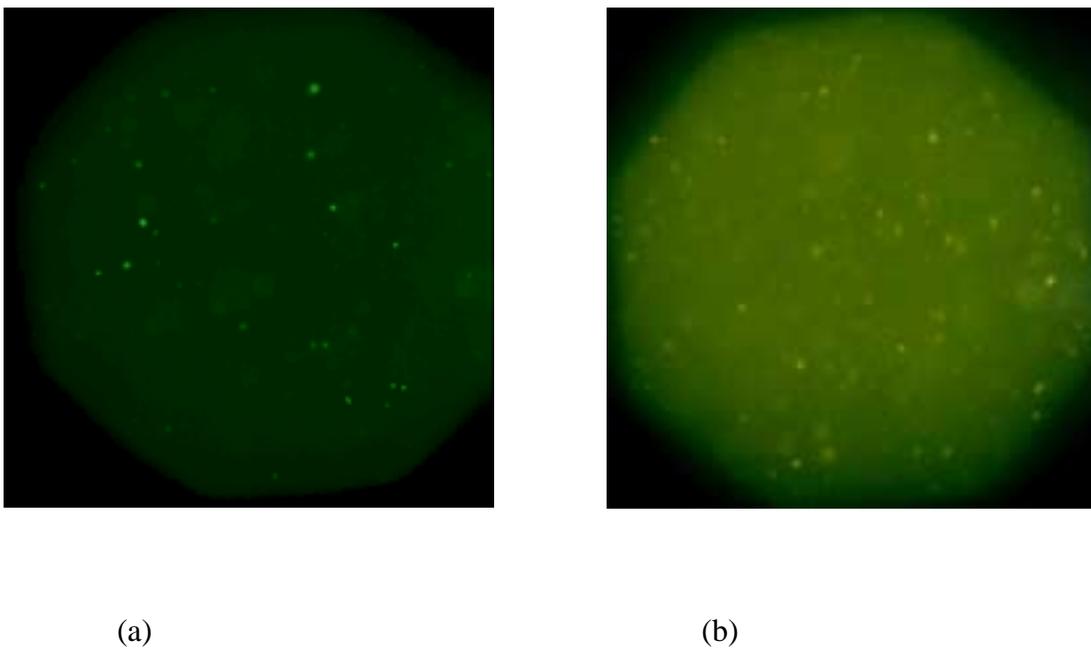
Figure 3.1. Photographs of fluorescent liposomes immobilized in a sol-gel thin film: (a) A film containing a low density of liposomes. Individual liposomes can be seen indicating that the liposomes maintain their structural integrity when immobilized in the gel; (b) A photograph of a liposome containing sol-gel film of a typical liposome density used for our pH sensing measurements.
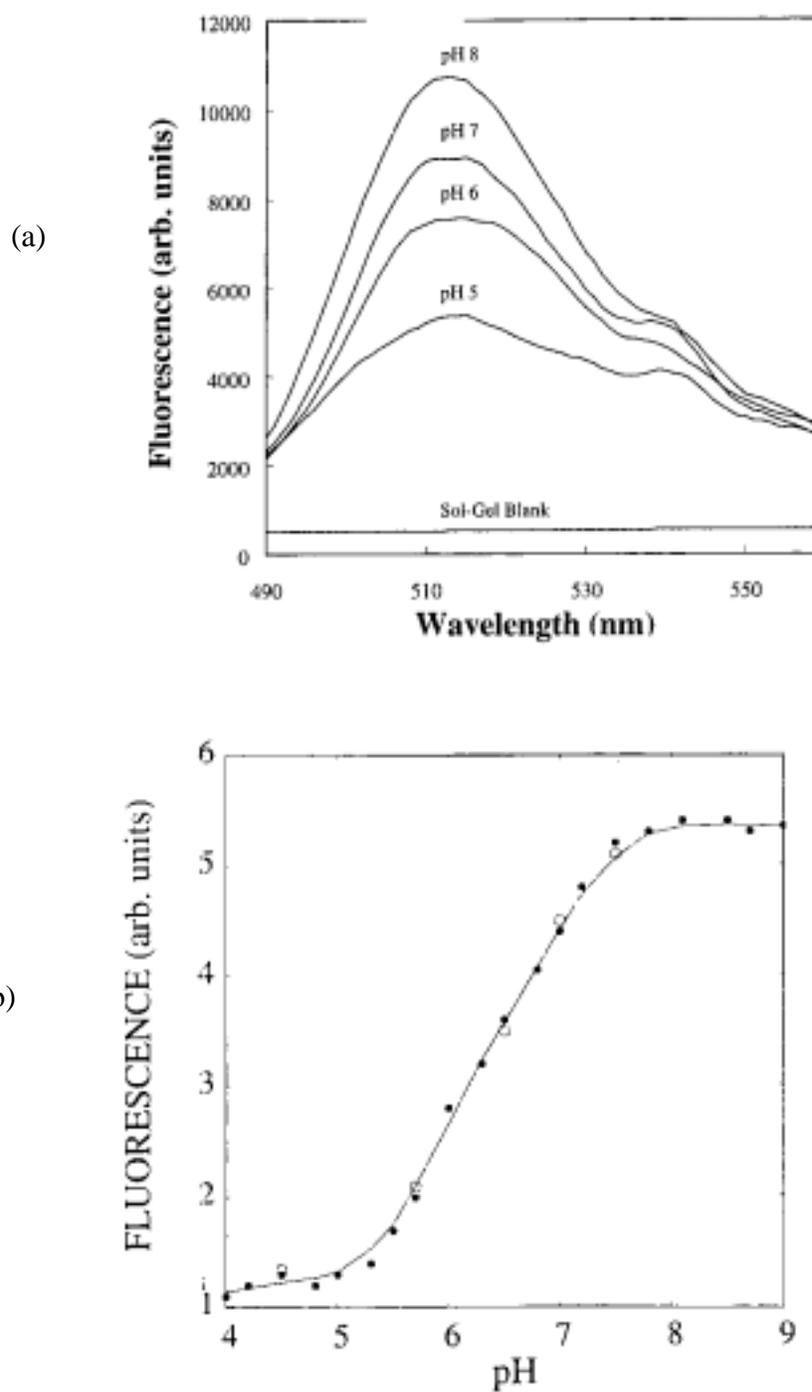
Figure3.2. pH sensitivity of a liposome containing sol gel film: (a) Fluorescence spectra of the gel in solutions of pH 5, 6, 7 and 8, (b) A calibration curve describing the pH dependence of the liposome containing sol-gel film (Filled circles - data points of standard solutions, unfilled circles – data points of solutions of unknown pH).

3.3.2. Leaking stability of a sol-gel film containing carboxyfluorescein encapsulating liposomes

As previously mentioned, leaking of dye molecules is a major concern in fluorescence-based sensors. To characterize the leaking stability of our sol-gel based sensors, carboxyfluorescein containing sol gel films were placed in MOPS buffer solutions of pH 7.2 for 48 hours. The fluorescence intensity of the sol-gel sensors and the solutions in which they are placed were measured periodically. The fluorescence intensity of the MOPS solution placed on top of a liposome containing sol-gel film show only a residual fluorescence intensity and did not increase throughout the experiment. The fluorescence intensity of the MOPS solution placed on a free carboxyfluorescein containing sol-gel film show a rapid increase during the first 12 hours of observation, a clear indication of a significant leakage of carboxyfluorescein from the sol-gel support. The fluorescence intensity of a sol-gel film containing carboxyfluorescein-encapsulating liposomes remained stable throughout the experiment. The fluorescence intensity of a sol-gel film containing free carboxyfluorescein lost about 60% of its initial intensity in 12 hours before reaching a relatively stable fluorescence signal. These leaking experiments clearly show that the encapsulation of fluorescent liposomes in sol-gel films prevents its leakage from the sol-gel matrix support. To further verify this observation, free dye and liposome containing sol gel thin films have been stored in air instead of in a buffer solution. The films have been exposed to the same excitation conditions used to measure the leaking stability of the films in buffer solutions. Under low level excitation conditions, the fluorescence intensity of these films remains stable throughout the 48 hours experiment. To prevent photodecomposition of the carboxyfluorescein molecules,

the exposure time used to obtain each data point is only 100 msec.   As a result, the

fluorescent sol-gel films are exposed for only a few seconds to the excitation light during

the 48 hour- experiment.   Under these experimental conditions, the observed

fluorescence decrease observed in sol-gel films that contain free carboxyfluorescein

results from dye leaking and not from photodecomposition.

3.3.3. Photobleaching stability of a sol-gel film containing carboxyfluorescein encapsulating liposomes

During the work with samples of carboxyfluorescein encapsulating liposomes, it is

noted that the background fluorescence (from remaining free dye) photobleaches faster

than the dye that is encapsulated within the liposomes.   Figure 3.3a shows a fluorescence

image of a sol-gel film containing liposomes that have only been washed once to

incompletely remove free carboxyfluorescein prior to gel formation.   While the fluorescent

liposomes can be clearly seen, the signal to noise ratio of this film is only about 4.   Figure

3.3b shows the same sample following a 3 min of continuous illumination with a 488-nm

light of the fluorescence microscope excitation burner.   The liposome sample is virtually

free of any significant background fluorescence, and the signal to noise ratio increases by

almost an order of magnitude to about 26. One possible explanation for this phenomenon

may be less preferable conditions for the formation of singlet oxygen inside the internal

compartment of the liposomes that in turn leads to a reduced photobleaching rate.   It is also

possible that the interaction of the encapsulated carboxyfluorescein molecules with the

phospholipid bilayer membrane makes them less susceptible to photobleaching.   Further

experiments and theoretical studies are needed to fully explain this interesting observation.

It should be noted that there would not be any suggestion to illuminate fluorescent dye encapsulating liposomes as an effective protocol for "removing" free dye from an unwashed sample, as the liposomes themselves are also bleached, albeit at a much slower rate.

T=0   3 min

(a)   (b)

Figure3.3: Photobleaching stability of a sol-gel film containing carboxyfluorescein-encapsulating liposomes: (a) A fluorescence image of a sol-gel film containing incompletely washed fluorescent liposomes, with a signal to noise ratio of about 4; (b) The same sol-gel film following 3 minutes continuous illumination with a 488-nm light. The signal to noise ratio increases by almost an order of magnitude to about 26.

3.3.4. Response time of a sol-gel film containing carboxyfluorescein-encapsulating liposomes

A response time characterization of a liposome containing sol-gel thin film is shown in Figure 3.4 where the fluorescence response, I_{490}/I_{440}, of the sensor is plotted against a time coordinate. The response time of the pH sensitive sol-gel film is determined

as follows: First, the ratio I_{490}/I_{440} is measured when the sensor is in contact with a 200 μl aqueous solution of pH 4 (adjusted with 0.01 N HCl). Then, 50 μl of a 0.1 mM NaOH solution are injected into the solution to instantly increase the pH to about 9. A rapid increase in the ratio I_{490}/I_{440} is observed in less than 1s. It is possible that the response curve follows the injection of the alkaline solution, which is slower than the actual response time of the sensor. In comparing the response time of a liposome containing sol-gel film to the response time of a free carboxyfluorescein containing sol-gel film we find a minimal and inconsistent difference in the response time. This observation indicates that the diffusion of protons across the bilayer membrane of the liposome does not have a significant affect on the response time of the sensor, which is regulated primarily by the thickness of the sol-gel film itself.

To characterize the reversibility of the sensor, the pH of the analyte solutions is changed repeatedly between pH 5 and 10. As can be seen in Figure 3.4, the effect of consecutive pH changes of the analyte solution on the sensor is marginal. Consecutive pH measurements in standard buffer solutions show that the deviation of I_{490}/I_{440} data points from their average value is approximately 5%. This result is comparable with previously described fluorescence-based pH sensors [120-121].
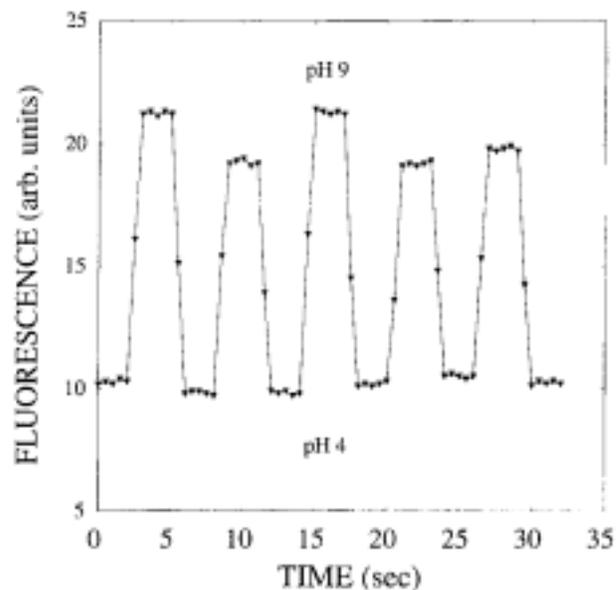
Figure 3.5. Characterization of the response time, reproducibility and reversibility of a micrometer thickness sol-gel film, containing carboxyfluorescein-encapsulating liposomes. The sensor shows sub-second response time, about 95% reproducibility, and high reversibility.

3.4. Summary

A new method for physical immobilization of hydrophilic sensing reagents in sol-gel thin films is described. The immobilization of fluorescent dye encapsulating liposomes in a sol-gel film is an effective way to prevent dye leaking and to increase the chemical stability of sol-gel based optochemical sensors. Water-soluble fluorescence dyes are readily encapsulated in liposomes and the presence of conjugating functional groups is not necessary. The major advantage of this new immobilization method is its simplicity. Dye encapsulating liposomes form spontaneously when a cocktail containing phospholipids and cholesterol is injected into an aqueous solution of the sensing reagent. Encapsulation efficiencies vary between 5% to 70%

depending on the specific dye and composition of the cocktail used to make the liposomes, which are then added to the aqueous buffer used to prepare the sol-gel film. The pH sensor fabricated using this new immobilization protocol is more stable than previously described optochemical pH sensors prepared by physical immobilization. It shows sensitivity and linear dynamic range that are comparable with previous sensors. The sub-second response time of the sensor to rapid pH changes indicates that the diffusion of protons across the bilayer membrane does not slow the response time of the sensor, which depends greatly on the thickness of the sol-gel film. It is difficult to control the size of these sensors in a consistent manner as they are immobilized in a sol- gel matrix. It is also not feasible when the examined cells are not dispersed in solution and needed to grow on a support platform. The next chapter shifts to a new unique approach for fabrication of liposome-based sensors. For the first time, a liposome-based biosensor for Ca^{2+} by encapsulating fluorescein labeled calmodulin, a calcium binding protein, in unilamellar liposomes is introduced. Upon binding, calmodulin undergoes a conformational change that exposes its hydrophobic core and affects the fluorescence intensity of the attached fluorophors.

CHAPTER FOUR: CALCIUM ION FLUORESCENCE DETECTION USING

LIPOSOMES CONTAINING ALEXA-LABELED CALMODULIN

4.1. Introduction

There has been a growing interest in the development of fluorescence detection techniques for the analysis of calcium ions in biological samples and single cells [122-123]. In most recent optochemical calcium ion sensors, calcium ion sensitive fluorescence indicators were immobilized to particles, polymer films or to the distal end of optical fibers [124-126]. The analysis of calcium ion levels was based on a direct interaction between calcium ions and the fluorescence indicators. The fluorescence intensity of these sensors was calcium ion concentration dependent. The principle of this measurement is identical to the principle of intracellular calcium ion level measurements using cell permeable calcium ion fluorescence indicators such as indo-1, quin-2, fura-2, fluo-3, calcium orange, and calcium crimson [127-128]. These dyes may show up to 50-fold fluorescence increase when binding to calcium ions. The high signal-to-noise (S/N) ratio in these measurements enables the determination of submicromolar calcium ion levels in cells.

Quantitative analysis of calcium ion levels and calcium ion signaling processes using common fluorescence indicators is not always accurate. This is due to the limited photostability of the dyes, interference from other divalent ions such as magnesium ions, heterogeneous distribution of the dyes in cells and poor stability in the cellular environment. Recent studies have been focusing on the use of conformational changes of proteins, peptides and DNA structures as an alternative way to sense ions in biological samples. The detection

strategy is based on fluorescent allosteric signal transduction proteins. Binding to a ligand causes these proteins to undergo a large conformational change at their binding sites. This conformational change yields a measurable optical signal [129-134]. The proteins usually possess a chain that folds into two domains connected together by a hinge region. The ligand binding sites are located in the interface between the two domains. Such a protein would have two stable conformations: an "open" form when binding to the ligands, and a "closed" form when free of the ligands [135]. For example, Miki et al have revealed that the amino acid sequence of the protein BRCA1, encoded by the familiar breast and ovarian cancer susceptibility gene, has an amino terminal ring finger domain, which is a zinc-binding motif [136]. A distinct conformational change of the ring finger is observed when zinc ions bind to the protein. Roehm et al characterized the metal binding and metal –dependent folding properties of a peptide encompassing the BRCA1 ring finger by using cobalt (II) as a spectroscopic probe [137]. Proteins can be covalently labeled with various fluorophores, thus producing fluorescent protein conjugates. Hence, tagging a protein with fluorescent labels is an important and valuable tool for studying structure and microenvironment. In this project, the conformational change of calmodulin (CaM), a calcium ion binding protein, is used as a principle for selective calcium ion sensing. This conformation change strongly affected the fluorescence intensity of the covalently bound fluorophore, Alexa Fluor488.

Calmodulin (CaM) is a major membranal calcium ion binding protein in eukaryotic cells. CaM plays an important role in cell signaling and regulates a wide variety of cellular processes including nucleotide metabolism, cell proliferation, microtubular function, exocytotic secretion, calcium regulation of smooth muscle contraction, ion pumps and channels, and cell

cycle control [138-142]. CaM contains two globular lobes joined by a linker region as shown in Figure 4.1. Each globular lobe consists of two helix-loop-helix Ca^{2+}-binding sites called EF hands [143-144]. Upon binding to calcium ions, CaM undergoes an induced conformational change that exposes its hydrophobic cores, which may act as active sites for the interactions with target enzymes or CaM antagonists. Both the carboxy- and amino- terminal domains of CaM then undergo large structural rearrangements from the " closed" conformation (the two helices of each hand are almost anti-parallel) to the "open" conformation (the two helices are more perpendicular) [145-151].   When a fluorophore, Alexa Fluor488, covalently bound to the protein, a calcium ion induced conformational change affects its fluorescence intensity [152-154].

Baccas et. al have previously fabricated a fiber optic fluorescence sensor for calcium ions using fluorescein labeled calmodulin as a calcium ion sensitive indicator [155]. In their sensor, a solution containing calmodulin was encased between two membranes. This assembly was attached to the distal end of an optical fiber. The sensor was large and exhibited a long response time in the minutes time scale due to the presence of the encasing membrane designed to prevent leakage of calmodulin into the sample solution.   The use of fluorescein limited the accuracy of the measurement because of its poor photostability. In our study, calmodulin is immobilized to the bilayer membrane of liposomes, which may serve as individual calcium ion nanosensors, or immobilized to a glass surface to form calcium ion sensitive films. Furthermore, the highly photostable fluorophore Alexa 488 is used to label the calmodulin molecules.
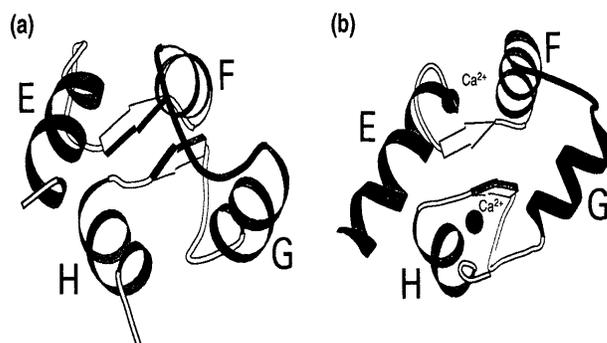
Figure 4.1. The carboxy-terminal domain of calmodulin (CaM) (a) in the " closed" Ca^{2+} - free states (b) in the "open" Ca^{2+} - bound states.

Alexa Fluor 488 dye (chemical structure shown in Figure 4.2) is the best fluorescein FITC substitute available for most applications. Fluorescence spectra of Alexa Fluor 488 and fluorescein are almost identical with excitation/emission maxima of 491/515 nm. It has the fluorescence lifetime of about 4.1 nanoseconds. Alexa Fluor 488 is much more photostable than fluorescein, and pH-insensitive fluorescence between pH 4 and pH 10.   This pH insensitivity is a major improvement over fluorescein, which emits fluorescence that is affected by pH. Protein conjugates prepared with Alexa Fluor 488 dye are much better conjugates with significant brighter, more photostable and pH insensitive compared than that of fluorescein FITC.
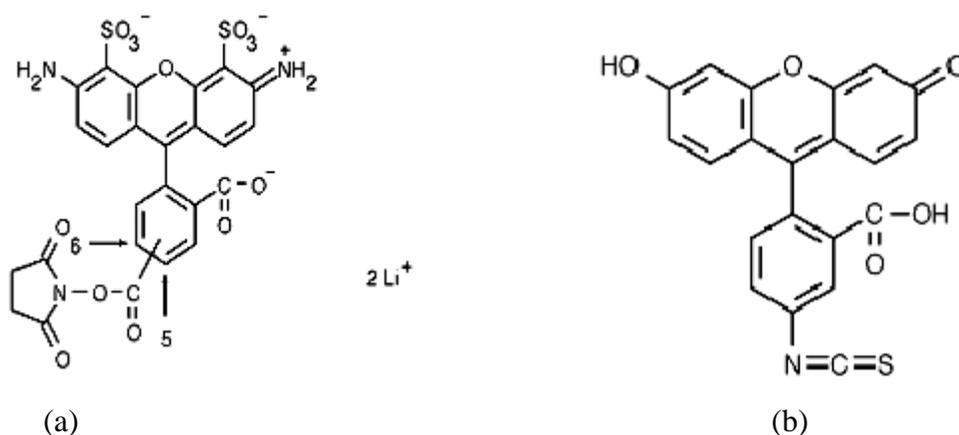
Figure 4.2. Chemical structures of (a) Alexa Fluor® 488 carboxylic acid, succinimidyl ester, (b) fluorescein-5-isothiocyanate (FITC).

4.2. Specific experimental and Technical Details

a) The detection system

Digital florescence imaging microscopy and a fluorometer are used to measure the fluorescence of the calcium response of calmodulin labeled liposomes. A filter cube containing a 480 nm narrow band excitation filter, a 500 nm dichroic mirror, and a 515 nm long pass emission filter is used to ensure spectral imaging purity.

b) Preparation of CaM-Alexa encapsulating liposomes

A 5: 4: 1 molar ratio (50 mM) lipid stock solution is prepared with dimyristoylphosphatidylcholine, cholesterol, and dihexadecyl phosphate in 0.5 mM EGTA/ 5.0 mM Tris-HCl buffer (pH 7.0) and dispersed using probe sonicator (Fisher Model 60 Sonic Dismembrator) at 40W for 2 minutes. The solution is stored in a sealed vial at room temperature until use. A 200 μL aliquot of the phospholipid stock solution is added to 200

µL of Alexa-labeled calmodulin solution (0.5 mg/ml) in 0.5 mM EGTA/ 5.0 mM Tris-HCl buffer (pH 7.0). The solution is then dried at room temperature using a rotating flask evaporator under nitrogen to form a film of phospholipids and calmodulin at the bottom of the flask. The film is rehydrated by adding 0.4 ml of 0.5 mM EGTA/ 5.0 mM Tris-HCl buffer (pH 7.0) to form liposomes with embedded Alexa-labeled calmodulin molecules in their bilayer membrane. The rehydrated sample is then incubated for 1 hour at room temperature to form small unilamellar vesicles (SUV) [156-161]. A micro-column centrifuge technique, previously described by Fry et al. [162] is used to separate the calmodulin containing liposomes from the excess free protein molecules remaining in the solution. To prepare the separation column, a 10g sample of Sephadex G-100 is allowed to swell overnight in a 175 ml 0.9% NaCl solution. Glass wool is placed at the bottom of an empty 1 ml tuberculin syringe. A volume of 1 ml Sephadex solution is transferred into the syringe to form a plug above the glass wool. The Sephadex containing syringe is then centrifuged in a low speed centrifuge (Adam Dynac) at 2000 rpm for 3 minutes to form a dry solid Sephadex column, absent of cracks or voids. Sephadex solution is added and the syringe is again centrifuged until a plug of dry Sephadex of ~ 8 cm long is formed in the syringe. To separate the free calmodulin from the calmodulin containing liposomes, 200 µL of the liposome solution is added drop wise to the top of the column and the syringe is placed in a 10 mm diameter, 13 cm height centrifuge tube. The syringe, inserted into the tube, is centrifuged at 700 rmp for 10 minutes (Fisher, Model Marathon 8K). The liposomes are collected in the centrifuge tube while the Sephadex column retains the free proteins. The process is repeated at least three times to ensure complete washing of free

protein from the liposome solution. The washed liposome solution is stored at room temperature in a light tight environment.

c) Preparation of a calcium ion sensing film on a glass surface

Calmodulin entrapping liposomes are immobilized to poly L-lysine coated glass microscope cover slips as follow: the Corning glass cover slips are washed in 70% ethanol / water solution (v/v), followed by washing with deionized water. The cover slips are then dipped in 10 ml of 0.1 % poly-L- lysine solution and left overnight, at room temperature and in the dark. They are removed from the coating solution and rinsed with a phosphate buffer solution at pH 7.2. 1 ml of liposome solution is then placed on the glass cover slip surface. The cover slip is placed in a sample holder on the top of a homemade spinner and briefly spinned at 500 rpm to generate the sensing film. Unbound liposomes are washed with a phosphate buffer at pH 7.2. The liposome-coated cover slips are stored in a phosphate buffer solution at pH 7.2 at room temperature until use. Under these storage conditions the sensor maintains its calcium ion sensitivity for up to 3 days.

4.3. Results and Discussion

4.3.1. Calcium Sensitivity of Alexa-Labeled Calmodulin in Solution

The calcium ion response of Alexa-CaM in aqueous solution at concentrations of 1, 5 and 10 µM is shown in Figure 4.3. The fluorescence intensity of Alexa-CaM decreases with increasing calcium ion concentration due to the binding of calcium ions to the CaM active binding sites.   The optimal concentration of Alexa-CaM is 5 µM where a dynamic

range between 0.1 and 1.3±0.05 µM of calcium ion in solutions is observed.   In our measurements, Alexa-CaM is dissolved in a phosphate buffer solution at pH 7.4 and kept at room temperature. Under these conditions, the calcium ion binding affinity of Alexa-CaM gradually degrades and the protein becomes inactive within 2 hours. The lifetime of the calcium ion binding activity of Alexa-CaM is extended up to 6 hours when the protein solution is kept at 4°C. The encapsulation efficiency of Alexa labeled calmodulin in the liposomes was estimated by comparing the fluorescence of liposomes containing Alexa-labeled calmodulin with the fluorescence of free Alexa labeled calmodulin at known concentrations. Based on these measurements we found the encapsulation efficiency to be about 10%.
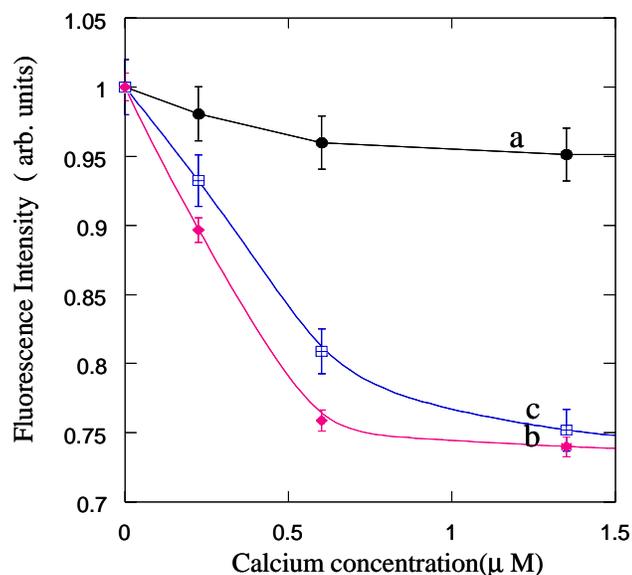
Figure 4.3. Calcium ion response of increasing concentrations of Alexa-CaM in aqueous solution: (a) 1µM, (b) 5µM, and (c) 10 µM.

4.3.2. Digital Fluorescence Imaging of Calmodulin Containing Liposomes

Calcium sensitive liposomes are prepared by embedding Alexa-CaM in the bilayer membrane of unilamellar liposomes. The liposomes are immobilized directly to a glass microscope cover slip treated with poly-L-lysine. Digital fluorescence images of Alexa-CaM containing liposomes are shown in Figure 4.4. Figure 4.4a shows an image of individual liposomes in a pH 7.2 phosphate buffer solution . A digital fluorescence intensity analysis of this image indicates that the ratio between the fluorescence intensity of individual liposomes and the background noise is 50±5. Figure 4.4b shows an image of a large number of liposomes embedded in a poly-L-lysine film. This film could be used to obtain an average measurement of the level of calcium ions in a larger sample. The images are taken using a 20x microscope objective (NA =0.25) and an exposure time of 100 msec. This exposure time is optimal for imaging the liposomes. The time is short enough to prevent capturing their lateral diffusion and sufficiently long to detect their fluorescence signal. Each spot represents the fluorescence of an individual liposome. The encapsulation efficiency depends on the mass ratio of lipid to solute. We find that under our experimental conditions, the mass ratio of lipid to solute is approximately 1:1.

0.1µm
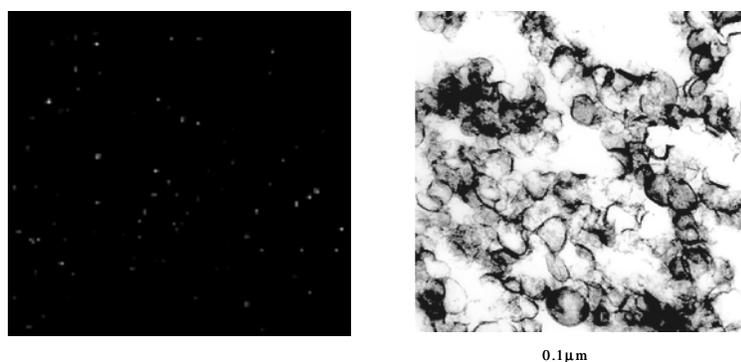
Figure 4.4. a) A digital fluorescence image of Alexa-CaM containing liposomes. The image is taken   using a 40x microscope objective (NA =0.25) and an exposure time of 100 msec; b) A 82,600 X transmission electronic micrograph of uranylacetate labeled liposomes.The average size of liposomes about 100 nm in diameter.

4.3.3. Photostability of Alexa-CaM Containing Liposomes

Figure 4.5 shows a comparison between the photostability of Alexa-CaM and Fluorescein-CaM containing liposomes. Samples of the fluorescent liposomes are illuminated by a 100 Watt/cm^2 beam of a continuous mercury lamp (Oriel). The fluorescence intensity of fluorescein-CaM containing liposomes decreases rapidly (curve a) while the fluorescence signal of Alexa-CaM containing liposomes (curve b) decreases initially by 45 % and remains constant for up to 1 hour of continuous illumination. The initial decrease in the fluorescence intensity of Alexa-CaM containing liposomes may be attributed to photodecomposition of unstable isomers. It should be noted, however, that the photon flux in our fluorescence microscopy experiment is much lower and the exposure time of the sample to the excitation light is only 100 msec per measurement. Under these conditions, no photodecomposition of Alexa-CaM containing liposomes is observed.
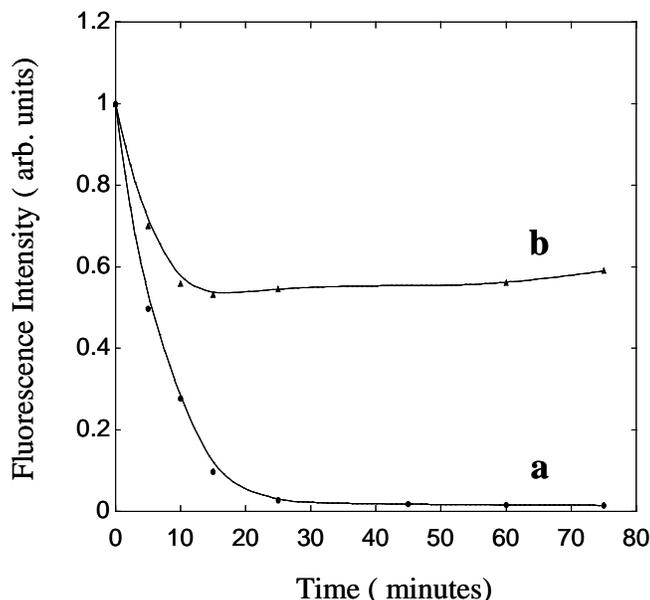
Figure 4.5. Photostability of (a) fluorescein-CaM containing liposomes and (b) Alexa-CaM containing liposomes. Samples of fluorescent liposomes are continuously illuminated using a 100 Watt/cm^2 beam of a mercury lamp (Oriel).

4.3.4. Analytical Properties of Alexa-CaM Containing Liposomes

The concentration dependence of the fluorescence intensity of Alexa-CaM containing liposomes is shown in Figure 4.6. The fluorescence intensity of the liposomes at saturating calcium ion concentration of 39.8 µM, I_{min}, is subtracted from the fluorescence intensity of the liposomes at a given calcium ion concentration, I. The corrected fluorescence signal is then normalized to the difference between the fluorescence intensity of the liposomes in a calcium ion free solution, I_{max}, and I_{min}. The normalized fluorescence intensity of the liposomes is described as a function of –log $[Ca^{2+}]$ or PCa^{2+}. Each data point represents the average of 3 replicate measurements. The error bar of each data point is the standard deviation between these 3 measurements. The dynamic range of calcium ion sensitive liposomes is between 0.1 and 40 µM ± 0.05. It is similar to the dynamic range of free

calmodulin in solution. We therefore conclude that embedding calmodulin in the liposome bilayer membrane does not inhibit the calcium ion binding activity and the conformational changes that occur as a result of calcium ion binding. This result confirms our prediction that since calmodulin is a membrane protein, its activity would not be degraded when embedded in a liposome bilayer membrane. Furthermore, we find that calmodulin-containing liposomes maintain their calcium ion sensitivity for 24 hours when kept in a phosphate buffer solution of pH 7.2 at room temperature. As previously mentioned, in solution, calmodulin maintains its calcium ion binding activity for only 2 hours under the same experimental conditions. The liposome solution is kept under light tight conditions to prevent photodecomposition of the fluorescence indicator. Exposure of liposomes to a step change in calcium ion concentration between 0 and 1.5μM results in an immediate signal decrease indicating that the response time of the calmodulin containing liposomes is in the second time scale. This is a significant improvement compared to previously described calmodulin-based sensors in which a response time of several minutes was reported. The interaction between calcium ions and CaM encapsulating liposomes at room temperature is not reversible. However, the calcium ions can be extracted from the liposomes and their fluorescence intensity could be restored to its calcium ion free level by increasing the temperature or by adding a chelating compound with a stronger binding constant like EGTA to the sample. Our calcium ion sensitive liposomes also show high selectivity for calcium ions over magnesium ions. As previously reported by Bachas et. al., calmodulin also binds to magnesium ions [163]. However, the corresponding binding constants are $2x10^3$ and $3x10^2$ M^{-1} for the high and low affinity sites of calmodulin. To evaluate the

calcium ion selectivity of our liposomes, we measured the fluorescence intensity of Alexa-CaM containing liposomes in solutions of increasing magnesium ion concentrations. No response was observed in solutions of up to 5 mM magnesium ions.
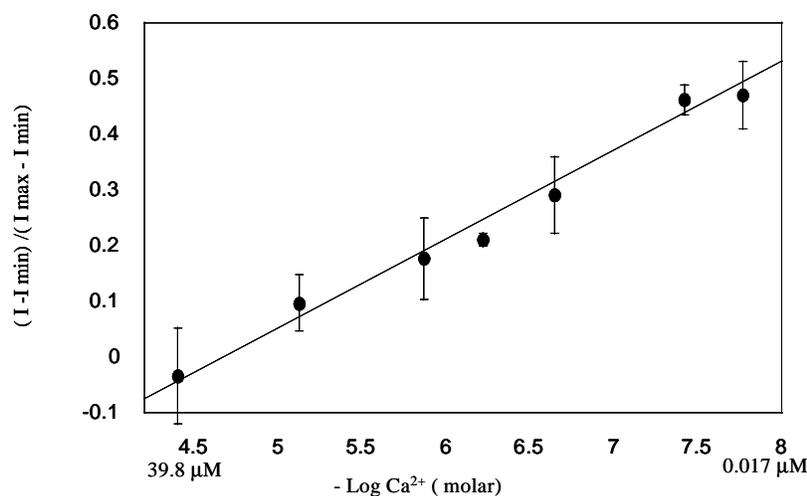
Figure 4.6. The concentration dependence of the fluorescence intensity of Alexa-CaM containing liposomes. The fluorescence intensity of the liposomes at saturating calcium ion concentration of 39.8 μM, I_{min}, is subtracted from the fluorescence intensity of the liposomes at a given calcium ion concentration, I.   The normalized fluorescence intensity of the liposomes is described as a function of –log $[Ca^{2+}]$ or PCa^{2+}. The error bar of each data point is the standard deviation between these 3 measurements.

4.4. Summary

Liposomes containing Alexa labeled calmodulin show high sensitivity to calcium ions. The calcium ion sensitivity of Alexa-CaM containing liposomes improves significantly compared to the calcium ion sensitivity of Alexa-CaM in aqueous solution. When embedded in liposomes the calcium ion response of Alexa labeled calmodulin is 4 fold higher than its calcium ion response in solution. This is attributed to the increasing stability of calmodulin when embedded in the liposome membrane. The dynamic range of Alexa-CaM containing

liposomes is between 0.1 and 40 μM $\pm$0.05. The calcium ion sensitive liposomes show very high calcium ion selectivity. Unlike in commonly used fluorescence indicators, physiological levels of magnesium ions do not interfere with the calcium ion response of the Alexa-CaM containing liposomes. The stability of the liposomes in biological samples is still a concern. Currently we are developing phospholipid coated polymeric particles, named lipobeads for ion sensing in and near cells. In lipobeads the indicator would still be embedded in a bilayer membrane. However, unlike in liposomes this membrane would coat polymer particles to increase the physical stability of the sensors. Characterization studies of this new system are underway.

In summary, chapters 3 and 4 describe liposome-based sensors for pH and calcium ions. Their instability in the cellular environment has led to the development of lipobead-based sensors. Chapters 5 and 6 describe the development of pH and zinc ion sensing lipobeads and their application in neuron cell cultures.

CHAPTER FIVE: A LIPOBEAD-BASED pH FLUORESCENCCE SENSOR FOR SITE
SPECIFIC pH MEASUREMENTS IN NEURON CELLS IN CULTURES

5.1. Introduction

Neuronal activity gives rise to rapid shifts of extracellular pH that occur in either

the alkaline or acid direction [164]. The activity-dependent pH shifts in a given cell or

brain region might lead to a decrease or increase in excitability and affect neuronal

functions. Extracellular alkaline shifts related to neuronal activity are due to channel-

mediated flux of acid equivalents such as the net efflux of HCO_3^- through gamma-

aminobutyric acid $GABA_A$ receptor channels, or bicarbonate-insensitive flux of hydrogen

ions through cationic channels, activated by glutamate or aspartate [165-169]. The basis

of activity dependent acidic shifts has generally been considered to be metabolic,

involving the efflux of lactic acid, or classic acid extrusion membrane transport systems

(Na^+ / H^+ or $Na^+ / HCO_3^- / Cl^- / H^+$). The Na^+ / H^+ exchange across cell membranes is

enhanced due to increased Na^+ permeability. The resulting influx of Na^+ and efflux of H^+

leads to extracellular acidification [170-171].   In general, alkalosis increases neuronal

excitability and initiates seizure activity. Acidosis decreases neuronal excitability and

suppresses seizure activity [172].

Cortical spreading depression (CSD) is a phenomenon that involves a breakdown

of neuronal ion gradients [173], increase of regional cerebral blood flow [174], release of

a variety of neurotransmitters such as glutamate [175], and nitric oxide [176], and

permanent cell swelling [177]. During CSD initiation, the concentration of extracellular K^+, $[K^+]_0$, rapidly rises, causing brief neuronal excitation then depolarization and a period of electrical silence during which the direct current (DC) potential at the brain surface falls. Extracellular $[Na^+]$ and $[Cl^-]$ levels decrease as these ions enter cells. Consequently, water enters the cells, and the extracellular space is reduced. Neurons, especially dendrites, swell because NaCl uptake exceeds the discharge of K^+ and organic anions. Ca^{2+} influx movements follow K^+ effluxes. Additional negative ion species move outwards to maintain electrical balance [178]. Extracellular acidic shifts of several tenths of a unit of pH could be observed during CSD [179]. If the depolarization due to CSD is prolonged beyond a critical time, the neurons become permanently unresponsive. If, however, the depolarization induced influx of Ca^{2+} into neurons is prevented, then the neurons can regain function after extended CSD-like depolarization that otherwise would cause irreversible injury [180]. CSD might be associated with some clinical disorders and behavioral consequences, including migraine, cerebrovascular diseases, head injury, and transient global amnesia [181].

Currently, CSD in the nervous system can be triggered using high-frequency electrical nerve stimulation (10-100 Hz, 20- 60 seconds) [182], chemical injury evoked by local pressure ejection of glutamate and gamma-aminobutyric acid (GABA) [183], ouabain [184], benzolamide [185], or 4,4'-Diisothiocyanostilbene-2, 2'-disulfonic acid (DIDS) [186]. A pH electrode is placed in the cell medium to measure pH changes. However, the ability to visualize targeted and site- specific (as opposed to global) pH changes external to the neurons has been lacking.

In our laboratory, we focused in recent years on the synthesis of phospholipid-coated particles, called lipobeads, and their use as submicrometric fluorescence sensors. The phospholipid membrane formed on the surface of the polystyrene core is biocompatible and provides the protection for the sensing fluorophore from the surrounding environment. It also minimizes leakage of indicators into cells when the particles are used for extracellular measurements. The new sensing particles with cell-like lipid bilayer surface similar to natural cells combine complementary advantages of liposomes and polymeric beads. Unlike other particle-based sensors the use of phospholipid coating enables the stable immobilization of hydrophilic and hydrophobic indicators to the particles. To date, phospholipid coated nanoparticles, with pH, and oxygen-sensing capabilities were fabricated and applied for intracellular measurements in murine macrophages. [187-188]. The technique is highly versatile since it is possible to incorporate biomolecules such as antibodies, enzymes, and receptors into the membrane of the particles and use them as selective and sensitive biosensors. These types of lipobeads could be used to trace site-specific physiological events in neurons and other cells, and provide a novel technique for presenting growth, differentiation, and survival factors.

In this chapter, the fabrication of pH sensing lipobeads with cellular targeting capability towards neuron cells is described. The lipbeads are labeled with Succinyl Concanavaine A (Succ. Con A), a lectinic protein that binds specifically to α-D-Mannose on the external membrane of neurons [189]. While these lipobeads attached to cell surface areas as well as the plate area covered with matrigel, many beads aligned

along the neuronal processes and attached to the cell soma. The small size of these sensors, combined with the technique to target the lipobeads to the neuronal surface, provide an important advancement in visualizing extracellular pH changes during cortical spreading depression in neuron cells.

5.2. Specific Experimental and Technical Details

a) The detecting system

A 460/50 nm band-pass excitation filter, 500 nm dichroic mirror, and 515 nm long pass emission filter are used to ensure spectral imaging purity. An exposure time of 0.3 second is used to acquire the fluorescence spectra of the lipobeads. Excitation and emission spectra are carried out using a PTI international (model QM-1) fluorimeter, equipped with a 75-W continuous Xe arc lamp as a light source.

b) Synthesis of pH sensing lipobeads

The synthesis was carried out using the following procedure: Four milligrams of polystyrene microspheres 1.6 μm in diameter were dispersed in 100 μl of ethanol/hexane (1:1 v/v). A 50 mM lipid stock solution was prepared with a 5:4:1 molar ratio of DMPC, cholesterol, and DP in chloroform. 250 μl of the lipid solution and 10μl of 5 mM fluorescein - DHPE in chloroform were added to 100 μl of microsphere suspension. The mixture was then sonicated by using a 47 kHz Bransonic sonicator for 15 minutes, held at room temperature for 2 hours, and then dried under nitrogen overnight. The dried phospholipid microsphere sample was then resuspended in 1 ml of phosphate buffer pH 7.0 and sonicated for 15 minutes. 0.25

mg / ml of Succ. ConA (final concentration) was then added to the resulting lipobead suspension and the whole mixture gently stirred for 4 hours to ensure the absorption of lectin molecules onto/into phospholipid membrane on the beads. Free unbound lectin molecules, excess phospholipid, and unreacted microsphere particles were removed by centrifugation (2600 rpm, 15 minutes). The coated lipobeads with Succ. Con A were thus collected at the bottom of a glass centrifuge tube while the supernatant and unreacted beads were discarded. Succ. Con A incorporated lipobeads were suspended in 1 ml of phosphate buffer (pH 7.0) and stored in glass vials covered with aluminum foil at 4° C until use.

c) Immobilization of lipobeads on the surface of chambered coverglass for pH sensitivity measurements

To immobilize the lipobeads, a chambered coverglass was dipped in 70% ethanol/water for 15 minutes. The chamber was dried in a 60^0C oven. The chambered coverglass was incubated in a 200µl solution of 10 % poly-L-lysine for 2 hours. It was then drained and left to dry at room temperature overnight. A 200µl lipobead suspension was then placed in the chambered coverglass for 4 hours. The unimmobilized lipobeads were then rinsed out with a phosphate buffer at pH 7.0.

5.3. Results and discussion

5.3.1.   Choice of Indicator

Fluorescein was chosen here because of its high absorptivity and emission quantum yield in the visible range of the electromagnetic spectrum. Fluorescein and many of its derivatives exhibit multiple, pH dependent ionic equilibria as shown in Figure 5.1.
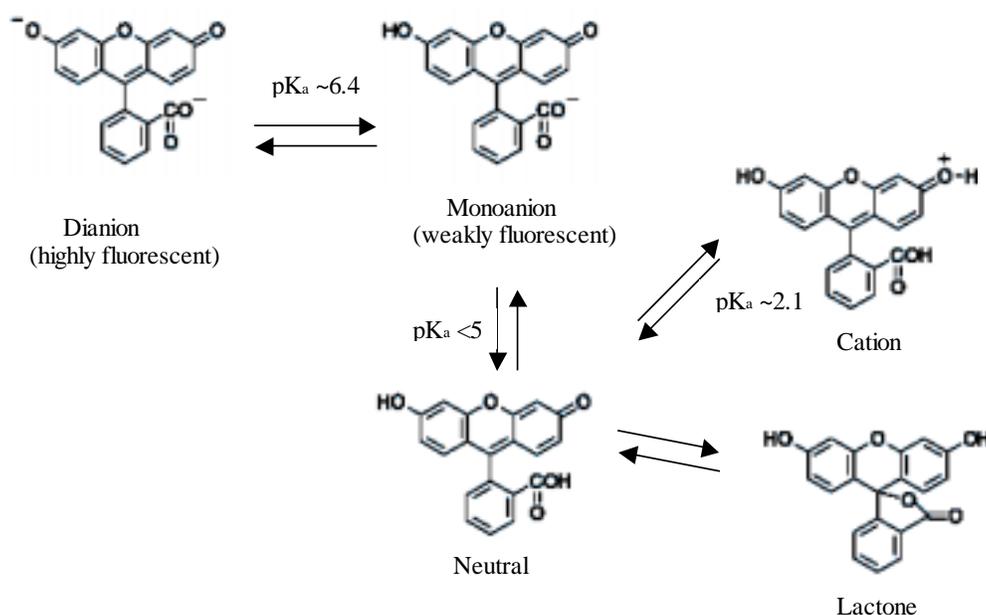
Figure 5.1. Ionization equilibria of fluorescein

Only the monoanion and dianion are fluorescent with quantum yields of 0.37 and 0.93, respectively. Excitation of either the neutral or cationic species also produces emission from the anion with effective quantum yields of 0.31 and 0.18. A further equilibrium involves formation of colorless, non- fluorescent lactone. The lactone is not formed in aqueous solution above pH 5 but may become dominant form

of neutral fluorescein in solvents such as acetone. The fluorescence emission spectrum of fluorescein or fluorescein derivatives, even in acidic solution, is dominated by the dianion, with only small distributions from the monoanion.

In this work, fluorescein derivatized dihexadecanoylglycerophosphoethanolamine (fluorescein DHPE) is used (chemical structure shown in Figure 5.2). Fluorescein DHPE is a membrane surface probe that is sensitive to both the local electrostatic potential and pH. Since the dye molecules of fluorescein are covalently attached to phospholipid, this will prevent the leakage of dye molecules from the sensing particles to the observed environment. This leakage is the most common problem in fluorescence sensors fabricated by physically entrapping hydrophilic sensing reagents like pH indicators in a polymer matrix. The fluorescein DHPE has excitation wavelength at 480nm and emission wavelength at 525 nm.
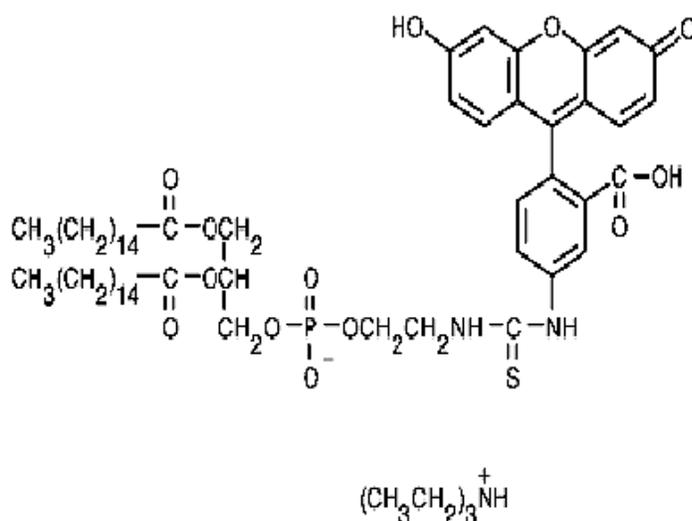
Figure 5.2. Structure of phospholipid component, *N*-(fluorescein-5-thiocarbamoyl)- 1,2-dihexadecanoyl-*sn*-glycero-3- phosphoethanolamine, triethylammonium salt (fluorescein DHPE).

5.3.2. Site-Specific Targeting of pH Sensing Lipobeads to Primary Rat Cortical Neuron Cells

Lectins can be found in many organisms and are involved in a variety of cellular processes that depend on specific recognition of complex carbohydrates. Their preferential binding to neuronal tissue has been studied extensively [190-191]. We chose Succ. Con A, which favors binding to neurons, to enable cell specific extracellular pH measurements under conditions simulating cortical spreading depression. 1.6 μm sized Succ. Con A coated lipobeads with neuron cells in cell cultures were incubated for 4 hours. Unbound lipobeads were washed off the cover slips with 5 exchanges of medium with Locke's solution. Figure 5.3a shows a transmission phase image of particles attached to cells and the culture cover slip under baseline conditions. Figure 5.3b shows a fluorescence image of the particles attached to neuron cells. The images were taken using a 40X microscope objective and an exposure time of a 100ms. Digital image analysis indicates that the ratio between the fluorescence intensity of individual lipobeads and the background noise, S/B, is ~ 40. The lipobeads bound to neuronal cellular structures, including individual neuronal processes and cell soma. The lectin-coated lipobeads adhered strongly to the neuronal cell surfaces, and remain attached to these cells during stimulus conditions.
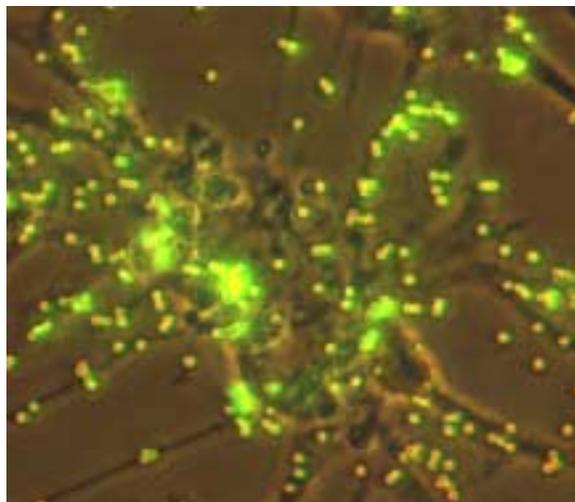
Figure 5.3. Image of 1.6 µm pH sensing lipobeads attached to a confluent cell culture of neurons and glial cells. Light source: 100W mercury lamp. Excitation filter: 460/50; Dichroic mirror: 500nm; Emission filter: BA 515 nm. Objective: 40X with N.A= 0.9. Neutral density: 1.3. Exposure time: 0.1sec. The imaging conditions remain the same throughout the experiments unless stated otherwise.

5.3.3. Photostability of pH Sensing Lipobeads

The photostability of submicrometric sensors is always a concern because of the limited number of fluorophors in each individual particle-based sensor. To test the photostability of the fluorescent lipobeads, samples were placed on the microscope stage and illuminated continuously at 435-485 nm. The fluorescence intensity of the pH sensing lipobeads decreased by about 3 folds during 15 minutes of continuous illumination (data not shown). To overcome this problem, we limited the exposure time and the number of exposures of the fluorescent lipobeads to the excitation light during our kinetic measurements. Figure 5.4 describes the photobleaching of pH sensing lipobeads with 3 different neutral density filters. Following 30 exposures of 100 msec the fluorescence intensity of the pH sensing lipobeads decreased by 65% when a neutral density filter was not used to decrease the excitation intensity (curve a). The utilization of neutral density filters improves the photostability of the lipobeads. The fluorescence

intensity decreased by 40% (curve b), 20% (curve c), and 13% (curve d) when neutral density filters of 0.6, 1.0 and 1.3 were used to decrease the excitation intensity. For this reason, we used a 1.3 OD neutral density filter and a small number of exposure times to minimize the photobleaching problem.
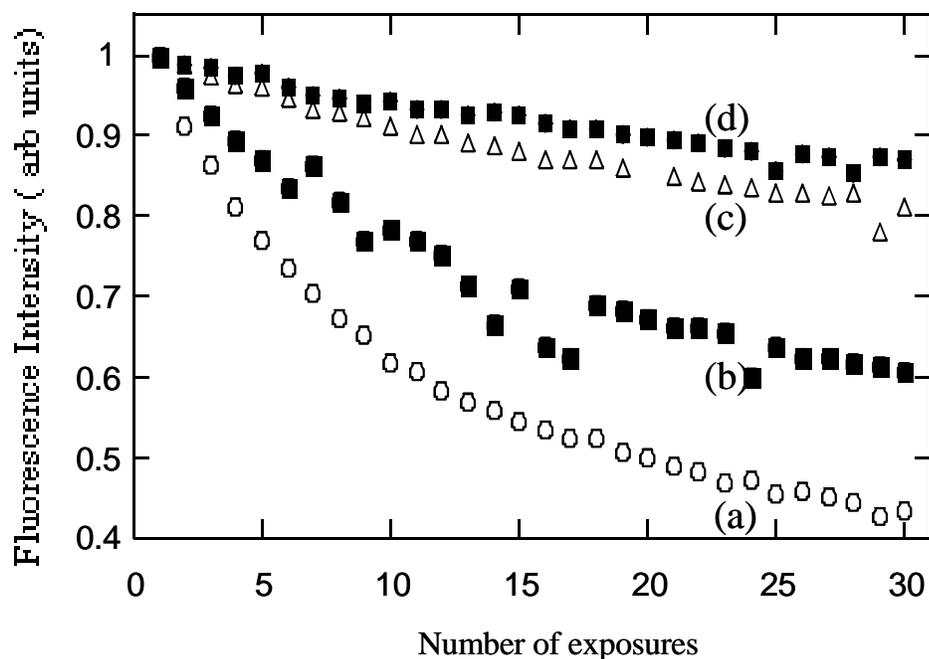
Figure 5.4. Photostability of pH sensing lipobeads using different neutral density filters: (a) 0 OD (b) 0.6 OD, (c) 1.0 OD, and (d) 1.3 OD.

5.3.4. Calibration of the pH Sensing Particles

The pH sensing particles were calibrated against standard solutions of pH 4.5 to 9. The particles were immobilized to the negatively charged surface of a glass cover slip coated with poly-L-lysine. The particles adsorb strongly to the poly-L-lysin surface allowing replacement of solutions over the immobilized lipobeads. To acquire the fluorescence spectrum of the lipobeads 5-10 lipobeads were positioned at the center of the field of view. The field of view was imaged through a slit allowing only the

fluorescence of these lipobeads to be dispersed by the attached spectrograph. A CCD camera was used to collect the fluorescence spectra of these same lipobeads at different pHs. We prepared two types of pH sensing lipobeads to characterize the effect of Succ. ConA on the sensitivity and stability of the pH sensing lipobeads, one type of lipobeads contained fluorescein-DHPE and lectins. The second type of lipobeads contained Succ. Con A labeled with fluorescein (Succ, Con A –FITC). Figure 5.5 shows a comparison between the pH dependence of the fluorescence intensity of lipobeads labeled with fluorescein-DHPE and unlabeled Con A (a) and Succ. Con A–FITC containing lipobeads. A 10% reduction in sensitivity was observed when Succ. Con A-FITC was used for pH measurements. This decrease in sensitivity could be attributed to steric or electrostatic hindrances when FITC is attached directly to the lectinic protein. The dynamic range of both lipobead types was between pH 5 and 8.5 with a pH sensitivity of 0.1 pH units. The response time of the particles was less than 1 second.
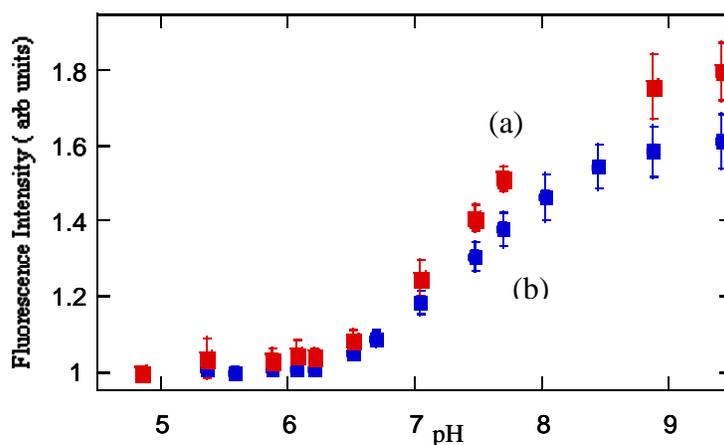
Figure 5.5. A calibraion curve of the pH sensing lipobeads (a) fluorescein DHPE and unlabeled lectin containing lipobeads, and (b) Succ.Con A-FITC labeled lipobeads.

5.3.5. Response of pH Sensing Lipobeads in a Lipobead-Neuron Mixture Induced by Acetazolamide

As previously mentioned the particles bound to neuron cellular structures, including individual neuronal processes and cell soma. During the stimulation, the lipobeads remained bound to cells. The lipobeads maintained their structural integrity and fluorescence intensity for more than 24 hours. To demonstrate the utility of these fluorescence-sensing particles we used them to monitor the extracellular pH when the cells were exposed to increasing concentrations of acetazolamide. Acetazolamide is a membrane – permeate carbonic anhydrase inhibitor that causes rapid inhibition of interstitial carbonic anhydrase activity leading to extracellular acidification and acidic spreading depression [192]. Similar results were previously observed when neurons were exposed to elevated concentration of KCl [193]. Cell swelling occurred minutes after CSD was induced by a single exposure of acetazolamide. It is characterized by a complete breakdown of ion gradients and an uptake of extracellular fluid into the intracellular compartment. Exposure of cortical neurons to acetazolamide resulted in marked extra- and intracellular pH shifts. The fluorescence intensity at 525 nm decreases by about 50% indicating a pH decrease of 0.5 units. Figure 5.6 describes the temporal dependence of the pH of the sensing lipobeads during the induced cortical spreading depression process triggered by (a) 0, (b) 5, (c) 10, and (d) 20 mM acetazolamide. A sharp drop in the fluorescence of the lipobeads was observed when the cells were exposed to acetazolamide. The acidic shift was prolonged and enhanced over time. There was no recovery of extracellular pH (pHe) following the removal of acetazolamide from the sample after 40 minutes. These results are in agreement with previous studies that

use pH electrodes to quantify extracellular pH changes during CSD. However, the use of high-resolution digital fluorescence imaging and spectroscopy allows us to monitor in real time the pH response of individual primary cortical neurons to conditions of CSD.
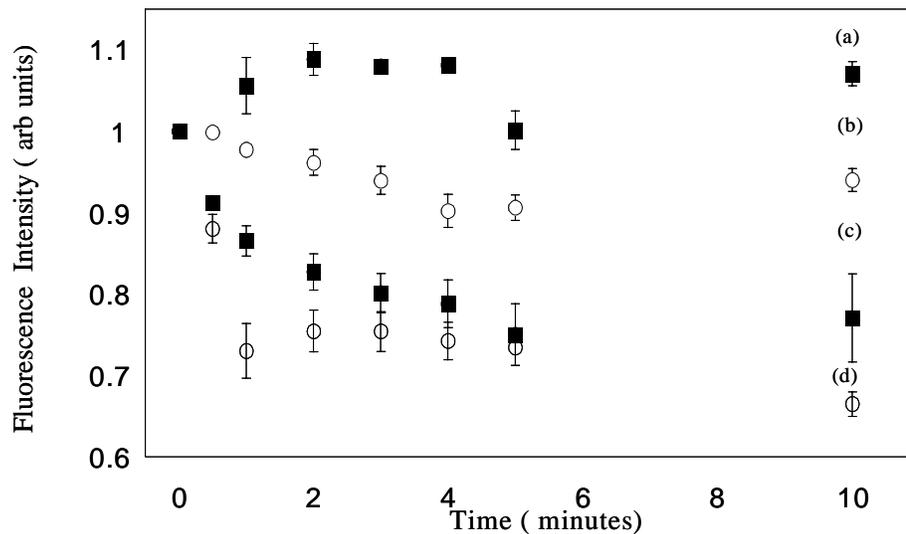
Figure 5.6. Temporal response of the pH sensing lipobeads during to the application of acetazolamide - (a) acetazolamide free solution   (b) 10 mM acetazolamide (c) 15 mM acetazolamide (d) 20 mM acetazolamide

Figure 5.7describes the response of individual cells from 3 different wells to induced spreading depression caused by 10 mM of acetazolamide. It is clearly seen that the cells response to acetazolamide varies greatly from cell to cell. This contributes greatly to the large variation observed in the kinetic data. Furthermore, the ability of the cells to recover from acidic spreading depression depends on the number of unaffected cells in a well. Cell cultures recovered from the acidic depression only when adjacent cells were not affected by the acidic conditions. Our results suggest that neuron cells cannot survive when isolated from other neuron cells or astrocytes in culture.
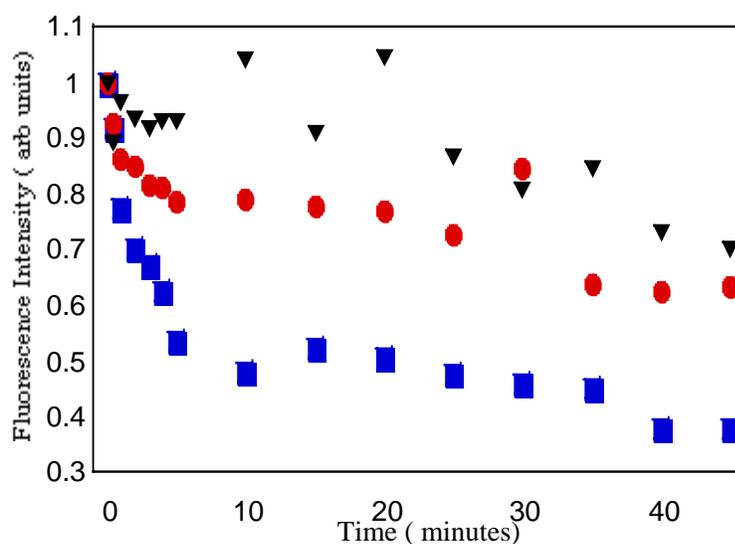
Figure 5.7. The response of cells from 3 different wells to induced spreading depression caused by 10 mM of acetazolamide.

5.4. Summary

In the present study we show that adhesive molecules like lectins are easily incorporated into the phospholipid membrane of lipobead-based sensors. The lectinic residues enable us to target the lipobeads selectively to neuron cells in culture. The micrometric lectin-coated lipobeads adhered to the neuronal cell soma and processes, remaining attached to the neurons in culture for up to 13 days without slowing cell growth or affecting cell viability. The lipobeads remained stably attached to the cells under depolarizing conditions. This is a very important observation, which suggests that lipobeads could not only be used for ion measurements of neuron functions but also as submicrometric carriers in future drug delivery applications. Our site-specific pH sensors show that exposing cortical neurons to mM concentrations acetozalamide causes depolarization of the membrane and a change in extracellular pH at the proximity of the cells of up to 0.5 pH units. The use of high resolution fluorescence imaging and

spectroscopy system allows us to monitor in real time dynamic pH changes during depolarization induced cortical spreading depression in rat cortical neurons. Our results are in agreement with previous work done on global extracellular pH change measurements during cortical spreading depression. However, with the current system, we can target where pH measurements are made and possibly reveal subpopulations of different responses in real time. Presumably, the choice of different lectin coatings and/or lipobead composition might assist in targeting different cell types. The next chapter focuses on the use of sensing lipobeads to measure chemical changes at the neuronal surface, which is in which free zinc ion sensing fluorophors and confocal microscopy are employed to follow zinc ion bursts in cells. The approach is to synthesize new sensing particles where the hydrophobic indicator, which is zinc ion sensing fluorophor, is embedded in the lipid-like layer. The technique not only improves the chemical and photostability of particle-based fluorescence nanosensors, but also enables hydrophobic indicators to be used for sensing applications in aqueous samples. This new lipobead-based fluorescence sensing technique is simpler than currently used zinc ion detection methods cells during experiments that last more than 40 minutes.

CHAPTER SIX: A LIPOBEAD-BASED ZINC ION FLUORESCENCE PROBE FOR
TARGETED RELEASE MEASUREMENT OF ZINC IONS FROM SINGLE NEURON
CELLS

6.1. Introduction

Zinc is one of the most abundant metals in the body. It is required by all cells

and plays a critical role in the control of gene transcription and metalloenzyme function.

Zinc ions are required for brain development and are needed for various brain functions.

In the central nervous system (CNS), zinc ions mediate cell-cell signaling. Moreover,

zinc ions function as endogenous neuromodulators of several important receptors

including the γ – aminobutyric acid (GABA) and N-methyl-D-aspartate (NMDA)

receptors. Neurons containing zinc ions sequester zinc ions in presynaptic vesicles and

release them in a calcium dependent manner. These neurons are thought to form neural

circuits of learning and memory functions. The CNS contains a high level of chelatable

zinc ions, which are primarily localized in the synaptic vesicles of excitatory nerve

terminals. Zinc ions are released from neurons by high K^+ or electrical stimulation of

the perforant path and then translocated from presynaptic sites into postsynaptic

neurons [194-201].

Zinc ion release has been characterized as similar to that of neurotransmitters: it

is Ca^{2+}- dependent and tetrodotoxin-sensitive [202]. One possible synaptic signaling role

for zinc ions is revealed by its interaction with amino acid receptors such as the NMDA,

AMPA, and GABA subtypes [203-204]. While this and other evidence suggests that zinc ions may act in concert with neurotransmitters such as glutamate in the CNS, a specific role for synaptically released zinc ions in physiological and pathological processes appears complex, and has yet to be defined. Zinc ions, which are synaptically stored in the brain, were shown to elicit neurotoxicity after brief exposure to cortical neurons in culture [205]. Moreover, the synaptic localization of zinc ions appears to have great negative potential as far as neuronal health when the release of zinc ions is uncontrolled as is occurred in stroke and epilepsy.

Currently, zinc ions in the nervous system can be detected using classical histochemical methods, i.e. Timm's stain [206], the sulphide-osmium method [207], and a fluorochrome based stain [208]. These histological methods cannot trace real-time events. More recently, real-time zinc ion indicators have been developed and utilized in living neuron cells. However, these have demonstrated zinc ion release by disappearance of an intracellular loaded dye [209], or by detecting global zinc ion release outside of the neuronal tissue [210]. The ability to visualize targeted and site-specific (as opposed to global) zinc ion release external to the neurons has thus been lacking.

In this chapter, the fabrication of submicrometric lipobead-based zinc ion fluorescence probes is described. The small size of these sensors, combined with the techniques to attach the lipobeads to the neuronal surface, provide an important advancement in visualizing zinc ion synaptic release events.

6.2. Specific Experimental and Technical Details

a) Synthesis of TSQ - immobilized lipobeads

Four milligrams of polystyrene were suspended in 100 μl ethanol/hexane solution (1:1 v/v). 50 mM lipid stock solution with a 5:4:1 molar ratio of dimyristoylphosphatidylcholine, cholesterol, and dihexadecyl phosphate in chloroform. To prepare zinc-sensing lipobeads, the lipid mixture was added to 100 μl of 9.44 mM TSQ and sonicated for 15 minutes by using a 47 KHz Bransonic sonicator. The mixture was then added to the particle suspension and sonicated again for 15 minutes. The whole mixture was incubated at room temperature for 2 hours and dried under nitrogen at room temperature overnight. The dried suspension was then resuspended in 1 ml of phosphate buffer pH 7.0 and sonicated for 15 minutes. The suspension is incubated for 2 hours to allow the indicator and the phospholipid molecules to absorb onto the surface of the particles. During these coating steps, there is a simultaneous formation of liposomes formed in addition to the coated particles. These formed liposomes, free unbound TSQ molecules, and unbound microsphere particles were easily removed by centrifugation a few times at 1500 rpm, 15 minutes each. The coated lipobeads with TSQ molecules and phospholipids were collected at the bottom of the glass centrifuge tube while the supernatant and unbound beads were discarded. The TSQ- incorporated lipobeads were resuspended in 1 ml of phosphate buffer pH 7.0 and stored in a glass test tube covered with aluminum foil at room temperature until use.

b) Immobilization of lipobeads on the surface of chambered coverglass for zinc sensitivity measurements

To immobilize the lipobeads, a chambered coverglass (borosilicate, Nalge Nunc International) is dipped in 70% ethanol/water for 15 minutes. The chambered coverglass is dried by placing it in a 60 ^{0}C oven for 5 minutes. The chambered coverglass is then incubated in a 200µl solution of 10 % poly-L-lysine for 2 hours. It is then drained and dried in a 60°C oven for 1 hour. A 200µl lipobead suspension is then placed in the chambered coverglass for 3 hours. The unimmobilized lipobeads are then rinsed out with a phosphate buffer at pH 7.0.

c) Preparation of rat cortical neurons and cell culture plates for imaging

Primary cultures of rat cortical neurons were prepared and grown in neuronal culture medium as previously described in section 2.5. 200 µl of prepared lipobeads were added into the 2 ml of culture media already in the petri dish. Coverslips were incubated with beads in CO_2 incubators as above for 2 hours. Immediately before imaging coverslips, dishes were washed extensively (5 exchanges of 2 ml volume) with Locke's solution pH 7.4, lacking $MgCl_2$. Coverslips were then imaged in the petri dish in 2 ml of Locke's solution with an Olympus inverted microscope and a slow scan CCD.

6.3. Results and Discussion

6.3.1. Choice of Indicator

The fluorescent molecular probe, N- (6-methoxy-8-quinolyl)-p-toluenesulfonamide (TSQ), was used as extrinsic fluorescence sensing probe for the

quantitative measurements of zinc ion release from the depolarization-induced release of zinc from rat cortical neurons. TSQ is selective for zinc ions in the presence of physiological concentrations of Ca^{2+} and Mg^{2+} ions. TSQ has an excitation wavelength at 367nm and emission wavelength at 495 nm. The incorporated TSQ molecules react with zinc ions to form a highly fluorescent complex, which has a stoichiometry of two dye molecules per metal atom (shown in figure 1.6) [211]. Although the probe itself is fluorescent, its fluorescent intensity is negligible relative to that of the Zn-complex.

(a)　　　　　　　　　　　　　　　(b)
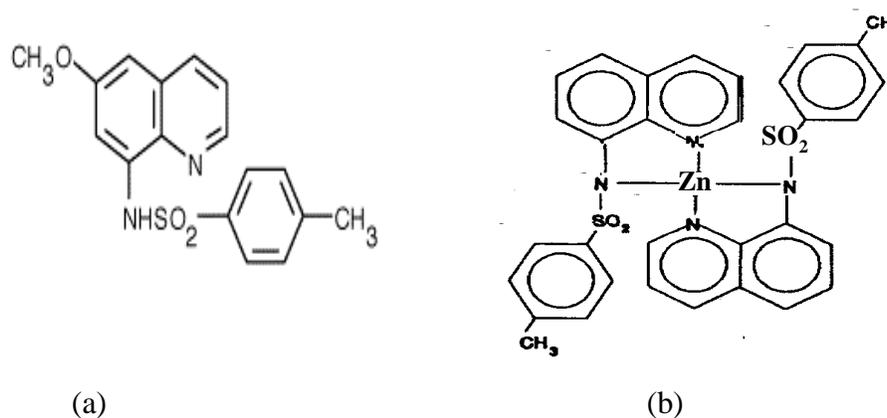
Prat, M.D. et al, *Journal of Fluorescence,* **1(4)** (1991)

Figure 6.1. Zinc ion sensing dye and its complex (a) N- (6-methoxy-8-quinolyl)-p-toluenesulfonamide (TSQ) (b) Complex of TSQ with Zn (II).

TSQ has been used to measure Zn^{2+} levels in artificial lipid vesicles and live sperm cells by flow cytometry [212]. In these studies, the fluorescence yield of the TSQ- Zn^{2+} complex was shown to be much higher when bound to lipids than in aqueous solution.

6.3.2. Zinc Ion Sensing Lipobeads in Aqueous Solution

Figure 6.2. shows a fluorescence image of zinc ion sensing lipobeads. The TSQ-embedded lipobeads show weak fluorescence in the absence of zinc ions. When placed in a solution of 1 µM zinc ions the formation of a complex between zinc ions and TSQ ligands leads to about 10-fold increase in the fluorescence intensity of the lipobeads. The images are taken using a 40× microscope objective and an exposure time of a 100ms. Digital image analysis indicates that the ratio between the fluorescence intensity of individual lipobeads and the background noise, S/B, is ~ 40. The sensing lipobeads show a variation of 10% in the average signal intensity.
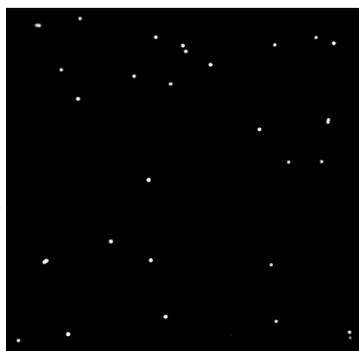
Figure 6.2. Digital fluorescence image of 2.1µm zinc sensitive lipobeads. Light source: 100W mercury lamp. Excitation filter: D480/30X; Dichroic mirror: 500nm; Emission filter: BA 515nm. Objective: 20X with N.A= 0.5. Neutral density: 1.0. Exposure time: 0.5sec. The imaging conditions remain the same through the experiments unless otherwise stated.

6.3.3. Calibration of the Zinc Sensing Particles

The particles were immobilized to the negatively charged surface of a glass cover slip coated with poly-L-lysine. The particles adsorb strongly to the poly-L-lysine surface allowing replacement of solutions over the immobilized lipobeads. To acquire the fluorescence spectrum of the lipobeads 5-10 lipobeads were positioned at the

center of the field of view. The field of view was imaged through a slit allowing only the fluorescence of these lipobeads to be dispersed by the attached spectrograph. A CCD camera was used to collect the fluorescence spectra of these same lipobeads at different zinc ion concentrations. Zinc sensing lipobeads are added to either pH 7.0 buffer or Locke's buffer containing 2.3 mM $CaCl_2$ to characterize selectivity of the zinc sensing lipobeads.
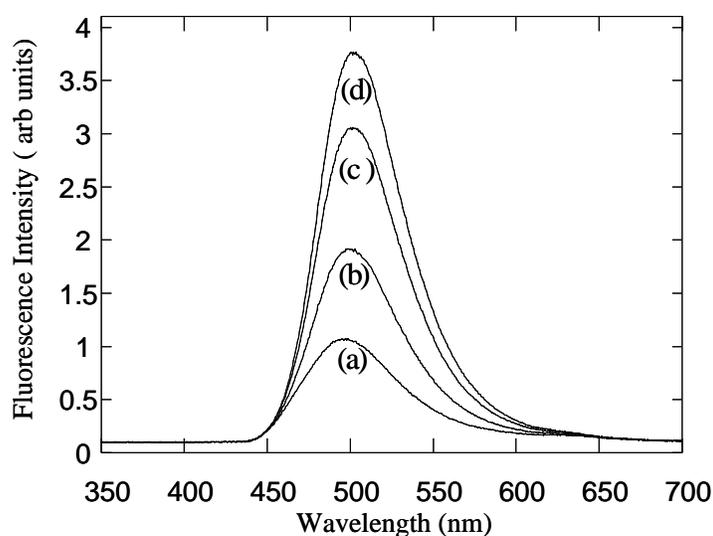
Figure 6.3. A spectrum of zinc sensing concentration dependence of TSQ lipobeads. Concentrations of zinc ions (a) 0, (b) 0.01, (c) 0.10, and (d) 8.40 μM.

Figure 6.3 describes the fluorescence spectra of solutions of various zinc ion concentrations and TSQ containing lipobeads. The fluorescence increase was measured using spectrofluorometry and digital fluorescence imaging microscopy. The excitation light was at 360 nm and the emission was observed at 480 nm. The peak maxima of the fluorescent lipobeads are similar to that of free TSQ in solution. The fluorescence of TSQ increases with increasing zinc ion concentration due to the

formation of a Zn $(TSQ)_2$ complex. A 4-factor of magnitude dynamic range between 10 nM and 10 μM is observed. Figure 6.4 shows a comparison between the zinc ion dependence of the fluorescence intensity of lipobeads. As shown in Figure 5.4, TSQ-lipobeads show high sensitivity to Zn^{2+} with a linear dynamic range of 0.01 - 2 μM. The lipobeads are selectively to zinc ions and did not respond to calcium ions at physiological levels. The measured limit of detection is 10 nM.
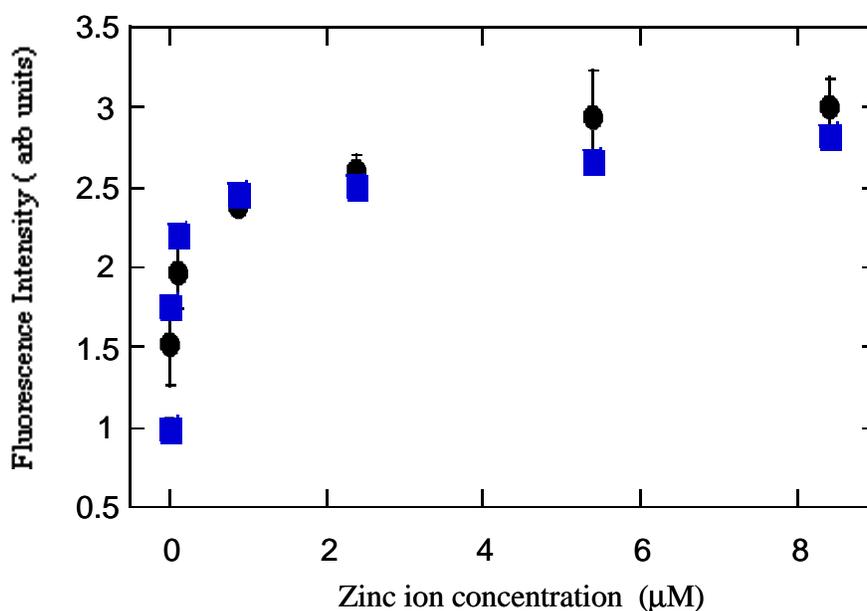
Figure 6.4. A zinc calibration curve of the zinc sensing lipobeads in pH 7.0 buffer●
and in Lockes' buffer containing 2.3 mM $CaCl_2$.■

6.3.4. Photostability of Zinc Sensing Lipobeads

The photostability of submicrometric sensors is always a concern because of the limited number of fluorophors in each individual particle-based sensor. To overcome this problem, we limited the exposure time and the number of exposures of the fluorescent lipobeads to the excitation light during our kinetic measurements. Figure

6.5 describes the photobleaching of zinc sensing lipobeads with 2 different neutral density filters. Following 30 exposures of 100 msec the fluorescence intensity of the zinc sensing lipobeads decreased by ~60% when a neutral density filter of 1.0 was used (curve b) to decrease the excitation intensity. The utilization of neutral density filters increased the photostability of the lipobeads. The fluorescence intensity decreased by ~ 13% (curve a) when neutral density filters of 1.3 was used to decrease the excitation intensity. For this reason, we used a 1.3 OD neutral density filter and a small number of exposure times to minimize the photobleaching problem. No substantial photobleaching was seen under these conditions.
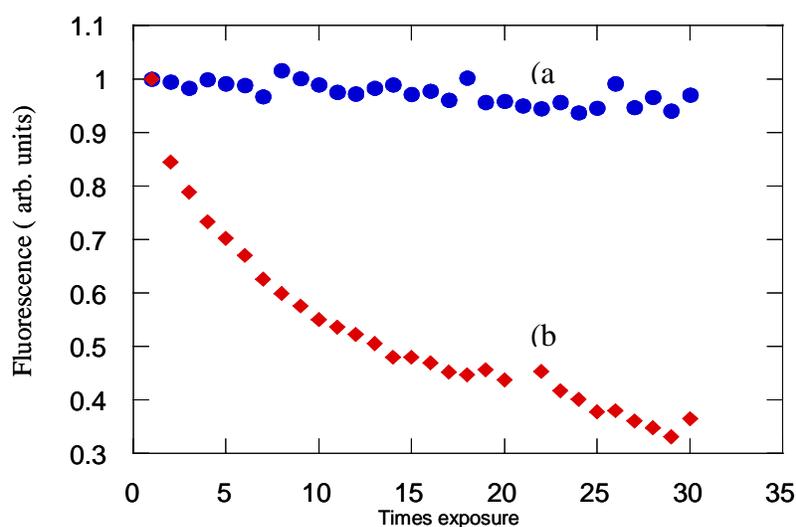
Figure 6.5 Photostability of zinc sensing lipobeads using different neutral density filters: (a) 1.3OD, and (b) 1.0 OD

6.3.5 Selectivity of Zinc Ion Sensing Lipobeads

The response of the zinc ion sensing particles to increasing zinc, calcium and magnesium ion concentrations is described in Figure 6.6.
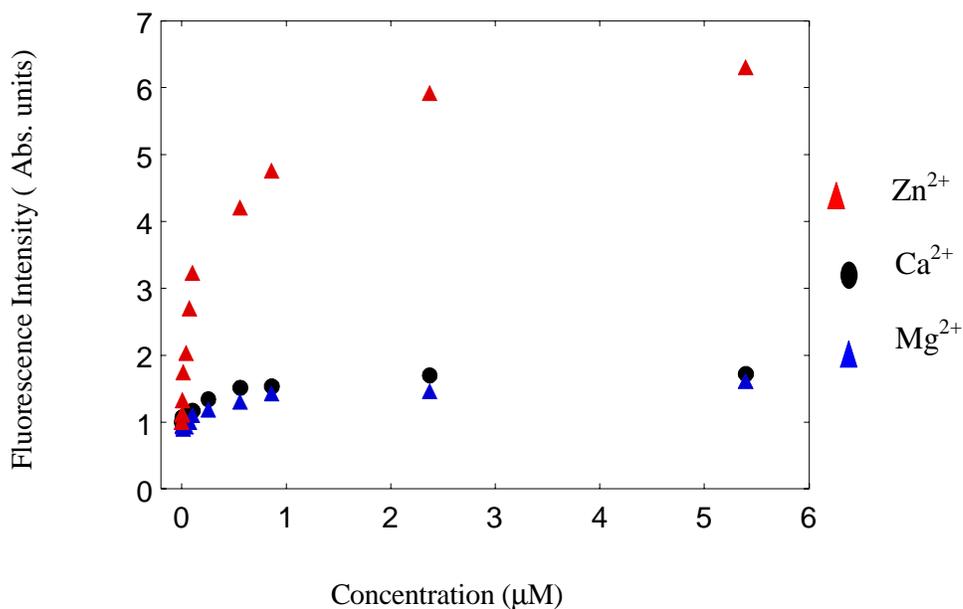
Figure 6.6. Selectivity of zinc sensing lipobeads

The fluorescence intensity of the lipobeads increases by 6 folds in a 5 μM zinc ion solution compared to zinc ion free solution. Similar levels of calcium and magnesium ions increase the fluorescence intensity by about 30%. More importantly the effect of these ions is saturated at these concentrations. This observation is of particular importance since zinc ion release measurements from neuron cells in culture are conducted in a Locke's buffer containing mM levels of calcium ions.

6.3.6. Response of Zinc Sensing Lipobeads in a Lipobead/Liposome Mixture

To demonstrate the utility of these zinc-sensing particles, these zinc sensing lipobeads were used to monitor the release of zinc ion from liposomes encapsulating $ZnCl_2$. The response of TSQ lipobeads to liposomes containing zinc ion in aqueous solution is shown in Figure 6.7. The liposomes are lysed with a detergent to release the zinc ion content. The fluorescence increase, resulting from leaking of zinc ion from liposomes, is measured as a function of time. The fluorescence of the lipobead increases up to nearly 4 folds right at the time of adding zinc containing liposome solution. This shows that the technique has the sufficient sensitivity to monitor the secretion of zinc ions from cells.
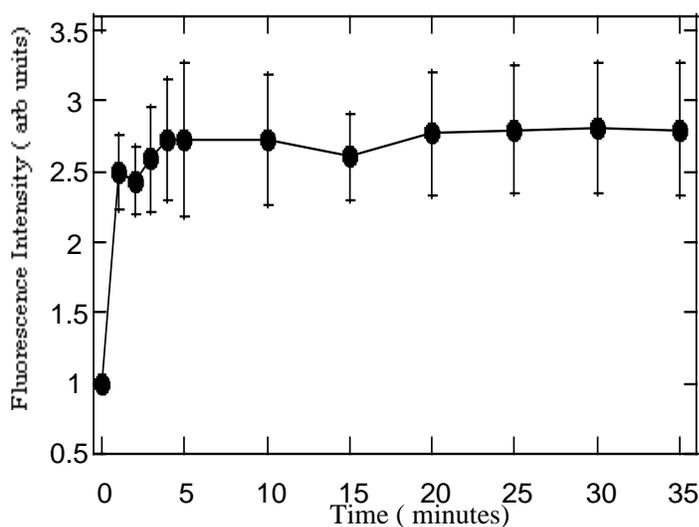
Figure 6.7. Fluorescence response of zinc sensing lipobeads upon the addition of zinc containing liposome solution over the period of time.

6.3.7. Site Specific Zinc Sensing Lipobeads Targeting to Rat Cortical Neurons

In a previous chapter, the attachment of lectins to micrometric phospholipid coated polystyrene beads has been applied successfully. To demonstrate the ability of

lectins to attach the zinc ion sensing particles to neuron cells, these 1.6 μmeter zinc sensing lipobeads, which embedded glycinemax manose binding lectin, were incubated with neuron cells for 2 hours under cell culture conditions. Unbound beads were washed off cover slips with 5 exchanges of medium with Locke's solution. Transmission phase images of the particles attached neuron cells are shown in Figure 6.8. Figure 6.8 a shows a phase image of beads attached to cells and the culture cover slip. Figure 6.8 b shows a digital fluorescence image of the beads.
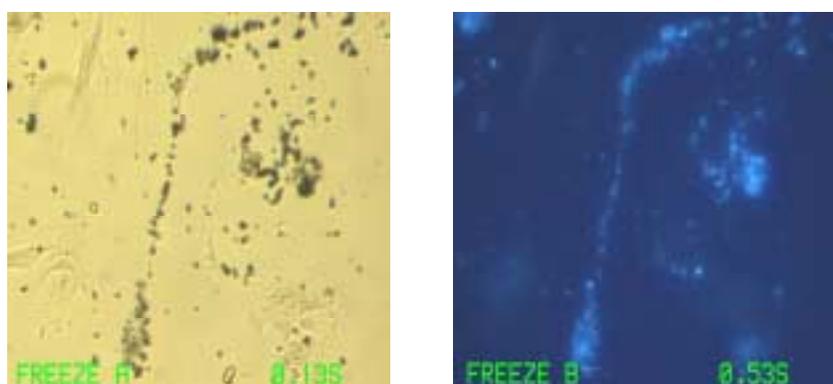
Figure 5.8. Phase and digital fluorescence images of TSQ-Glycine max lipobeads/ rat cortical neuron mixture. Light source: 100W mercury lamp. Excitation filter: BP 330-385; Dichroic mirror: 400nm; Emission filter: BA 420 nm. Objective: 40X with N.A= 0.9. Neutral density: 1.3. Exposure time: 0.1sec

While it is possible to target neurons with phospholipid coated polystyrene particles containing lectins, the physical attachment of lectins to the phospholipid membrane of the particles has been inconsistent.

6.4. Summary

In the study, the water-insoluble dye, N- (6-methoxy-8-quinolyl)-p-toluenesulfonamide (TSQ) and adhesive molecules are easily incorporated into the

phospholipid membrane. The zinc sensing lipobeads could be used to measure zinc ion concentrations in volume limited aqueous samples and to monitor the release of zinc ions from neurons in culture. These studies prove that particle-based sensors have the capability to quantitatively monitor cellular release events. Furthermore, this new measurement technology is unique since the ion probe is positioned at or near the site of release where the ion concentration is much higher than the ion concentration in the diluted bulk solution. Our experiments show that the attachment of lipobeads to the cells does not affect their viability for up to 14 days. This is a very important observation, which suggests that lipobeads could not only be used for ion measurements of neuron functions but also as submicrometric carriers in drug delivery applications. Experiments to this end are currently being conducted in the laboratory.

CHAPTER SEVEN: CONCLUSIONS AND DISCUSSIONS

The advantages of using fluorescence detection, rather than absorbance methods, in medical testing, biotechnology, and drug discovery include high sensitivity and signal specificity. Combined with a variety of optochemical probes and sensors, imaging fluorescence microscopy has become a primary choice for single cell analysis. A fluorescence bio/chemical sensor designed for single cell measurements must be highly compatible with the cellular environment, show low cytotoxicity, and high chemical stability as well as photostability.

During the last four years I introduced a new analytical sensing technology that is based on fluorescent liposomes. The main advantages of liposomes include their biocompatibility, ability to effectively encapsulate hydrophilic or hydrophobic fluorescent probes and the sensitivity of their fluid-like membrane to temperature and pH. Chapter 3 presents a new method for physical immobilization of polar fluorescence dyes in a sensing support. The method is based on the immobilization of fluorescence dye encapsulating liposomes in a sol-gel film of micrometer thickness. This is the first example of liposome- based sensors. The encapsulation of the dye molecules in the liposomes effectively increases the molecular dimensions of the sensing reagent, thus prevents its leakage from the matrix support. This chapter describes the analytical properties of a pH sensor fabricated by immobilizing carboxyfluorescein-encapsulating liposomes in a sol-gel thin film. The sensor shows excellent stability with respect to dye

leaking, which in turn leads to high reproducibility and sensitivity of about 0.05 pH units. The linear dynamic range of the sensor is between pH 6 and 7.5 and its response time is at the sub-seconds time scale. Chapter 4 describes the development of calcium ion sensor as another example of a liposome-based biosensor. It employed a calcium ion binding protein for recognition and a sensing fluorophore for signal transduction. To fabricate the sensor, Alexa-488 labeled calmodulin (CaM) molecules were encapsulated in the membrane of liposomes. Upon binding calcium ions, CaM shows large structural rearrangements from the " closed" conformation (the two helices of each hand are almost anti-parallel) to the "open" conformation (the two helices are more perpendicular). This conformation change strongly affected the fluorescence intensity of the fluorophore Alexa-488 that was covalently bound to calmodulin. Liposomes containing Alexa-labeled calmodulin show sensitivity to calcium ions in the micromolar range. The calcium ion response of the liposomes was 4 folds higher than the calcium ion response of Alexa-labeled calmodulin in solution. This was attributed to the increasing stability of calmodulin when embedded in the liposome membrane. Unlike in commonly used fluorescence indicators, physiological levels of magnesium ions did not interfere with the calcium ion response of Alexa-CaM containing liposomes. It was not possible to use the fluorescence sensing liposomes for cellular measurements due to their instability in the cellular environment. The lipsomes fuse with the neurons and released their content inside the cell. This led to the development of fluorescence sensing lipobeads.

To overcome the high leakage rate and poor stability in the cellular environemt, phospholipid-coated particles lipobeads are synthesized and used as particle-based fluorescent sensors in single cell measurements. Lipobead- based sensors are for the first

time designed to focus on the improvement of liposome- based sensors. The new hybrid sensing particles with cell-like lipid bilayer surfaces similar to natural cells combine complementary advantages of liposomes and polymeric beads. The use of phospholipid coating enables the stable immobilization of hydrophilic and hydrophobic indicators to the particles and provides the protection of the dyes from the complex cellular environments. The technique is highly versatile since it is also possible to incorporate biomolecules such as antibodies, enzymes, and receptors into the membrane of the particles and use them as selective and sensitive biosensors. These unique particles could be applied to measure the level of intracellular ion flux in a non-invasive manner with high reproducibility, selectivity and sensitivity. The newly prepared fluorescent sensing lipobeads show significant improvement in mechanical stability and size homogeneity compared to liposomes.

Chapter 5 describes the miniaturization of pH sensitive lipobeads and the applications of these fluorescence lipobeads as sensors in targeted, real time kinetic studies of extracellular pH changes in cortical neuron cells under conditions simulating cortical spreading depression. Succinyl Concanavalin A (Succ. Con A), which is a carbohydrate-specific binding membranal protein, was incorporated into the phospholipid membrane of the lipobeads and used to target the lipobeads to the membrane of neuron cells. The unique hydrophobic core-hydrophilic shell structure of the lipobeads enabled stable immobilization of the protein in the lipobead membrane while maintaining the mono-dispersity of the particles in aqueous solution. The lipobeads were highly biocompatible and did not cause cell death or structural changes to the cells even during long experiments that lasted up to 14 days. The biocompatibility of the lipobeads is

attributed to the similarity between the phospholipid membranes of the lipobeads to the cell membrane. Site-specific pH sensors show that exposing cortical neurons to acetazolamide causes a depolarization of the membrane and a large change in extracellular pH at the proximity of the cells of up to 0.3-0.5 pH units. It is importantly noted here that lipobead based sensors revealed differences in the response of different neurons to conditions of chemical injury. This is the first time that an analytical technique shows a clear difference in the response of different neurons to injury like conditions.

Chapter 6 describes the fabrication of zinc sensing lipobead-based sensors. The micrometer -sized sensor was prepared by immobilizing N- (6-methoxy-8-quinolyl)-p-toluenesulfonamide (TSQ) to the phospholipid coating of the particles. The incorporated TSQ molecules react with zinc ions to form a highly fluorescent complex. The fluorescence intensity of these lipobeads is zinc ion concentration dependent. TSQ-lipobeads were used effectively to monitor the release of zinc ions from liposomes. TSQ-lipobeads show high sensitivity to Zn^{2+} with a dynamic range of 0.1 - 2 μM. The lipobeads are selective to zinc ions and did not respond to calcium ions at physiological levels. The application of the zinc ion sensing lipobeads for zinc ion release from neuron cells proved to be problematic because of the very small number of zinc containing vesicles in prenatal primary neurons and neuron cell-lines. And also the unavailability of zinc containing neurons prevented the application of zinc ion sensitive lipobeads for real time zinc ion release measurements in neuron cell cultures. Currently the study is to focus on using the lipobeads to monitor zinc ion release from preloaded cells.

These studies show that compared to other sensing techniques, such as electrodes or particle-based sensors, lipobeads are non-invasive, and biocompatible because of the

unique phospholipid membrane. The cytotoxicity of the dye, and the unwanted interactions between the dye and cellular interfering species are minimized. However, there are several limited factors that need to be addressed for increasing the precision and accuracy of the quantitative power of miniaturized sensors. Lipbead based fluorescence sensors need to be miniaturized to nanodimensions. Size reduction of lipobeads down to nanometer scale will increase the spatial resolution of these sensors. This also implies that miniaturization of the sensors to nanometer scale would result in a decrease in the number of sensing fluorophores available for sensing per particle, which translates to lower signal to noise ratio and limited analytical performance. Previous studies that utilized nanometric particle-based sensors like PEBBLEs in cellular applications were based on the incorporation of a large number of particles (hundreds and more) into cells. The signal was measured from an ensemble of particles rather than from individual particles. This is remaining a problem, particularly because the concentration of the sensing dye in the particles cannot be higher than the self-quenching limit of the sensing dyes. It is possible to compensate for the loss of fluorophores due to miniaturization by increasing the excitation power. However, increasing the excitation power will lead to a rapid photobleaching of the sensor since the photostability of the organic sensing dyes is limited. In the future, this could be done with a significant improvement of the imaging instrumentation such as a CCD camera with highly improved sensitivity and signal to background ratio, electronic shutters to enable illumination of the observed lipobeads only during actual CCD exposure times, and a laser port to enable illumination of the sample with laser beams to enhance the fluorescence signals obtained from the beads. A laser based digital imaging fluorescence microscope will also provide a higher precision.

The reason is that there is about ~5% fluctuation of the light source, the mercury lamp. This might add to the error found in the data. Difficulties in separating between the nanometric lipobeads and the excess of phospholipids and fluorophores used to coat the polystyrene particles might be encountered during the process of nanometric lipobead synthesis. Increasing the speed of centrifugation and lengthening the centrifugation time degraded the structure of the lipobeads due to excessive heat and led to their aggregation. Improvement in centrifugation conditions will include the use of a temperature-controlled centrifuge. This will enable the use of longer centrifugation times at low speed and low temperature to precipitate the nanometric size lipobeads.

Improvement of the lipobead system will also include the covalent attachment between the phospholipid membrane, indicator, and the core surface of the particles to increase the stability of the sensors. It is also desirable to control the synthesis in order to achieve more homogenous particle formulations, as well as to develop better data processing techniques since the large number of observed particles would generate huge amount of data in 5 dimensions (x, y, z, intensity, spectrum).

Lastly, it is sometimes unreliable to use fluorescence intensity-based measurements for variety of reasons. The sensing method is based on the fluorescence intensity of the probe changing in response to the analyte. Changes often occur in fluorophores due to quenching by oxygen or other interfering substances. Also due to inherent chemical and poor photostability problems of organic fluorophores, the intensity based sensing sensors are limited in their applicability in the cellular environment to relatively large changes in analyte concentration that lead to fluorescence signal changes of at least 10%. One approach is to replace the organic fluorophors with luminescent

semiconductor nanoparticles, quantum dots. Luminescent quantum dots offer significant advantages over organic fluorophors such as higher emission quantum yield, higher chemical and photostability. Another approach is to design new mechanisms for signal generation that are not based only on intensity measurements such as fluorescence resonance energy transfer (FRET). The development of FRET based lipobeads is under construction in our laboratory. In FRET sensing mechanisms, the signal transduction generation is based on the use of a biomolecular recognition component to selectively bind the analyte of interest to the beads and on FRET between donor and acceptor fluorophores. In this case, the sensor's response would not depend on direct interaction between an analyte and an analyte selective fluorophore. The response of the sensor will be given as a ratio between the donor and acceptor emission.

REFERENCES

1. Georganopoulou, D.G., Carley, R., Jones, D.A., and Boutelle, M.G. *Faraday Dicuss.* **2000**, 116, 291-303.

2. Brauel, M., Kopelman, R., Miller, T., Tjalkens, R., and Philbert, M.A *Anal. Chem* **2001**, 73 (10), 2221-2228.

3. Schuhmeier RP, Tewes S, Szentesi P, and Melzer W., *Pflugers Arch* **2000**, 439(3), 385-93.

4. Aspinwall, C.A.; Huang, L.; Lakey, J.R.T., and Kennedy, R.T. *Anal Chem* **1999**, 71 (24), 5551-5556.

5. Zhou, Z.; and Misler, S. *Proc. Natl. Acad. Sci. U.S.A.* **1995**, 92, 6938-6942.

6. Griffith, A.W.; and Cooper, J.M. *Anal. Chem*. **1998**, 70, 2607-2612.

7. Bratten, C.D.T.; Cobbold, P.H.; and Cooper, J.M. *Anal. Chem*. **1998**, 70, 1164-1170.

8. Kissinger, P.T.; Hart, J.B.; and Adams, R.N. *Brain Res*. **1973**, 55, 209-213.

9. Adams, R.N. *Prog. Neurobiol*. **1990**, 35, 297-311.

10. Zimmerman, J.B.; and Wightman, R.M. *Anal. Chem*. **1991**, 63, 24-28.

11. Wightman, R.M.; Jankowski, J.A.; Kennedy, R.T.; Kawagoe, K.T.; Schroeder, T.J.; Leszczyszyn, D.J.; Near, J.A.; Diliberto, E.J., Jr.; and Viveros, O.H. *Proc. Natl. Acad. Sci. U.S.A.* **1991**, 88, 10754-10758.

12. Weng, Q. , and Jin, W. *Electrophoresis* **2001**, 22(13), 2797-803.

13. Jin, W., Li, W., and Xu, Q. *Electrophoresis* **2000**, 21(4), 774-9.

14. Michael DJ, and Wightman, RM *J Pharm Biomed Anal* **1999,**19(1-2), 33-46.

15. Dong, Q.; and Jin, W. *Electrophoresis* **2001**, 22(13), 2786-92.

16. Anderson, BB; and Ewing, AG *J Pharm Biomed Anal* **1999**,19(1-2), 15-32.

17. Snanek, F.D.; Chen, G., and Ewing A.G. *Anal. Chem.* **1996**, 68, 3912-3916.

18. Henry, J.P.; Darchen, F.; and Cribier, S. *Biochimie* **1998**, 80, 371-377.

19. Jardemark, K.; Orwar, O.; Jacobson, I.; Moscho, A.; and Zare, R.N. *Anal. Chem.* **1997**, 69, 3427-3434.

20. Wilson, G.S.; and Hu, Y. *Chem. Rev*. **2000**, 100(7), 2693-2704.

21. Lakowicz, J. Principles of Fluorescence Spectroscopy, 2 nd Ed., Kluwer Academic/Plenum Publishers: New York, **1999**.

22. D'Auria, S., and Lakowicz, J.R., *Current Opinion in Biotechnology* **2001**,12, 99-104.

23. Rethi B, Detre C, Gogolak P, Kolonics A, Magocsi M, and Rajnavolgyi E. *Cytometry* **2002**, 47(4), 207-16.

24. Richards B, Zharkikh L, Hsu F, Dunn C, Kamb A, and Teng DH. *Cytometry* **2002**, 48 (2), 106-12.

25. Colavita, A.; Capello, G.; Ijaduola, RB.; Cunei, A.; Lagostena, L.; and Canepari, M. *Proceedings of SPIE-The International Society for Optical Engineering* **1999**, 3604(Optical Diagnostics of Living Cells II), 100-106.

26. Li, Y.; Sasaki, S; Inoue, T; Harata, A; and Ogawa, T. *Applied Spectroscopy* **1998**, 52(8), 1111-1114.

27. McNamara, K.; Yeung, ES.; Rosenzweig, N; and Rosenzweig, Z., *Analytica Chimica Acta* 1997, 356(1), 75-83.

28. Tong, W; and Yeung, E S. *Applied Spectroscopy* **1998**, 52(3), 407-413.

29. Littlefield, R; and Fowler, VM. *Biophysical Journal* **2002**, 82(5), 2548-2564.

30. Hedley, DW; and Chow, S. *Cytometry* **1994**, 15, 349-358.

31. Kosomer, E.M.; and Kosomer, N.S. *Methods Enzymol*. **1995**, 251, 133-148.

32. Rosenzweig, Z; and Kopelman, R. *Sens. Actuators B* **1996**, 35-36, 475-483.

33. Kopelman, R; Miller, MT; Brasuel, M; Clark, HA; Hoyer, M; and Philbert, M. *Proceedings of SPIE-The International Society for Optical Engineering* **1999**, 3540 (Chemical, Biochemical, and Environmental Fiber Sensors X), 198-205.

34. Mcculloch, S; and Uttamchandani, D. *Proceedings of SPIE-The International Society for Optical Engineering* **1997**, 2980(Advances in Fluorescence Sensing Technology III), 228-239.

35. Cullum, BM; Griffin, GD.; and Vo-Dinh, T. *Proceedings of SPIE-The International Society for Optical Engineering* **2001**, 4254 (Biomedical Diagnostic, Guidance, and Surgical-Assist Systems III), 35-40.

36. Sasaki K.; Shi Z.; Kopelman R.; and Masuhara H. *Chem. Letter.* **1996**, 2, 141-142.

37. Jin J.; Rosenzweig N.; Griffin C.; and Rosenzweig Z*. Anal. Chem.* **2000**, 72(15), 3497-350.

38. Clark, H.A.; Marion, H.; Martin, A.; and Kopelman R. *Anal. Chem.* **1999**, 71, 4831-4836.

39. Clark H.A.; Marion, H.; Kopelman, R.; Tjalkens, R.; and Philbert, M. Sensors. *Anal Chem*. **1999**, 71, 4837-4843.

40. Xu, H.; Aylott, JW.; and Kopelman, R. *Analyst* **2002**, 127(11), 1471-7.

41. Xu, H.; Aylott, JW.; Kopelman, R.; Miller TJ.; and Philbert, MA. *Anal Chem* **2001**, 73(17), 4124-33.

42. Uyechi, LS; Gagne, L.; Thurston, G.; and Szoka, FC Jr. *Gene Ther* **2001**, 8(11), 828-36.

43. Liang, Y.; Belford, S.; Tang, F.; Prokai, L.; Simpkins, JW.; and Hughes JA. *Brain Res Bull* **2001**, 54(6), 661-8.

44. Wu, J; Lizarzaburu, ME; Kurth, MJ.; Liu, L; Wege, H.; Zern, MA.; and Nantz, MH *Bioconjug Chem* **2001**,12(2), 251-7.

45. Piva, R. del Senno, L.; Lambertini, E.; Penolazzi, L.; and Nastruzzi, C. *J Steroid Biochem Mol Biol* **2000**, 75(2-3), 121-8.

46. Toultou, E.; Godin, B.; Dayan, N.; Weiss, C.;, Piliponsky, A.; and Levi-Schaffer, F. *Biomaterial* **2001**, 22(22), 3053-9.

47. Batzri, S.; and Korn, ED. *Biochimica et Biophysica Acta* **1973**, 298, 1015-9.

48. Shew RL.; and Deamer, DW. *Biochimica et Biophysica Acta* **1985**, 816, 1-8.

49. Brandl, M.; and Gregoriadis, G. *Biochimica et Biophysica Acta* **1994**,1196, 65-75.

50. Schubert, R.; and Stauch, O. *Biomacromolecules* **2002**, 3, 565-578.

51. Paclet, MH.; Coleman, AW.; Vergnaud, S.; and Morel, F. *Biochemistry* **2000**, 39, 9302-9310.

52. Robert, MA.; Locasscio-Brown, L.; MacCrehan, WA.; and Durst, RA. *Anal. Chem* **1996**, 68, 3434-3440.

53. Wiedmer, SK.; Hautala, J.; Holopainen, JM.; Kinnunen, PKJ.; and Riekkola, ML. *Electrophoresis* **2001**, 22, 1305-1313.

54. Chandaroy, P.; Sen, A.; and Hui, SW. *J Control Release* **2001**, 76(1-2), 27-37.

55. Shew, RL.; and Deamer, DW. *Biochimica et Biophysica Acta* **1985**, 816, 1-8.

56. McNamara, KP.; and Rosenzweig, Z. *Anal. Chem*. **1998**, *70* (22), 4853-4859.

57. McNamara, KP.; Rosenzweig, Z.; and Rosenzweig, N. *Mikrochimica Acta* **1999**, 131, 57-64.

58. Floch,V.; Le Bolc'h, G.; Audrezet, MP.; Yaouanc, JJ.; Clemen, JC.; des Abbayes, H.; Mercier, B.; Abgrall, JF.; Ferec,C. *Blood Cells, Molecules, and Diseases*, **1997**, 23, 69-87.

59. Muller, WJ.; Zen, K.; Fisher, AB.; and Shuman, H.; *Am. J. Physiol.*, **1995**, 269, L11-19.

60. Ji, J.; Rosenzweig, N.; Jones, I., and Rosenzweig, Z. *Anal. Chem.* **2001**, 73 (15), 3521-3527.

61. Asiedu, J.K.; Ji, J.; Nguyen, M.; Rosenzweig, N., and Rosenzweig Z. *Anal. Chem.* **2001**, 6 (2), 116-121.

62. Nguyen, T.; DeCoster, M.; Nicolas, B.; and Rosenzweig, Z. *Anal. Chem.* **2003** (Submitted).

63. Deitmer, JW; and Rose, CR. *Prog Neurobiol* **1996**, 48, 73-103

64. Fykse, EM.; and Fonnum, F. *Neurochem Res* **1996**,21, 1053-1060.

65. Lindgren, CA.; Emery, DG.; and Haydon, PG. *J. Neurosci* **1997**, 17, 3074-3084.

66. Trudeau, L.; Parpura, V.; and Haydon, PG. *J. Neurophysiol* **1999**, 81, 2627-2635.

67. Huang, RQ.; and Dillon, GH. *J Neurophysiol* **1999**, 82, 1233-1243.

68. Chesler, M.; and Kaila, K. *Trends Neurosci* **1992**, 15, 396-402.

69. Cowan, AI.; and Martin, RL. *J Neurophysiol* **1995**, 74 (6), 2713-2721

70. Scheller, D.; Kolb, J.; and Tegtmeier, F. *Neuroscience Letters*, **1992**, 135, 83-86.

71. Deitmer, JW; and Rose, CR. *Prog Neurobiol* **1996**, 48, 73-103.

72. Chen, JCT.; and Chesler, M. *Proc. Natl. Acad. Sci. USA*, **1992**, 89, 7786-7790.

73. Powell, JJ; Burden, TJ.; Greenfield, SM.; Taylor, PD.; Thompson, RP.; *J. Inorg Biochem* **1999**, 75, 159-165.

74. Frederickson, CJ. *Int. Rev. Neurobiol*. **1989**, 31, 145-238.

75. Frederickson, CJ.; and Danscher, G. *Prog. Brain Res.* **1990**, 83, 71-84.

76. Frederickson, CJ.; Suh, SW.; Silva, D.; Frederickson, CJ.; and Thompson, RB. *J. Nutr* **2000**, 130, 1471S-1483S.

77. Frederickson, CJ; and Bush, A. *BioMetals* **2001**, 14, 353-366.

78. Franco-Pons, N.; Casanovas-Aguilar, C.; Arroyo, S.; Rumia, J.; Perez-Clausell, J.; and Danscher G. *Neuroscience* **2000**, 98, 429-435.

79. Frederickson, CJ; and Bush, A. *BioMetals* **2001**, 14, 353-366.

80. Varea, E.; Ponsoda, X.; Molowny, A.; Danscher, G.; and Lopez-Garcia, C. *J Neuroscience Methods* **2001**, 110, 57-63.

81. Sensi, SL.; Yin, HZ; and Weiss, JH. *European J Neuroscience* **2000**, 12, 3813-3818.

82. Colvin, RA; Davis, N.; Nipper, RW; and Carter, PA. *Neurochemistry Internaltional* **2000**, 36, 539-547.

83. Takeda, A. *Brain Res Rev* **2000**, 34, 137-148.

84. Sensi, SL.; Canzoneiro, LMT.; Yy, SP.; Ying, HS.; Koh, JY.; Kerchner, GA.; and Choi, DW. *J Neuroscience* **1997**, 17(24), 9554-9564.

85. Howell, GA.; Welch, MG.; and Frederick, CJ. *Nature* **1984**, 308, 736-738.

86. Perez-Clausell, J.; and Danscher, G. *Brain Res.* **1986**, 362, 358-361.

87. Gee, KR.; Zhou, ZL.; Ton-That, D.; Sensi,SL.; and Weiss, JH. *Cell Calcium* **2002**, 31(5), 245-251.

88. Frederickson, CJ.; Suh, SW.; Jensen, MS.; Hayes, D.J.; and Danscher, G.; *Soc. Neurosci*.**1998**, 24, 234.

89. Weiss, JH.; Sensi, SL.; and Koh, JY. *Trends Pharmacol Sci* **2000**, 21, 395-401.

90. Colvin, RA. *Am J Physiol Cell Physiol* **2002**, 282, C317-329.

91. DeCoster, M. A., Klette, K. L., Knight, E. S., and Tortella, F. C *Brain Research* **1995**, 671, 45-53.

92. DeCoster M.A., Lambeau G., Lazdunski M., and Bazan N.G. *J. Neurosci. Res.* **2002**, 67, 634-645.

93. Liu, W.; Wang, Y.; Tang, J.; Shen, G.; and Yu, R. *Analyst* **1998**,123(2), 365-369.

94. Potyrailo, R.A.; and Hieftje, G.M.. *Anal. Chem*. **1998**, *70* (16), 3407-3412.

95. Healey, B.G.; and Walt,DR. *Anal. Chem.* **1997**, 69 (11), 2213-2216.

96. Barker, SL.; and Kopelman, R. *Anal. Chem.* **1998**, *70* (23), 4902-4906.

97. Xin, Q.; and Wightman, RW. *Anal. Chem.* **1998**, 70(9), 1677-1681.

98. Plaschke, M.; Geyer, M.; Reichert, J.; and Ache, HJ. *Proc. SPIE-Int. Soc. Opt. Eng.* **1997**, 3105 (Chemical, Biochemical, and Environmental Fiber Sensors IX), 31-37.

99. Whitaker, JE.; Haugland, RP.; Ryan, D.; Hewitt, PC.; and Prendergast, FG. *Anal. Biochem*. **1992**, 207 (2), 267-279.

100. Haugland, RP. Handbook of Fluorescent Probes and Research Chemicals, 6th Ed*.;* Molecular Probes, Inc.: Eugene, OR, **1996.**

101. McNamara, KP.; and Rosenzweig, Z. *Anal. Chem.* **1998**, *70* (22), 4853-4859.

102. McNamara, KP.; Rosenzweig, Z.; and Rosenzweig, N. *Mikrochimica Acta*, in press.

103. New, R. Liposomes: A Practical Approach; Oxford University Press: Oxford, **1990.**

104. Bangham, AD.; Standish, MM.; and Watkins, JC. *J. Mol. Biol.* **1965**,13, 238-252.

105. Braganza, LF.; Blott, BH.; Coe, TJ.; and Melville, D. *Biochim. Biophys. Acta* **1983**,731 (2), 137-144.

106. Hartnett, AM.; Ingersoll, CM.; Baker, GA.; and Bright, FV. *Anal. Chem.* **1999**, 71(6), 1215-1224.

107. R. Armon, R.; Dosoretz, C.; Starosvetsky, J.; Orshansky, F.; and Saadi,, I. *J. Biotechnol* **1996**, 51 (3), 279-285.

108. Shtelzer, S.; and Braun, S. *Biotechnol. Appl. Biochem* **1994**, 19, 293-305.

109. Lavin, P.; Mcdonagh, CM; and Maccraith, BDJ. *Sol-Gel Sci. Technol*. **1998**, 13(1/2/3), 641-645.

110. Jaeger, KE.; and Reetz, MT. *Trends Biotechnol* **1998**, 16 (9), 396-403.

111. Williams, AK.; and Hupp, JTJ. *Am. Chem. Soc.* **1998**, 120(18), 4366-4371.

112. Zheng, L.; Reid, WR.; and Brennan, JD. *Anal. Chem*. **1997**, 69, 3940-3949.

113. Okabayashi, Y.; and Ikeuchi, I. *Analyst* **1998**, 123(6), 1329-1332.

114. Lim, SJ.;and Kim, CK. *Anal Biochem*. **1997,** 247(1), 89-95.

115. Singh, AK.; Kilpatrick, PK.; and Carbonell, RG *Biotechnol Prog*. **1996**,12(2), 272-280.

116. Locascio-Brown, L.; Plant, AL.; Chesler, R.; Kroll, M.; Ruddel, M.; and Durst, RA. *Clin Chem* **1993**, 39(3), 386-91.

117. Yager, P.; and Abrams, SB. *Proc. SPIE-Int. Soc. Opt. Eng*. **199**2, 1648 (Fiber Opt.

118. Yamanaka, SA.; Charych, DH.; Loy, DA.; and Sasaki, DY. *Langmuir* **1997**, 13(19), 5049-5053.

119. Fry, DW.; White, C.; and Goldman, DJ. *Anal. Biochem*. **1978**, 90, 809-814.

120. Ferguson, JA.; Healey, BG.; Bronk, KS.; Barnard, SM.; and Walt, DR. *Anal. Chim. Acta* 1997, 340(1-3), 123-131.

121. Nivens, DA.; Zhang, Y.; and Angel, SM. *Anal. Chim. Acta* **1998**, 376(2), 235-245.

122. Shalom, S., Strinkovski, A., Peleg, G., Druckmann, G., Krauss, A., Lewis, A., Linial, M., and Ottolenghi, M. *Anal. Biochem*. **1997**, 244(2), 256-59.

123. Clark, H.A., Hoyer, M., Philbert, M.A., and Kopelman, R. *Anal. Chem*. **1999**, 71(21), 4837-43.

124. Clark, H.A., Kopelman, R., Tjalkens, R., and Philbert, M.A. *Anal. Chem.***1999**, 71(21), 4831-6.

125. Sloan, W.D., and Uttamlal, M. *Luminescence* **2001**, 16(2), 179-86.

126. Kudo, Y., Akita, K., Nakamura, T., Ogura, A., Makino, T., Tamagawa, A., Ozaki, K., Miyakawas, A. *Neuroscience* **1992,** 50(3), 619-25.

127. Tsien, R.Y.(1989) *Ann. Rev. Neurosci*. **1989**, 12, 227-53.

128. Eberhard, M., and Erne, P. *Biochem Biophys Res Commun* **1991**, 180 (1), 209-215.

129. Flora, K., and Brennan, J.D. *Anal. Chem* **1998**, 70, 4505-4513.

130. Shetty, R.S., Ramanathan, S., Bard, I.HA., Wolford, J.L. and Daunert, S. *Anal.Chem.***1998**, 71, 763-768.

131. Marvin, J.S., Corcoran, E.E., Hattangadi, N.A., Zhang, J.V., Gere, S.A., and Hellinga, H.W. *Proc. Natl. Acad. Sci. USA* **1997**, 94, 4366-4371.

132. Salins, L.L.E., Schauer-Vukasinovic, V., and. Dauntert, S. *Proc. SPIE-Int. Soc. Opt. Eng.* **1998**, 3270 (Methods for Ultrasensitive Detection), 16-24.

133. Ri, C. and Yang, S. *Anal. Sci. Technol* **1995**, 80 (3), 221-7.

134. Blair, T.L., Yang, S., Smith-Palmer, T., and Bachas, L.G. *Anal. Chem.* **1994**, 66 (2), 300-2.

135. Marvin, J.S., and Hellinga, H.W. *J. Am. Chem. Soc.* **1998**, 120, 7-11.

136. Miki, Y., Swensen, J., Shattuck-Eidens, D., Futreal, PA., Harshman, K., Tavtigian, S., Liu, Q., Cochran, C., Bennett, LM., Ding, W. et al *Science* **1994**, 266, 66-71.

137. Roehm, P.C., and J.M. Berg, J.M. *Biochemistry* **1997**, 36(33), 10240-245.

138. Michael, S.F., Kilfoil, V.J., Schmidt, M.H., Amann, B.T., and Berg, J.M. *Proc. Natl. Acad. Sci. U.S.A* **1992** , 89 (11), 4796-4800.

139. Roehm, P.C., and Berg, J.M. *Biochemistry* **1997**, 36(33), 10240-10245.

140. Hinrichsen, R.D. *Biochem Biophys Acta* **1993**, 1155, 277-293.

141. Cheung, W.Y. *Science* **1980**, 207 (4), 19-27.

142. Persechini, A. and Cronk, B. *J.Biol Chem* **1999**, 274 (11), 6827-6830.

143. Tanaka, T. *Japan J. Pharmacol* **1988**, 46, 101-107.

144. Walsh, M.P. *Mol. Cell Biochem* **1994**, 135, 21-41.

145. Houdusse, A., Love, M.L., Dominguez, R., Grabarek, Z. and Cohen, C. *Structure* **1997**, 5(12), 1695-1711.

146. Crivici, A. and Ikura, M. *Annu. Rev. Biophys. Biomol. Struct.* **1995**, 24, 85-116.

147. Ikura, M. *Trends in Biochemical Sciences* **1996**, 21, 14-17.

148. Evenas, J., Malmendal, A., Thulin, E., Carlstrom, G. and Forsen, S. *Biochemistry* **1998**, 37, 13744-13754.

149. Trave, G., Lacombe, P., Pfuhl, M., Saraste, M., and Pastore, A. *EMBO J.* **1995**, 14(20), 4922-4931.

150. Nelson, M.R., and Chazin, W.J. *Protein Science* **1998**, 7, 270-282.

151. Wang, C.A. *Biochem Biophys Res Commun* **1985**, 130 (1), 426-430.

152. Johnson, J.D., and Wittenauer, L.A. *Biochem J.* **1983**, 211, 473-479.

153. Tsuruta, H. and Sano, T. *Biophys Chem* **1990**, 35, 75-84.

154. Johnson, J.D., and Wittenauer, L.A. *Biochem. J.* **1983**, 211, 473-479.

155. Miyawaki, A., Liopis, J., Helm, R., McCaffery, J.M., Adams, J.A., Ikura, M. and Tsien, R.Y. *Nature* **1997**, 388, 882-887.

156. Blair, T.L., Yang, S., Smith –Palmer, T., and Bachas, L.G. *Anal. Chem.* **1994**, 66, 300-302.

157. McNamara, K.P., and Rosenzweig, Z. *Anal. Chem.* **1998**, 70 (22), 4853-4859.

158. McNamara, K.P., Rosenzweig, N., and Rosenzweig, Z. *Mikrochim. Acta* **1999**, 131, 57-64.

159. New, R. Liposomes: Approach, Oxford University Press: Oxford, **1990**.

160. Bangham, A.D., Standish, B.H., and Watlins, J.C. *J .Mol. Biol* **1965**, 3, 238-252.

161. Lasic, D.D. *Trends in Bio. Tech* **1998**, 16, 307-321.

162. Shew, R.L., and Deamer, D.W. *Biochim Biophys Acta* **1985**, 816, 1-8.

163. Fry, D.W., White, C., and Goldman, D.J. *Anal. Biochem* **1978**, 90, 809-814.

164. Chesler, M and Grichtchenko G *Neuroscience* **1994**, 62(4), 1057-70.

165. Sykova, E and Chvatal, A *J. Chemical Neuroanatomy* **1993**, 6, 247-260.

166. Chesler, M and Kaila, K *TINS* **1992**, 15(10), 396-402.

167. Stella, N, Pellerin, L, and Magistretti, PJ *The Journal of Neuroscience* **1995**, 15(5), 3307-3317.

168. Deitmer, JW, and Rose, CR *J. of Neurophysiology* **1995**, 73(1), 132-139.

169. Voipio J, Paalasmaa P, Taira T, Kaila K. *J Neurophysiol* **1995**, 74(2), 633-42.

170. Sykova E, Svoboda J, Chvatal A, Jendelova P. *Ciba Found Symp* 1988, 139, 220-35.

171. Woodbury DM, Engstrom FL, White HS, Chen CF, Kemp JW, Chow SY. *Ann Neurol* 1984, 16 Suppl, S135-44.

172. Xiong, Z, and Stringer, JL *Developmental Brain Research* **2000,** 122, 113-117.

173. Walz, W (1997) *Neuroscience and Biobehavioral Reviews* **1997**, 21(2), 135-142.

174. Lauritzen, M *Cephalalgia* **2001***,* 21, 757-760.

175. Basarsky, TA, Feighan, D, and MacVicar, BA *The Journal of Neuroscience* **1999**, 9(15), 6439-6445.

176. Chen, G, Dunbar, RL, Gao, W, and Ebner, TJ (2001) *The Journal of Neuroscience* **2001**, 21(24), 9877-9887.

177. Kempski, O, Otsuka, H, Seiwert, T, and Heimann, A (2000), *Acta Neurochir* **2000***,* 76 Suppl, 251-255.

178. James, MF, Smith, JM, Boniface, SJ, Huang CLH, and Leslie, RA (2001*) Trends in Neurosciences* **2001***,* 24(5), 266-271.

179. Mutch WAC, and Hansen, AJ *J. Cerebral Blood Flow and Metabolism* **1984**, 4, 17-27.

180. Somjen, G *Physiol Rev* **2001**, 81, 1065-1096.

181. Gorji, A *Brain Research Reviews* **2001**, 38, 33-60.

182. Chen JC, Chesler M. *J Neurophysiol* **1992**, 67(1), 29-36.

183. Avoli M, Louvel J, Drapeau C, Pumain R, Kurcewicz I. *J Neurophysiol* **1995**, 73(2), 468-84.

184. Menna, G, Tong CK, and Chesler, M *J. Neurophysiol* **2000**, 83, 1338-1345.

185. Huang, W, Smith, SE, and Chesler, M *J. Neuorphysiology* **1995,** 74(4), 1806-1809.

186. Krishtal, OA, Osipchuk, V, Shelest, TN, and Smirnoff, SV *Brain Research* **1987**, 436, 352-356.

187. Ji, J, Rosenzweig, N, Griffin, C, and Rosenzweig, Z *Anal. Chem.* **2000,** 72, 3497-3503.

188. Ji J, Rosenzweig N, Jones I, Rosenzweig Z *Anal. Chem.* **2001,** 73 (5), 3521-3527.

189. Zambenedetti, P, Giordane, R., and Zatta, P. *Glycoconjugate J.* **1996**, 13, 341-346.

190. Hart, CE, and Wood, JG *The Journal of Comparative Neurology* **1985**, 239, 155-162.

191. Elgavish, S, and Shaanan, B *Trends in Biochemical Sciences* **1997**, 22,462-467.

192. Huang, W, Smith, E., and Chesler, M. *Journal of Neurophysiology* **1995**, 74(4), 1806-1809.

193. Tong, CK., and Chesler, M. *Journal of Neurophysiology* **2000**, 84, 2449-2457.

194. Velazquez, R.A, Cai, Y., Shi, Q., and Larson, A. *J. Neuroscience* **1999**, 19(6), 2288

195. Lees, G.J., Cuajungco,M.P., and Leong W. *Brain Research* **1998**, 799 , 108

196. Suh, S.W., Chen, J.W., Motamedi, M., Bell, B., Listiak, K., Pons, N.F., Dnascher, G., and Frederickson, C.J. *Brain Research* **2000***,* 852, 268

197. Takeda, A. *Brain Research Review* **2002**, 34, 137

198. Canzoniero, L.M., Turetsky, D.M., and Choi, D.W. *J. Neuroscience* **1999**, 19, RC31

199. Sensi, S.L., Canzoniero, L.M., Yu, S.P., Ying, H.S., Koh, J., Kerchner, G.A., and Choi, D.W. (1997) *J. Neuroscience* **1997***,* 17 (24),9554.

200. Takeda, A., Sawashita, J., Takefuta, S., Ohnuma,M., and Okada, S. *J. Neuroscience Research* **1999**, 57, 405.

201. Nasir, M.S., Fahrni, C.J., Suhy, D.A., Kolodsick, K.J., Singer, C.P., and O'Halloran, T.V. *JBIC* **1999**, 4, 775

202. Prat, M.D., Compano,R., Guiteras, J. and Beltran, J.L. *J. Fluorescence* **1991**, 1(4),267

203. Koh, JY., and Choi,DW. *Neuroscience* **1994**, 60(4), 1049-1057.

204. McDonald, JW.; Bhattacharyya, T.; Sensi, SL.; Lobner, D.; Ying, HS.; Canzoneiro, LMT.; and Choi, DW. *J Neuroscience* **1998**, 18(16), 6290-6299.

205. Kim, EY.; Koh, JY.; Kim, YH.; Sohn, S.; Joe, E., and Gwag, BJ. *European J Neuroscience* **1999**, 11, 327-334.

206. Timm, F. Zur Histochemie der Schwermetalle. Das Sulfid-Silberverfahren. Dtsch. Z. *Ges Gerichtl. Med*. **1958**, 46, 706-711.

207. Lopez-Garcia C., Molowny A., Perez-Claussel J., Martinez-Guijarro F.J. *J Neurosci Methods*. **1984**, 11, 211-20.

208. Frederickson C.J., Kasarskis E.J., Ringo D., Frederickson R.E. *J. Neurosci. Methods.***1987,** 20, 91-103.

209. Budde T., Minta A., White J.A., Kay A.R. *Neuroscience*. **1997**, 79, 347-58.

210. Thompson R.B., Whetsell W.D. Jr., Maliwal B.P., Fierke C.A., Frederickson C.J. *J. Neurosci. Methods*. **2000**, 96, 35-45.

211. Prat, M.D. et al, *Journal of Fluorescence* **1991,** 1(4)**,** 267-272.

212. Andrews, JC; Nolan, JP., Hammerstedt, RH.; and Bavister, BD. *Cytometry* **1995**, 21, 153.

APPENDIX

GLOSSARY OF TERMS

AraC: Cytosine (beta)-D-arabinofuranoside

CNS: Central nervous system

CSD: Cortical spreading depression

DMPC: Dimyristoyl phosphatidylcholine

 DP: Dihexadecyl phosphate

EGTA: Ethylene glycol bis(2-aminoethyl ether)-N,N,N'N'-tetraacetic acid

FAD: Flavin adenine dinucleotide

Fluorescein DHPE: *N*- (fluorescein-5-thiocarbamoyl)- 1,2-dihexadecanoyl-*sn*-glycero-3-

phosphoethanolamine, triethylammonium salt

MOPS: 4-morpholino-propanesulfonic acid

NADH: Nicotinamide adenine dinucleotide reduced form

PBS: Phosphate buffered saline

Succ. Con A: Succinyl-concanavalin A

TMOS: Tetramethylorthosilicate

TSQ: N- (6-methoxy-8-quinolyl)-p-toluenesulfonamide

VITA

The author was born in Saigon City, Vietnam. She obtained her B.A. in Chemistry from University of New Orleans in 1998. In 1999, she joined the Department of Chemistry at the University of New Orleans and became a member of Professor Zeev Rosenzweig's research group.

DOCTORAL EXAMINATION REPORT

CANDIDATE: THUVAN HOANG NGUYEN

MAJOR FIELD: ANALYTICAL CHEMISTRY

TITLE OF DISSERTATION: MINIATURIZED FLUORESCENCE BIOSENSORS FOR

STUDYING NEURONAL EVENTS

APPROVED: *Zeev Rosenzweig*

PROFESSOR ZEEV ROSENZWEIG

Major Professor & Chair -

Robert C. Cashner

Dean of the Graduate School

EXAMINING COMMITTEE:
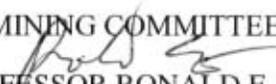
PROFESSOR RONALD F. EVILIA
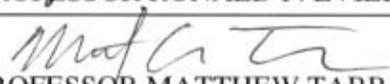
PROFESSOR MATTHEW TARR

PROFESSOR MARK L. TRUDELL
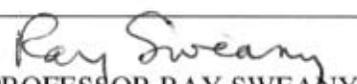
PROFESSOR RAY SWEANY

DATE OF EXAMINATION: APRIL 28, 2003